Role of sphingomyelinases in mycobacterial infection

Inaugural-Dissertation

zur

Erlangung des Doktorgrades

Dr. rer. nat.

der Fakultät für Biologie

an der

Universität Duisburg-Essen

vorgelegt von

Yuqing Wu

aus

Shanghai, China

im Februar 2019

Die der vorliegenden Arbeit zugrunde liegenden Experimente wurden am Institut für Molekularbiologie, Universität Duisburg-Essen durchgeführt.

1. Gutachter: Prof. Dr. Erich Gulbins

2. Gutachter: Prof.‘in Dr. Astrid Westendorf

3. Gutachter: Prof.‘in Dr. Elke Cario

Vorsitzender des Prüfungsausschusses: Prof.‘in Dr. Elke Cario

Tag der mündlichen Prüfung: 27.05.2019

DOI: 10.17185/duepublico/70191
URN: urn:nbn:de:hbz:464-20190612-144629-4

I dedicate this work to my supervisors, who inspired and encouraged me; my colleagues, who worked with and helped me; my friends, for entertaining and comforting me; and my family, for supporting and loving me.

Abstract

Mycobacterial infection-induced diseases, particularly tuberculosis (TB), cause more than 1 million deaths annually. Mycobacteria initially infect lungs, invade alveolar macrophages and can develop a systemic infection with high lethality. However, currently available drugs are only partially effective due to the development of drug-resistant mycobacteria.

The sphingomyelinase/ceramide system has been implicated to play many roles in mycobacterial infections. Thus, this study aims to identify the mechanisms of sphingomyelinase/ceramide-regulated mycobacterial infection and provide potential therapeutic strategies.

The present work investigated roles of neutral sphingomyelinase (Nsm) and acid sphingomyelinase (Asm)/ceramide system in the systemic infection of murine macrophages and mice with *Mycobacterium bovis* Bacillus Calmette-Guérin (BCG).

Nsm has been shown to allow mycobacterial persistence in mice by suppressing autophagy. The present study focused on the role of Nsm in the generation of granuloma, the hallmark of mycobacterial infections. The results in this thesis reveal a novel mechanism of Nsm-dependent granuloma formation upon mycobacterial infection. The results indicate that the infection of bone marrow-derived macrophages (BMDMs) with BCG leads to rapid activation of Nsm and activation of surface β1-integrin via phosphorylation of p38 mitogen-activated protein kinases (p38K) and c-Jun N-terminal kinase (JNK). Nsm-dependent β1-integrin activation results in the activation of small GTPase Rac1 and reorganization of the cytoskeleton. This leads to macrophage migration and granuloma-like clusters *in vitro*. Mice heterozygous for Nsm or mice treated with neutralizing antibodies against β1-integrin contain fewer macrophage clusters *in vitro*, fewer granulomas *in vivo* and, most importantly, fewer bacteria *in vivo*. These findings indicate that the Nsm/ceramide system plays an important role in mycobacteria-induced granuloma formation by regulating a signaling cascade via p38, JNK, β1-integrin and Rac1.

Furthermore, the current study suggests a novel mechanistic link between Asm and mycobacterial infection. The results show that BCG infection of BMDMs triggers

activation of Asm and acid ceramidase (Ac), and elevated levels of sphingosine-1-phosphate (S1P) which increases reactive oxygen species (ROS) via nicotinamide adenine dinucleotide phosphate (NADPH) oxidase subunit $p47^{phox}$. ROS promote BCG degradation by the lysosomal enzyme, cathepsin D. BMDMs of Asm deficient mice abrogate these effects, and these mice are more susceptible to BCG infection than wild-type (Wt) mice. Transplantation of Wt BMDMs into Asm deficient mice confirmed the crucial role of Asm in macrophages. The transplantation partially reversed the susceptibility of Asm deficient mice to BCG infection. These findings indicate that Asm/ceramide system is important in the control of BCG infection.

These studies reveal the role of sphingomyelinases in mycobacteria-induced granuloma formation and bacterial elimination. The further study combines neutral and acid sphingomyelinases may provide a novel therapeutic strategy against mycobacterial infection.

Zusammenfassung

Infektionen durch Mykobakterien, insbesondere Tuberkulose (TB), verursachen jährlich mehr als 1 Million Todesfälle. Die anfängliche pulmonale Lokalisation der Erreger entwickelt sich oft zu einer systemischen Infektion mit hoher Letalität. Gegenwärtig verfügbare Arzneimittel sind jedoch aufgrund der Entwicklung von arzneimittelresistenten Mykobakterien nur teilweise wirksam.

Dass das Sphingomyelinase/Ceramid-System bei mykobakteriellen Infektionen bedeutsam ist, wurde bereits in einigen Publikationen beschrieben. Ziel dieser Studie ist es, die Mechanismen der Sphingomyelinase-regulierten mykobakteriellen Infektion detaillierter zu untersuchen, um dadurch potentielle Zielmoleküle für eine Therapie zu identifizieren.

In der vorliegenden Arbeit wurden die Rolle des sauren Sphingomyelinase (Asm) und des neutralen Sphingomyelinase (Nsm)/Ceramid-Systems bei der systemischen Infektion von Mäusen und von murinen Makrophagen mit *Mycobacterium bovis* Bacillus Calmette-Guérin (BCG) untersucht.

Die Ergebnisse zeigen, dass die Infektion von Makrophagen mit BCG zu einer raschen Stimulation der Nsm und einer Aktivierung von oberflächigem β1-Integrin über eine Phosphorylierung von p38K und JNK führt. Die Nsm-abhängige Aktivierung von β1-Integrin hat eine Stimulation von Rac1 und eine Reorganisation des Aktin-Zytoskeletts zur Folge, was zur Migration von Makrophagen und schließlich zur Granulombildung führt. Bedeutsam ist, dass die Inzidenz der Granulombildung bei Nsm-heterozygoten Mäusen oder bei Mäusen, die mit neutralisierenden Antikörpern gegen β1-Integrin behandelt wurden, viel niedriger ist, wodurch chronische Infektionen der Leber und Milz verhindert werden. Diese Befunde zeigen, dass das Nsm/Ceramid-System eine wichtige Rolle bei der Bildung von Mykobakterien-induzierten Granulomen spielt, indem es eine Signalkaskade über p38, JNK, β1-Integrin und Rac1 reguliert.

Darüber hinaus liefern die vorliegenden Daten eine neuartige mechanistische Verbindung zwischen mykobakteriellen Infektionen und der Funktion der Asm. Die Ergebnisse zeigen, dass die BCG-Infektion von Makrophagen über die Stimulierung der Sauer Sphingomylinase (Asm), Sauer Ceramidase (Ac), Sphingosin-1-Phosphat

erhöht und dann eine erhöhte Produktion von reaktiven Sauerstoffspezies über die NADPH-oxidase-Untereinheit $p47^{phox}$ auslöst. Die reaktiven Sauerstoffspezies ihrerseits aktivieren Cathepsin D, welches das Abtöten der Bakterien vermittelt. Mäuse, die für die Asm defizient sind, sind nicht in der Lage, die beschriebenen Prozesse zu induzieren und können somit die BCG-Infektion nicht abwehren. Die entscheidende Rolle von Makrophagen in der Asm-abhängigen Kontrolle von Mykobakterien wurde durch Transplantation von Wildtyp-Makrophagen in Asm-defiziente Mäuse bestätigt; durch diese Übertragung wurde die Empfindlichkeit von Asm-defizienten Mäusen gegenüber BCG-Infektionen partiell kompensiert. Diese Ergebnisse legen nahe, dass das Asm/Ceramid-System bei der Kontrolle von BCG-Infektionen wichtig ist.

Diese Studien zeigen die Rolle von Sphingomyelinasen bei der Mykobakterien-induzierten Granulombildung und der Bakterienbeseitigung. Die weitere Studie, in der neutrale und saure Sphingomyelinasen kombiniert werden, kann eine neuartige therapeutische Strategie gegen mykobakterielle Infektionen darstellen.

Contents

List of Tables

List of Figures

List of Abbreviations

Abbreviations	Meaning
A/L	aprotinin/leupeptin
ADAM9	a disintegrin and metalloproteinase domain-containing protein 9
ANOVA	analysis of variance
AP	alkaline phosphatase
APS	Ammonium persulfate
Asm/ASM	Acid sphingomyelinase (Asm for murine, ASM for human)
$Asm^{-/-}$	Asm-deficient
BCG	Bacillus Calmette-Guérin
BMDMs	bone marrow-derived macrophages
BODIPY FL	Boron dipyrromethene fluorophore, $C_9H_7BF_2N_2$
BSA	Bovine serum albumin
CD	Cluster of differentiation
CDase	ceramidase
CF	cystic fibrosis
CFUs	colony forming units
CK	ceramide kinase
CLRs	C-type lectin receptors
COPD	chronic obstructive pulmonary disease
cPKC	conventional protein kinase C
CR3	complement receptor 3
CRs	complement receptors
CTD	C-terminal subdomain
DAG	diacylglycerol
DCs	dendritic cells
DC-SIGN	Dendritic Cell-Specific Intercellular adhesion molecule-3-Grabbing Non-integrin
DMEM	Dulbecco's Modified Eagle Medium
DMSO	dimethyl sulfoxide

dpi	days post infection
E. Coli	*Escherichia coli*
EDTA	ethylenediaminetetraacetic acid
EEA1	early endosome antigen 1
EED	embryonic ectoderm development
ER	endoplasmic reticulum
ERK	extracellular signal-regulated kinase
ESI+	electrospray ion source operating in the positive ion mode
FBS	Fetal Bovine Serum
GCase	glucosylceramidase
GCS	glucosylceramide synthase
G-CSF	Granulocyte-colony stimulating factor
GFP-BCG	green fluorescent protein (GFP)-expressing BCG
GTPase	guanosine triphosphatase
H&E	hematoxylin and eosin
H/S	HEPES/saline buffer
HIV	human immunodeficiency virus
hpi	hours post infection
hvPS34	human vacuolar protein-sorting 34
I-EGF2	Integrin-epidermal growth factor domain 2
IFN-γ	interferon-γ
IgG	immunoglobulin G
IL	Interleukin
ILVs	intraluminal vesicles
iNOS	inducible nitric oxide synthase
JNK	c-Jun N-terminal kinases
L. monocytogenes	*Listeria monocytogenes*
LAM	lipoarabinomannan
LAMPs	lysosomal-associated membrane proteins
L-Asm	lysosomal Asm
LC3B	microtubule-associated protein 1 light chain 3 beta
LM	lipomannan
LPS	lipopolysaccharide

M. abscessus	*Mycobacterium abscessus*
M. avium	*Mycobacterium avium*
M. bovis	*Mycobacterium bovis*
M. leprae	*Mycobacterium leprae*
M. marinum	*Mycobacterium marinum*
M. tuberculosis	*Mycobacterium tuberculosis*
M. ulcerans	*Mycobacterium ulcerans*
MAPKs	mitogen-activated protein kinases
MA-Smase	mitochondria-associated sphingomyelinases
M-CSF	macrophage colony-stimulating factor
MEM	Minimum Essential Medium
MGCs	multinucleated giant cells
MHC	major histocompatibility complex
MTC	*Mycobacterium tuberculosis* complex
MV	*Measles virus*
N. gonorrhoea	*Neisseria gonorrhea*
NADH	nicotinamide adenine dinucleotide
NADPH	nicotinamide adenine dinucleotide phosphate
NBD	nitrobenzoxadiazole
NOX	NADPH oxidase
Nsm/NSM	Neutral sphingomyelinase (Nsm for murine, NSM for human)
$Nsm^{+/-}$	Nsm heterozygous
NSMAF	Neutral sphingomyelinase activation–associated factor
NTM	nontuberculous mycobacteria
O_2	oxygen
O_2–	ROS superoxide
OADC	oleic acid, albumin, dextrose, and catalase
P. aeruginosa	*Pseudomonas aeruginosa*
p38K	P38 mitogen-activated protein kinases
PAMPs	pathogen-associated molecular patterns
PBS	Phosphate buffered saline
PC	phosphatidylcholine
PCR	polymerase chain reaction

pERK	phospho-extracellular signal-regulated kinase
PFA	Paraformaldehyde
PI-3K	phosphoinositide 3-kinase
PIM	phosphatidylinositol mannosides
PI-PLC	phosphoinositide-specific phospholipase C
PL	proline-rich linker
PLD	phospholipase D
RANTES	regulated and normal T cell expressed and secreted (chemokine)
RIP1	receptor-interacting serine-threonine kinase 1
RIP3	receptor-interacting serine-threonine kinase 3
ROI	region of interest
ROS	reactive oxygen species
S. aureus	*Staphylococcus aureus*
S. tryphimurium	*Salmonella enterica serovar Typhimurium*
S1P	sphingosine-1-phosphate
S1PR1	S1P receptor-1
S1PR2	S1P receptor-2
SapM	secreted acid phosphatase M
S-Asm	secretory Asm
SD	standard deviation
SDS	sodium dodecyl sulfate
SDS-PAGE	SDS polyacrylamide gel electrophoresis
SK	sphingosine kinase
SMase	sphingomyelinase
Smpd1	Sphingomyelin Phosphodiesterase 1, murine
SMPD3/Smpd3	Sphingomyelin Phosphodiesterase 3 (SMPD3 for human, Smpd3 for murine)
SMS	sphingomyelin synthase
Sort1	Sortilin 1
SP	signal peptide
SphK	Sphingosine kinase
SPN2	S1P transporter spinster homolog 2
SPPase	sphingosine phosphate phosphatase

SPT	serine palmitoyltransferase
SRs	scavenger receptors
TB	tuberculosis
TBS	Tris-buffered saline
TDM	trehalose dimycolate
TGFβ	Transforming growth factor beta
Th	T-helper
TLC	thin-layer chromatography
TLR2	Toll-like receptor 2
TNF	tumor necrosis factor
TNF-R	TNF-receptor
V-ATPase	vacuolar-ATPase
wpi	weeks post infection
Wt	wild-type

1 Introduction

1.1 Mycobacteria

The genus Mycobacterium was first introduced by Lehmann and Neumann in 1896 as the only member of Mycobacteriaceae (Liu, 2005; van Ingen, 2017). Until now, over 150 species of mycobacteria have been recognized, and all of them are aerobic, non-motile, slightly curved or straight rod and nonspore-forming bacteria. Mycobacteria are characterized as acid-fast bacteria which prevent the de-colorization during Gram staining with hydrochloric acid and cannot be stained well by Gram dyes (van Ingen, 2017). Therefore, they are being considered as gram neutral bacteria (van Ingen, 2017).

1.1.1 Structure of mycobacterial cell envelope

Mycobacteria are covered by a thick cell envelope which consists of a covalently linked cell wall and a variety of lipids (Daffe, 2015; van Ingen, 2017) (Figure 1). The covalently linked cell wall defines the size and shape of the mycobacteria and contains peptidoglycan, arabinogalactan and mycolic acids (Daffe, 2015). The mycolic acids (mycolate) consist of short chain fatty acids and medium chain fatty acids. These fatty acids complement the hydrocarbon chains and form a flat surface. As well as other microorganisms, mycobacteria contain a plasma membrane. However, unlike other bacteria, the constituents of the mycobacterial plasma membrane are lipids, as lipoarabinomannan (LAM), lipomannan (LM) and phosphatidylinositol mannosides (PIM) (Figure 1) (van Ingen, 2017). The lipid-rich cell envelope functions as a hydrophobic permeability barrier which protect the bacteria from osmotic pressure and deleterious environment (van Ingen, 2017).

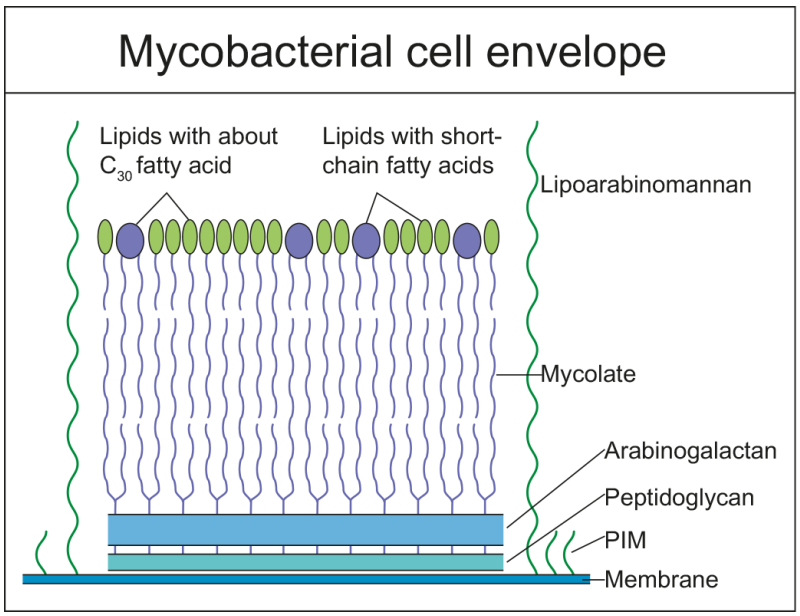

Figure 1. The structure of the mycobacterial cell envelope.
The mycobacterial cell envelope consists of the plasma membrane and a thick cell wall. The plasma membrane of mycobacteria is a lipid-rich structure associated with lipoarabinomannan (LAM), and phosphatidylinositol mannosides (PIM). The cell wall of mycobacteria is a covalently bound structure and contains mycolate (with short, medium chain fatty acids and hydrocarbon chains), arabinogalactan and peptidoglycan. Adapted from van Ingen, 2017.

1.1.2 Mycobacteria-induced diseases

Mycobacterium tuberculosis (*M. tuberculosis*) and *Mycobacterium leprae* (*M. leprae*) are two of the most well-known pathogens of the genus Mycobacteria, leading to tuberculosis (TB) (see section 1.2) and leprosy in humans, respectively. During the last decades, other diseases caused by other mycobacteria species are also gaining attention, such as Buruli ulcer disease caused by *Mycobacterium ulcerans* (*M. ulcerans*) and some diseases caused by nontuberculous mycobacteria (NTM).

Leprosy, also called Hansen's disease, is a chronic, severe disease characterized by lesions or granulomas in the skin, nerves, and mucous membranes. It affected about 170,000 people worldwide at the end of 2015 (WHO, 2018a). Long-term infection with *M. leprae* is causative of leprosy. Leprosy is curable with 2-3 multidrug therapies including rifampicin, clofazimine, and dapsone (WHO, 2018a).

Buruli ulcer is the third most common mycobacteria-induced disease which is caused by the toxin mycolactone, released by *M. ulcerans* (Guarner et al., 2003). The disease is characterized by chronic and necrotizing ulcers in the skin. There was no effective

medication for this disease. Until the last decade, as reported being treatable by multi-antibiotics, such as rifampin, streptomycin, and clarithromycin (Nienhuis et al., 2010). However, the transmission routes of *M. ulcerans* are still unclear.

NTM cause a wide range of diseases in humans. *Mycobacterium avium* (*M. avium*), which commonly exists in soil, water and animals, is the cause of chronic pulmonary infections. This concerns especially patients who already have pulmonary diseases or are severely immunocompromised, such as patients with chronic obstructive pulmonary disease (COPD) or people who are infected with human immunodeficiency virus (HIV), as well as children with lymphadenitis (Griffith et al., 2007). Except for *M. avium*, *Mycobacterium kansasii* is the second leading cause of pulmonary diseases (Griffith et al., 2007). *Mycobacterium abscessus* (*M. abscessus*), *Mycobacterium chelonae,* and *Mycobacterium fortuitum* are species leading to cutaneous infection, as well as to postsurgical infections in soft tissues or bones (van Ingen, 2017). *Mycobacterium abscessus* gains increasing interest due to its high risk of infection in cystic fibrosis (CF) patients (Nessar et al., 2012).

1.2 Tuberculosis: a worldwide emergency

Tuberculosis (TB) is an infectious disease which exists in humans as well as in other animals and is caused by one of the *Mycobacterium. tuberculosis* complex (MTC). MTC includes *M. tuberculosis*, *M. africanum*, *Mycobacterium. bovis* (*M. bovis*), *Mycobacterium. microti* (*M. microti*), *Mycobacterium. canettii* (*M. canettii*) and others (Wayne, 1982). Robert Koch identified *M. tuberculosis* as the causative agent of TB in 1882 (Koch, 1882). *M. tuberculosis* caused TB is one of the top 10 causes of mortality worldwide, primarily in low-income and middle-income countries (over 95%). TB led to 10.4 million people falling ill, and 1.7 million people dying in 2016 (WHO, 2018b).

From the clinical and public health perspective, patients with TB are pragmatically classified as having latent TB infection or active TB disease. Most people infected with *M. tuberculosis* exhibit no clinical symptoms; this state is called latent TB, and it is an asymptomatic and non-transmissible state (WHO, 2018b). Patients with active pulmonary TB disease, which is transmissible, experience symptoms which include fever, night sweats, lack of appetite, weight loss and coughing. These symptoms could

be mild for many months, which causes many affected people to handle the disease carelessly and delayed. This delay may result in transmission of the bacteria to others. Some patients are asymptomatic but with an active (transmissible) disease which is a state considered as subclinical TB (Esmail et al., 2014).

M. tuberculosis, *M. africanum,* and *M. bovis* are the most important MTC which can cause TB in humans (Wayne, 1982). A spoligotyping (a polymerase chain reaction-based method for genotyping) of historical samples (ancient skeletal and mummified materials) showed that humans have been in a constant battle with TB since ancient times. *M. tuberculosis* DNA has been discovered in Egyptian mummies dating from 2050 B.C. and 1650 B.C. (Zink et al., 2003). A previous hypothesis was that *M. bovis* might be the ancestor of *M. tuberculosis* which was transmitted from cattle to humans (Cockburn, 1964). However, Zink et al. suggested that human *M. tuberculosis* may have originated from a precursor bacterium probably related to *M. africanum* (Zink et al., 2003).

TB became a treatable disease with the discovery of streptomycin in 1943 by Dr. Selman Waksman. From then on, the incidence and lethality of TB decreased through the middle of the 20th century. However, interactions among the environment, the host, and the pathogen resulted in the resurgence of TB. Antibiotic resistance (the evolution of extensively drug-resistant forms of *M. tuberculosis*), the lack of effective, sensitive, and rapid diagnostic tools, the increased susceptibility of people with weakened immune systems to TB, the increased mobility of people because of globalization, and the relative ineffectiveness of the Bacillus Calmette-Guérin (BCG) vaccine have put TB back on the agenda during the past twenty years and have again rendered the infectious disease a recognized global threat (Dheda et al., 2010).

The BCG vaccine, a live attenuated variant of *M. bovis*, has been used since the early 20th century to prevent TB. However, it has recently been shown to be rather unsuccessful in preventing TB caused by *M. tuberculosis* (Kagina et al., 2010). A study of BCG vaccination of newborns showed that the frequency and cytokine profile of mycobacteria-specific T cells were not associated with protection from or susceptibility to the subsequent development of TB (Kagina et al., 2010). Therefore, a more effective vaccine is sorely needed. Public health and financial efforts, including improved access to health care, better control of transmission, improved and more available diagnostic tools, and better treatment methods are also mandatory to get this global disease

under control. New scientific insights into the underlying mechanisms of TB and more knowledge about how the host can overcome them is needed to develop a new, improved vaccine and new drugs that can tackle the emergence of antibiotic resistance (Dheda et al., 2010).

1.3 Pathogenesis of Tuberculosis: an orchestration of the immune system

Transmission of *M. tuberculosis* occurs when a new host inhales bacteria-containing droplets dispersed from the lungs of an infected person, for example, by coughing (Nunes-Alves et al., 2014). The infectious microorganisms are inhaled and deposited into the airways and alveoli (Figure 2A) (Pai et al., 2016).

TB pathogens, such as *M. tuberculosis*, are facultative intracellular bacteria that can infect various cell types, although alveolar macrophages seem to be the initially infected cell type. The primary stages of the host response to *M. tuberculosis* infection are characterized by innate immune responses that involve an influx of phagocytic cells, including resident alveolar macrophages and recruited neutrophils, to the lungs. Alveolar macrophages first phagocytose the bacteria. After the pathogens enter the airway and the lung parenchyma they are being taken up by macrophages, neutrophils and dendritic cells (DCs).

Macrophages and neutrophils are generally considered to be the first lines of defense against pathogen invasion. They express antimicrobial peptides as well as the property of several other antimicrobial factors. Activation of the adaptive immune response occurs after the spread of *M. tuberculosis* throughout the lymphatic system. In the lymph nodes, the presentation of bacterial antigens by DCs results in the priming and expansion of antigen-specific T cells. This stimulation promotes the differentiation of T cells from naïve T cells into effector T cells. The effector T cells migrate to the infected lung, interact with other leukocytes, and stimulate the formation of granulomas, organized structures that wrap mycobacteria with macrophages, lymphocytes, and fibroblasts (Figure 2A).

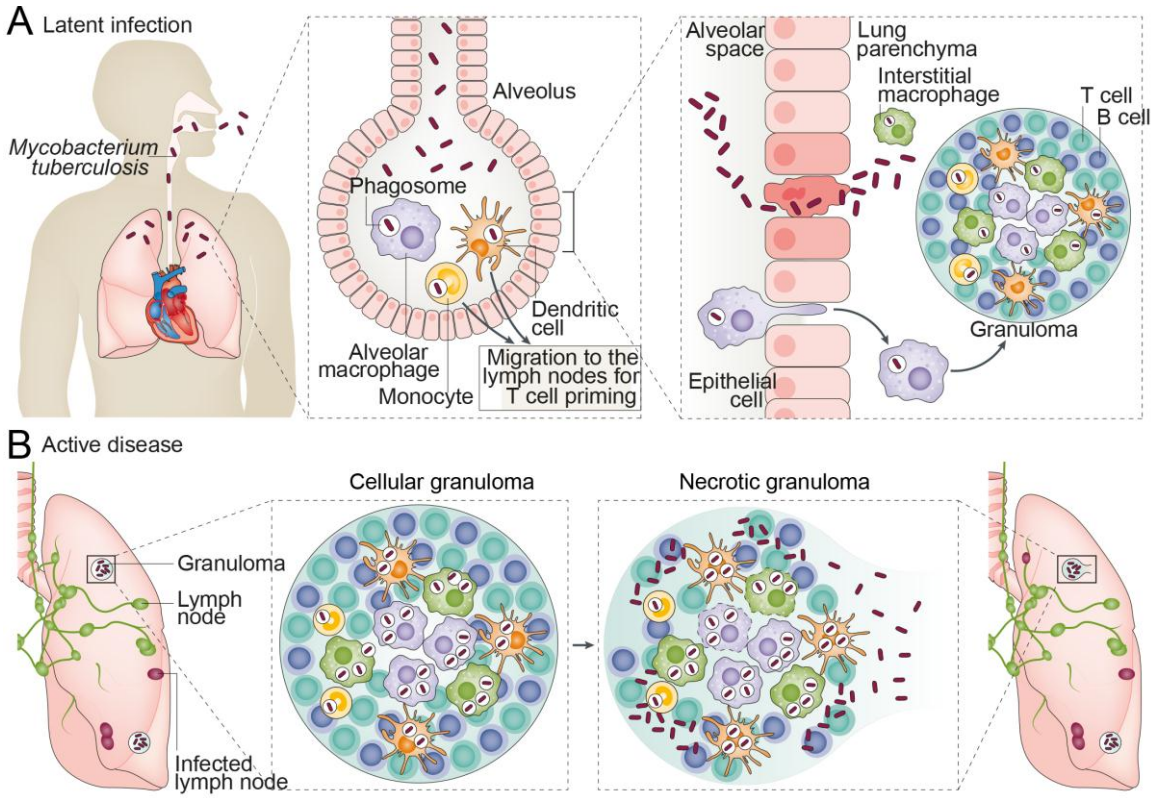

Figure 2. Pathogenesis of *Mycobacterium tuberculosis* infection.
(A) The infection starts with the inhalation of mycobacteria-containing droplets which enter the lungs, reach the alveolar space and encounter the resident alveolar macrophages. When the alveolar macrophages fail to eliminate the bacteria, the pathogen invades the alveolar epithelium or infect the lung parenchyma. Afterward, the bacteria are transported by either dendritic cells or monocytes to lymph nodes and subsequently activate T cells which leads to the successive activation of immune cells and finally the formation of granuloma. (**B)** Mycobacteria can survive and replicate within a granuloma. If a granuloma is overloaded with bacteria, it fails to control the infection and becomes necrotic. The overgrowth of bacteria eventually leads to the breakdown of granuloma, the entrance of bacteria into the respiratory tract or even bloodstream, and the infection of other organs with mycobacteria, such as liver, spleen and even brain. This step of the infection is considered as active TB disease with typical TB symptoms. Adapted from Pai et al., 2016.

Within the granulomas, the differentiated T-helper (Th) cells produce interferon-γ (IFN-γ), which leads to the activation of macrophages, the production of cytokines, the induction of microbicidal factors such as inducible nitric oxide synthase (iNOS), and thereby to the control of the bacteria (Nunes-Alves et al., 2014). Extrinsic innate immune factors, together with adaptive immune factors determine the outcome of the subsequent immune response: clearance or persistence of the pathogen. The reactions of macrophages and neutrophils finally result in ongoing latent infection or the development of active disease (Figure 2). When macrophages fail to control bacteria and mycobacteria over grow within granuloma, the bacteria are released into

the respiratory tract or the bloodstream, subsequently leading to the infection of other organs (Figure 2B).

1.4 Mycobacteria-induced granuloma

A mycobacteria-induced granuloma is a bacteria-containing, compact and organized immune cell aggregate which illustrates the dual character of *M. tuberculosis* infection (Figure 2B) (Pai et al., 2016). For the host, the granuloma is like a prison for the bacterium which limits the infection in a particular area. However, for the bacterium, the granuloma is a growing aggregate of phagocytic cells to infect and to replicate within.

A granuloma originates from an organized aggregate of macrophages, including mature macrophages, differentiated or epithelioid macrophages, foamy macrophages, and multinucleated (or Langhans) giant cells (MGCs) (Adams, 1976). These macrophages form a granuloma by fusing with each other with the plasma membranes but not the nuclei (Puissegur et al., 2007).

Real-time observations of granuloma formation by using *M. marinum* infected zebrafish embryos revealed that granulomas can be initiated with macrophages alone since the used embryos were at a stage before T lymphocytes were formed (Davis et al., 2002). Accordingly, utilization of human peripheral blood cells and *M. tuberculosis* demonstrated that macrophages are sufficient for the early stages of granulomas and MGC formation (Puissegur et al., 2004).

Puissegur and colleagues identified the molecular mediator of MGC formation. Specific mycobacterial glycolipids, such as lipomannan (LM), phosphatidylinositol mannosides (PIM), and trehalose dimycolate (TDM), promote MGC formation. These glycolipids exist on the exterior of the pathogen. LM induced MGC formation requires the host pattern-recognition molecule Toll-like receptor 2 (TLR2) and follows the β1-integrin expression as well as the expression of a disintegrin and metalloproteinase domain-containing protein 9 (ADAM9) (Puissegur et al., 2007). These MGCs exhibit a rather low efficiency in phagocytosis but express high levels of major histocompatibility complex (MHC) class II molecules (Lay et al., 2007).

Another type of macrophage which draws attention is the foamy macrophage. Foamy macrophages are lipid-rich macrophages which have been observed in granulomas and may be the cause of granuloma necrosis (Peyron et al., 2008). The center of the necrotic granulomas becomes caseous during active disease and contains necrotic macrophages which, in advanced TB, form cavities in the lung. Spillage of infectious bacteria into the airways occurs when the structure ruptures, allowing the spread of the bacteria to new hosts (Dheda et al., 2010; Nunes-Alves et al., 2014).

It has been demonstrated that *M. tuberculosis* uses the lipids within foamy macrophages as carbon and energy sources (Pandey and Sassetti, 2008) and that *M. tuberculosis*-containing phagosomes are adjacent to lipid bodies in cultured macrophages (Peyron et al., 2008). *In vitro* studies demonstrate that mycobacteria can induce the differentiation of human blood monocytes into foamy macrophages (Peyron et al., 2008). Mycobacteria stimulate as well as murine macrophages to differentiate into foamy cells through the involvement of TLR2 (D'Avila et al., 2006).

A recent study revealed an unexpected role of epithelioid macrophages within granulomas. Cronan and colleagues showed that in the *M. marinum* infected zebrafish model, granuloma macrophages were reprogrammed by macrophage-induced epithelial modules resulting in the formation of adherent junctions between single macrophages. These cells expressed macrophage markers and epithelial cells marker such as E-cadherin. The epithelial layer serves as a barrier for other immune cells and facilitates bacterial survival, and the disorganization of granuloma by disruption of cadherin-adhesion leads to a decreased bacterial burden and thereby increasing host survival (Cronan et al., 2016).

Apart from various phenotypes of macrophages, granulomas also contain dendritic cells (DCs), T cells and B cells. DCs can migrate from peripheral tissues to lymph nodes and present antigens to T cells (Briken et al., 2004; Maglione et al., 2007; Tailleux et al., 2003; Wolf et al., 2008). Although not essential for granuloma initiation, T cells have been shown to reside in the periphery of mature granulomas and contribute to the maintenance of granulomas structure (Egen et al., 2008; Randhawa, 1990; Tsai et al., 2006). Granulomas also contain B cells, but their function is still undefined (Maglione et al., 2007).

Therefore, studies of the mechanisms related to the initiation and maintenance of granulomas are essential to understanding how granulomas are involved in both killing and persistence of the pathogen (Lin et al., 2014).

1.5 Anti-mycobacterial mechanisms of macrophages

As facultative intracellular bacteria, mycobacteria prefer to infect and persist within macrophages, which are their favorite niche. Macrophages can ingest and eliminate pathogens by a complex process called phagocytosis, which is also crucial for elimination of apoptotic cells and for maintaining tissue homeostasis (Lim et al., 2017; Rosales and Uribe-Querol, 2017). Therefore, macrophages represent a unique battlefield between the host and the pathogen.

1.5.1 Phagosome formation

Phagocytosis starts with the recognition and ingestion of bacteria into a plasma-membrane derived vesicle, called phagosome. Cellular receptors achieve bacterial uptake in a direct way which can recognize pathogen-associated molecular patterns (PAMPs) on the surface of the microorganisms, or an indirect way which is mediated by opsonin (Flannagan et al., 2009; Flannagan et al., 2012). Opsonins are host factors which can attach to the pathogen's surface and can be recognized by phagocytic receptors such as Fcγ receptors and complement receptor 3 (CR3). These receptors trigger various signaling pathways followed by remodeling of actin and subsequent engulfment of pathogens and formation of phagosomes (Flannagan et al., 2009).

Numerous receptors expressed in phagocytic cells have been discovered to bind mycobacterial ligands, including C-type lectin receptors (CLRs), scavenger receptors (SRs), and complement receptors (CRs) (Table 1) (Philips and Ernst, 2012).

Table 1. Receptors implicated in *Mycobacterium tuberculosis* uptake in phagocytic cells.

Recptor	*M. tuberculosis* ligand(s)	Comment
Nonopsonic		
C-type lectin (transmembrane)		
Mannose receptor (CD207)	ManLAM, PIMs, arabinomannan, mannoproteins	Thought to be anti-inflammatory and to inhibit delivery of mycobacteria to the lysosome
DC-SIGN (CD209)	ManLAM, PIMs, arabinomannan, lipomannan, 19-kD antigen	Major uptake receptor in human DCs, thought to anti-inflammatory and inhibit DC maturation. There are seven paralogs in mice (SIGNR1-5, SIGNR7, SIGNR8)
Dectin-1	Unknown	Recognizes fungal β-glucan in cooperation with TLR2, *M. tuberculosis* ligand is unknown
Integrin family		
Complement receptor 3 (CD11b/CD18)	LAM, PIMs, antigen 85C	Has a lectin domain and mediates opsonic and nonopsonic uptake of *M. tuberculosis*
SRs		
Class A (SR-A1, MARCO) Class B (CD36, SR-B1)	Unknown	SRs display broad ligand-binding ability; ligands include lipoprotein, polyanionic molecules, gram-positive and gram-negative bacteria
Opsonic		
CRs		
CR1, CR3 (CD11b/CD18)	Host iC3b	CR3 is the major complement receptor involved in complement-opsonized *M. tuberculosis* uptake; *M. tuberculosis* activates the alternative complement pathway and is opsonized by C3b and iC3b
Collections (soluble C-type lectins)		
Surfactant protein A	ManLAM; lipomannan, a 60-kD glycoprotein; the glycoprotein Apa	Aggultinates *M. tuberculosis* and enhances macrophage internalization
Surfactant protein D	ManLAM	Aggultinizes *M. tuberculosis* and delays macrophage phagocytosis
Mannose-binding lectin	ManLAM, PIMs	Human studies suggest that low levels confer protection from tuberculosis
Fc receptor		
FcγR	Host IgG	Uptake through Fc receptors may direct *M. tuberculosis* to the lysosome

Abbreviations: DC, dendritic cell; IgG, immunoglobulin G; LAM, lipoarabinomannan; ManLAM, mannose-capped lipoarabinomannan; PIM, phosphatidylinositol mannan; SR, scavenger receptor; TLR, Toll-like receptor. Adapted from Philips and Ernst, 2012.

1.5.2 Phagosome maturation

Once the newly formed phagocytic cup is formed, the phagosome must undergo radical fusion and fission events with vesicles of the endocytic compartment to finally become a matured phagosome. The interactions between phagosomes and endosomes are transient with limited exchanges of contents and membranes (Levin et

al., 2016). The ultimate microbicidal structure, phagolysosomes, are formed after phagosomes fuse with lysosomes (Figure 3) (Uribe-Querol and Rosales, 2017).

The maturation starts when the phagosome fuses with an early endosome. The pH of the phagosome drops down from 7.4 to 6.1-6.5 by the acquisition of additional proton pumps, vacuolar-ATPases (V-ATPase) on its membrane (Kinchen and Ravichandran, 2008; Marshansky and Futai, 2008). Typical markers of an early phagosome include the small GTPase Rab5 (Gutierrez, 2013; Kitano et al., 2008), early endosome antigen 1 (EEA1) (Christoforidis et al., 1999), and the class III phosphoinositide 3-kinase (PI-3K) human vacuolar protein-sorting 34 (hvPS34) (Vieira et al., 2001).

Subsequently, the early phagosome matures into a late phagosome which is characterized by the presence of the small GTPase Rab7 (Rink et al., 2005; Vieira et al., 2003). Compared to the early phagosomes, the pH of the late phagosome is 5.5-6.0. The drop in pH within the phagosome is due to the acquisition of more V-ATPase molecules on its membrane. During this process, some proteins are no more necessary for the maturation of phagosome. Therefore, these proteins are separated in sorting (recycling) vesicles. Some transmembrane proteins which should be degraded are separated from intraluminal vesicles (ILVs) and directed into the lumen of the phagosome (Hanson et al., 2008). Lysosomal-associated membrane proteins (LAMPs) are a family of glycosylated proteins that accumulate on the lysosomal membrane and are required for fusion of lysosomes with phagosomes (Canton, 2014; Fairn and Grinstein, 2012; Huynh et al., 2007) (Figure 3).

The final microbicidal organelles, phagolysosomes, contain many degradative enzymes and are formed when late phagosomes fuse with lysosomes which are acidic (pH 5–5.5) (Bright et al., 2005; Pryor and Luzio, 2009). The various degradative enzymes, such as cathepsins, proteases, lysozymes, and lipases, are responsible for eliminating invading microorganisms. Phagolysosomes also acquire other scavenger molecules, thereby facilitating bacterial killing. These molecules include lactoferrin that sequesters iron which is required by some bacteria, and the nicotinamide adenine dinucleotide phosphate (NADPH) oxidase that generates superoxide, and other reactive oxygen species (ROS) (Masson et al., 1969; Minakami and Sumimotoa, 2006) (Figure3).

Numerous mycobacterial lipids and protein effectors have been reported to modulate the phagosome maturation (Philips, 2008). Mycobacteria have been demonstrated to arrest Rab5 positive phagosomes by blocking the fusion of the late endosomes with phagosomes (Vergne et al., 2005). The failure of the phagosome maturation is mediated by the expression of numerous bacterial effector proteins (e.g., secreted acid phosphatase SapM and a serine/threonine kinase PknG) and lipids (e.g., LAM) in mycobacteria (Philips, 2008).

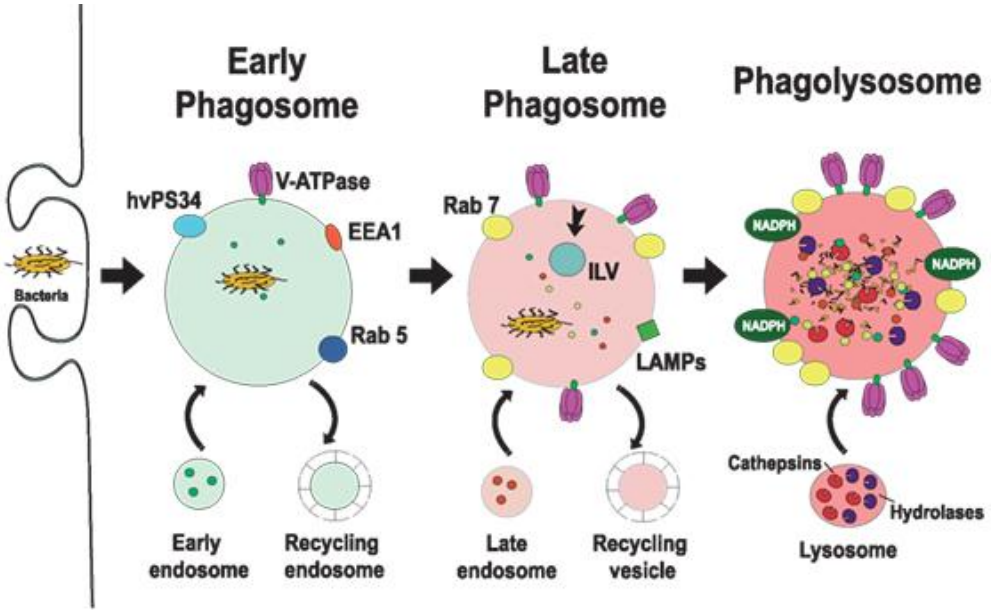

Figure 3. Phagosome maturation.
The scheme describes a typical process of phagosome maturation. The maturation of phagosome is a series of fusion and fission events. The early phagosome is mildly acidic (pH 6.1-6.5) and marked by the surface proteins of early endosomes, such as the small GTPase Rab5, early endosome antigen 1 (EEA1), and the class III PI-3K human vacuolar protein-sorting 34 (hvPS34). The late phagosome is more acid (pH 5.5-6.0) and marked with Rab7 and lysosomal-associated membrane proteins (LAMPs). Sorting (recycling) vesicles contain proteins to be recycled, while intraluminal vesicles (ILVs) collect proteins intended to be eliminated. Phagolysosomes are finally formed when late phagosomes fuse with lysosomes, and the pH of phagolysosomes turns into 5-5.5. Phagolysosomes contain many degradative enzymes and microbicidal components, such as various cathepsins, proteases, lysozymes, lipases and reactive oxygen species (ROS) generated by the NADPH oxidase. Adapted from Uribe-Querol and Rosales et al., 2017.

1.5.3 ROS and mycobacteria

The generation of ROS is one of the primary defense mechanisms used by the host's immune systems upon bacterial infection. ROS is mainly generated by the inducible nitric oxide synthase (iNOS) pathways, which is controlled by the activity of the NADPH

oxidase, and affected by NO. This system is one of the most critical antimicrobial systems of phagocytic cells (Fang, 2011). The NADPH oxidases are a family of enzymes which are specialized uniquely to produce ROS. One of the most well-known NADPH oxidases is Nox2. The catalytic center of Nox2 is gp91^{phox}, a transmembrane glycoprotein (Babior et al., 2002; Bedard and Krause, 2007). It forms a heterodimer together with another much smaller subunit is the transmembrane protein, p22^{phox} (Figure 4) (McCann and Roulston, 2013).

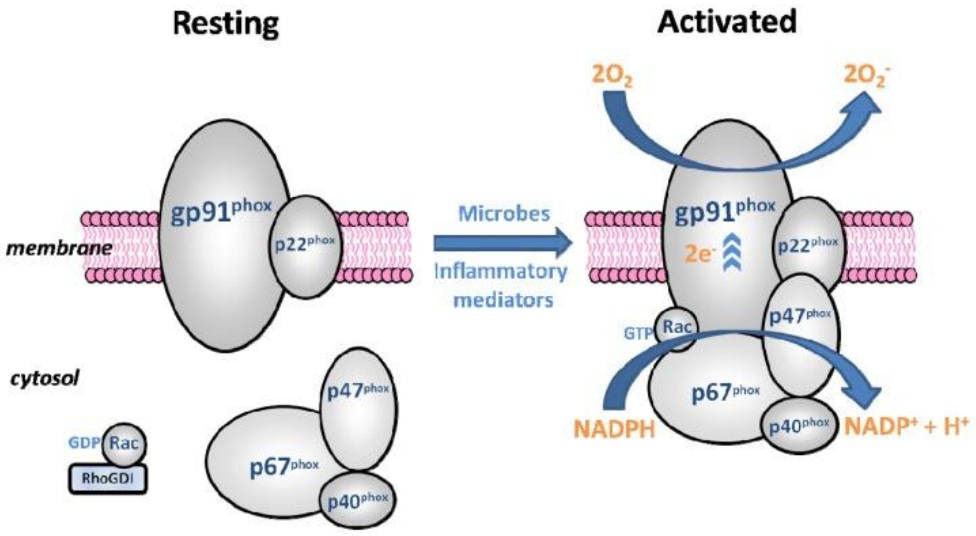

Figure 4. The resting and activated forms of the NADPH oxidase.
NADPH oxidase is consist of two transmembrane subunits and several cytosolic subunits. The transmembrane heterodimer contains gp91^{phox} and p22^{phox}, and the cytosolic subunits include p67^{phox,} p47^{phox}, p40^{phox} and Rac. The NADPH oxidase is activated when the cytosolic subunits bind to the transmembrane heterodimer. The activated NADPH oxidase generates reactive oxygen species by accepting electrons from cytosolic NADPH and transfers it to molecular oxygen. Adapted from McCann and Roulston, 2013.

The heterodimer is a central component of the NADPH oxidase and locates on the membrane. Four cytosolic components, p47^{phox}, p67^{phox}, p40^{phox,} and the small G-protein Rac1 or Rac2, also belong to the complex. The spatial segregation of these essential components defines the activity of the enzyme. In resting cells, the enzyme is dissociated. However, it rapidly assembles upon activation by exposure to microbes or inflammatory mediators. Upon activation, the 3 cytosolic components, p47^{phox}, p67^{phox} and p40^{phox} translocate to the membrane, docking to the gp91^{phox}-p22^{phox} heterodimer. Subsequently, GDP-bound Rac1, which is stabilized by RhoGDI, converts to a GTP-bound active form. GTP-Rac1 translocates to the membrane complex after its assembly; the NADPH oxidase generates the ROS superoxide (O_2^-)

by accepting electrons (e^-) from cytoplasmic NADPH and donating them to molecular oxygen (O_2) (Bedard and Krause, 2007; McCann and Roulston, 2013).

M. tuberculosis, like other bacterial species, has developed strategies to detect redox signals (such as O_2, NO, and CO) and to alter intracellular and extracellular redox states (Singh et al., 2007).

Recent research focused on the contribution of ROS to pro-inflammatory signaling in macrophages rather than on their direct microbicidal activity (Slauch, 2011). *M. tuberculosis* has been shown to downregulate both the production of ROS and the generation of pro-inflammatory cytokines in macrophages. NADPH oxidase-derived ROS mediate the TLR2 inflammatory responses that contribute to the clearance of *M. tuberculosis* via the enhancement of vitamin D receptor-induced cathelicidin expression in macrophages (Yang et al., 2009).

Additional studies showed that a subunit of type I nicotinamide adenine dinucleotide (NADH) dehydrogenase (NDH-1) of mycobacteria is essential for its virulence (Miller et al., 2010). NDH-1 can inhibit tumor necrosis factor (TNF)-induced macrophage apoptosis by neutralizing Nox2-derived ROS (Miller et al., 2010). The genetic deletion of NDH-1 in *M. tuberculosis* leads to the increased ROS in the phagosome, elevated TNF-α secretion, and apoptosis. These findings indicate that ROS are involved in the redox signaling pathway of apoptosis downstream of TNF, and in this case, ROS act as a defense by inducing host-cell apoptosis, which facilitates the elimination of microbes (Miller et al., 2010).

However, bacteria can escape this innate mechanism. In zebrafish model, TNF-induced ROS have been shown to participate in both, on the one hand in the elimination of *M. marinum*, on the other hand in triggering the infection, depending on the level of ROS (Roca and Ramakrishnan, 2013). Low quantities of ROS have been shown to be microbicidal and to contribute in control of the growth of the bacteria *M. marinum*, whereas high amounts induce necroptosis and release of bacteria into the surrounding microenvironment. This activity favors bacterial extracellular proliferation.

Recent studies have shown that ROS is a vital factor favoring foam-cell formation by inhibiting cholesterol efflux (Tavakoli and Asmis, 2012). This may be involved in the

differentiation of macrophages into foam cells, which is induced by *M. tuberculosis* allowing the bacteria to survive and replicate inside the host (Singh et al., 2012).

1.6 Ceramide and sphingomyelinases

Ceramide is a bioactive lipid, belonging to the class of sphingolipids. Sphingolipids are simple as well as complex lipids which contain 18-carbon amino-alcohol backbones. They are synthesized in the endoplasmic reticulum (ER) from nonsphingolipid precursors. Sphingolipid metabolism has a unique entry and exit point. The pathway of sphingolipid metabolism starts with serine palmitoyltransferase (SPT) and ends with the breakdown of sphingosine-1-phosphate (S1P) into non-sphingolipid molecules by S1P lyase (Hannun and Obeid, 2008).

1.6.1 Metabolism of ceramide

Ceramide can be formed by *de novo* synthesis, the salvage pathway or from sphingomyelin via the action of sphingomyelinases. Briefly, in the de novo synthesis, serine and palmitate are condensed to 3-keto-dihydrosphingosine by SPT (Linn et al., 2001). 3-keto-dihydrosphingosine is reduced to dihydrosphingosine and acylated into dihydroceramide by the dihydro-ceramide synthase (Pewzner-Jung et al., 2006). The desaturation of dihydroceramide forms ceramide by insertion of a double bond into the sphingoid backbone (Causeret et al., 2000). The generation of ceramide from sphingomyelin is catalyzed by one of three different sphingomyelinases which are classified according to their optimal pH of activity. These include acid sphingomyelinase, neutral sphingomyelinase and alkaline sphingomyelinase (Marchesini and Hannun, 2004).

Once synthesized, ceramide can be converted to other interconnected bioactive lipid species. In sphingolipid biosynthetic pathways (Figure 5) (Hannun and Obeid, 2008), ceramide can be phosphorylated by ceramide kinase, deacylated to generate sphingosine, glycosylated by glucosyl- or galactosylceramide synthase, or can receive a phosphocholine headgroup from phosphatidylcholine (PC) to generate sphingomyelin (Raas-Rothschild et al., 2004; Tafesse et al., 2006; Wijesinghe et al., 2005).

Ceramide can be cleaved ceramidases, leading to the formation of sphingosine (Galadari et al., 2006; Xu et al., 2006).

Sphingosine can be either salvaged into the sphingolipid pathways or is phosphorylated by sphingosine kinases to form S1P (Hait et al., 2006). S1P can be either dephosphorylated to regenerate sphingosine through S1P phosphatases or irreversibly cleaved by S1P lyase to generate ethanolamine phosphate and hexadecenal (Bandhuvula and Saba, 2007).

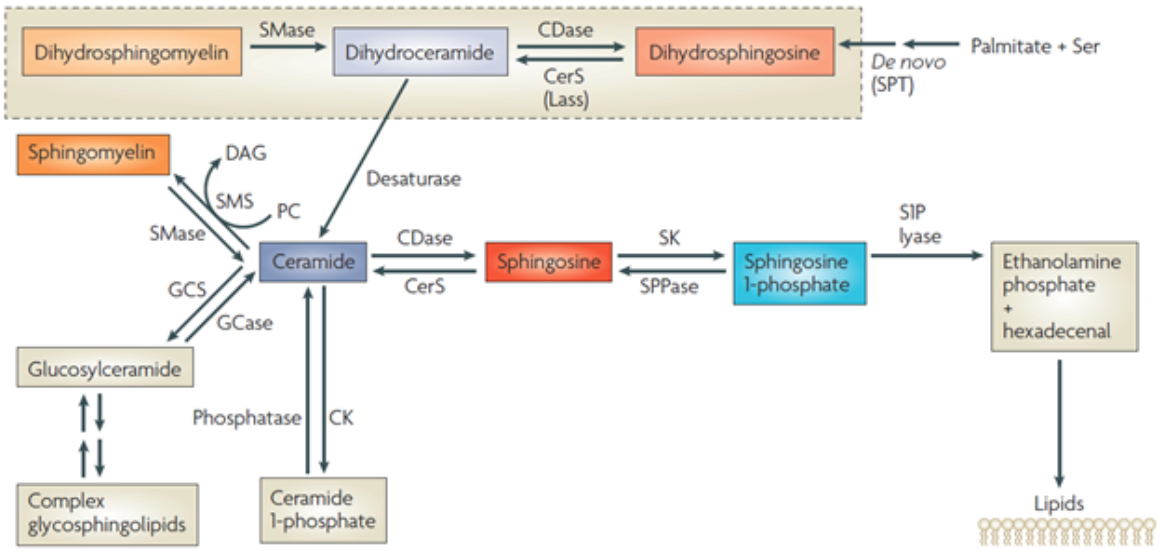

Figure 5. Sphingolipid metabolism and interconnection of bioactive sphingolipids. CDase, ceramidase; CK, ceramide kinase; DAG, diacylglycerol; GCase, glucosylceramidase; GCS, glucosylceramide synthase; PC, phosphatidylcholine; SK, sphingosine kinase; SMase, sphingomyelinase; SMS, sphingomyelin synthase; SPPase, sphingosine phosphate phosphatase; SPT, serine palmitoyltransferase. Adapted from Hannun and Obeid, 2008.

Of all sphingolipids, sphingosine, S1P, and ceramide are in focus because of their bioactivity. They have been shown to play roles in regulating the actin cytoskeleton, endocytosis, the cell cycle, apoptosis and various other cellular processes (Hannun and Obeid, 2008).

1.6.2 Bioactivity of ceramide

Ceramide plays an important role in modulating the biophysical properties of membranes and is involved in various cellular processes, such as apoptosis, inflammation, endocytosis, as well as in several infectious diseases (Grassme et al., 1997; Schutze et al., 1992; Schwandner et al., 1998; Venable et al., 1995).

Various types of stimulation can activate sphingomyelinases to generate ceramide from sphingomyelin, including cytokines, and viral or bacterial infections (see section 2.6), death receptor ligands, differentiation agents, and anti-cancer drugs (Carpinteiro et al., 2015; Cremesti et al., 2002; Grassme et al., 1997; Gulbins and Li, 2006; Zhang et al., 2009). The generation and further accumulation of ceramide within cellular membranes lead to the formation of ceramide-enriched domains in the plasma membranes (Cremesti et al., 2002; Grassme et al., 2001).

As all membrane lipids, ceramide contains both a hydrophobic and a hydrophilic part. The interactions among ceramide molecules occur between both parts. On the one hand, the hydrophobic tails interact with the hydrophobic tails of other ceramide molecules and with cholesterol via van der Waals interactions; and on the other hand, the polar heads interact with each other via hydrophilic forces (hydrogen bonds). These interactions result in the accumulation of ceramide molecules.

The ceramide enriched-domains are reported to sort proteins and to provide platforms for the spatial recruitment of receptors and intracellular signaling molecules upon various stimuli (Grassme et al., 2007; Zhang et al., 2009). These domains serve the reorganization and clustering of receptor molecules, including CD95, CD40, CD20, FcγRII, CD28, TNF, TNF-related apoptosis-inducing ligand and β1-integrin (Abdel Shakor et al., 2004; Bezombes et al., 2004; Boucher et al., 1995; Carpinteiro et al., 2015; Dumitru et al., 2007; Garcia-Ruiz et al., 2003; Grassme et al., 2017; Grassme et al., 2001; Grassme et al., 2002; Schutze et al., 1992). The clustered molecules, in turn, lead to amplified downstream signaling, the exclusion of inhibitory molecules, the conformational changes of receptors, and the stabilization of receptor-ligand interactions (Grassme et al., 2017; Grassme et al., 2007).

Many studies have shown that the sphingomyelinase/ceramide system plays an important role in infectious biology. Ceramides modify in the interaction of pathogens with host receptors, receptor clustering, and intracellular signaling molecules (Grassme et al., 2007). Several studies have demonstrated the participation of ceramide during the interaction between the host and specific pathogens, i.e., *Neisseria gonorrhoeae* (*N. gonorrhoeae*), *Pseudomonas aeruginosa* (*P. aeruginosa*), *Staphylococcus aureus* (*S. aureus*), and several viruses (see section 1.7).

In summary, ceramide and ceramide-enriched membrane domains are central molecules and motifs in reorganizing the topology of a given signalosome, thus permitting the transmission of pathogen-induced signals into the cell.

1.6.3 Acid sphingomyelinase

The Asm is encoded by the *Smpd1* gene, which is an endo-lysosomal protein of 629 amino acids (da Veiga Pereira et al., 1991; Marathe et al., 1998; Schuchman et al., 1992). Gatt and colleagues, in 1963, first described that Asm is a hydrolase, active at acidic pH of 4.5-5.5. Asm-encoding gene contains six exons and five introns, and it is 5 to 6 kb long and is localized on chromosome 11p15.1–11p15.4 (Schuchman et al., 1992). Human ASM cDNA encodes a 629 amino acids polypeptide, and it shares approximately 82% identities of amino acids with mouse Asm.

There are three main domains in the Asm: the N-terminal saposin domain, the proline-rich connector, and the catalytic domain (Figure 6A) (Gorelik et al., 2016). The Asm has two distinct conformations: a closed conformation and an open conformation in which the N-terminal saposin domain changes its fold and position relative to the catalytic domain (Gorelik et al., 2016). At the end of the catalytic domain, the Asm possesses an additional C-terminal subdomain (CTD). The CTD consists of four α-helices that pack against the core, which distinguishes the Asm from most other phosphodiesterases.

A linker connects the catalytic domain and the saposin domain of the Asm. The linker wraps itself around the catalytic domain as an L-shaped strap (Figure 6B). These elements form a spherical domain. In the center of the spherical domain, two zinc ions reside. A phosphate ion is bound to the active site in the catalytic domain of Asm and, thus, mediates several interactions with the protein and zinc ions. Additionally, His317 and His280, which are located near the bound phosphate, are potential proton donors and involved in the release of ceramide (Figure 6C) (Gorelik et al., 2016).

The signal peptide targets the Asm to the endoplasmatic reticulum where the enzyme is further glycosylated. The Asm is then destined for cellular trafficking: dependent from their location, the lysosomal Asm (L-Asm) and the secretory Asm (S-Asm) are distinguished (Hurwitz et al., 1994; Schissel et al., 1998). Qiu et al. reported a “cysteine switch” controls the activity of Asm (Qiu et al., 2003). The C-terminal cysteine residue

is cleaved in L-Asm. The loss of the C-terminal cysteine residue in L-Asm favors the hydration of zinc ions and enhance the L-Asm activity. The S-Asm still contains this cysteine which enables oxidation-driven dimerization for full activation (Jenkins et al., 2011; Qiu et al., 2003).

Asm deficiency results in the accumulation of sphingomyelin and causes lysosomal storage diseases: a fatal neuropathic and visceral disease, Niemann-Pick type A; and a visceral anomalies disease, Niemann-Pick type B (Takahashi et al., 1992).

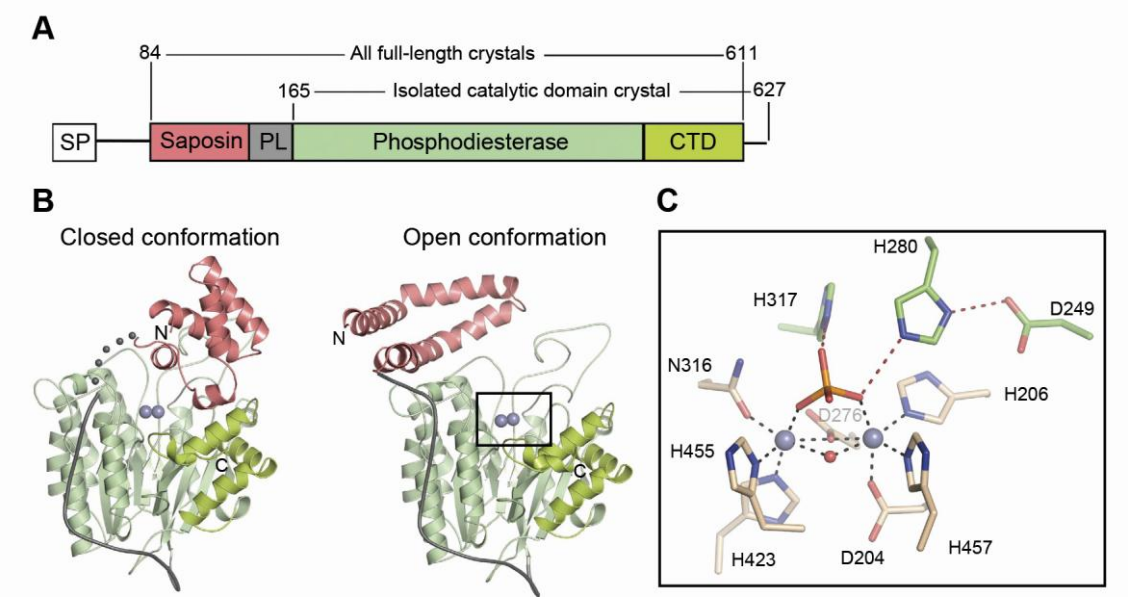

Figure 6. Structural overview of acid sphingomyelinase.
(A) Domain organization of acid sphingomyelinase (Asm). SP, signal peptide; PL, proline-rich linker. **(B)** Closed and open Asm colored as in **(A)**. Consecutive grey spheres indicate the disordered linker between the saposin domain and the catalytic center of the Asm. **(C)** The boxed region magnified in c shows the active site of the Asm. Glycans are omitted for clarity. Zincs are indicated as purple spheres. The interactions between zinc and amino acid residues are shown with dashes. The phosphate group is colored in orange and red. Shown are zinc-interacting residues (beige) and residues which are important for the protonation of leaving groups and substrate binding (green). CTD domain, C-terminal domain. Adapted from Gorelik et al., 2016.

1.6.4 Neutral sphingomyelinase

The genes *Smpd2* to *Smpd5* encode different isoforms of NSms which are translated into, namely, Nsm1, Nsm2, Nsm3, and mitochondria-associated sphingomyelinases (MA-SMase) (Hofmann et al., 2000). Nsm2 was first found in the spleen of patients with Niemann-Pick disease and was described as a hydrolase functioning like Asm but with a neutral pH and a Mg^{2+}-dependent conformation (Clarke et al., 2007; Hofmann

et al., 2000; Schneider and Kennedy, 1967). Amongst four separate mammalian neutral SMases, Nsm2 appears to be the most predominant and best characterized Nsm in cellular systems, physiologies, and pathologies (Goni and Alonso, 2002; Shamseddine et al., 2015; Tonnetti et al., 1999). The Nsm mentioned here on refers to the Nsm2.

Both the human NSM gene (*SMPD3*) and the mouse Nsm gene (*Smpd3*) encode for a 655-amino acid protein. The mouse Nsm and human NSM are very similar and share 90% sequence identity (Hofmann et al., 2000). The molecular weight of NSM and Nsm are both 71 kDa, and their optimal working pH is neutral. This protein is expressed mainly in brain tissues. Its N-terminal region contains two hydrophobic segments while its C-terminal region includes the catalytic domain (Figure 7) (Shamseddine et al., 2015; Wu et al., 2017).

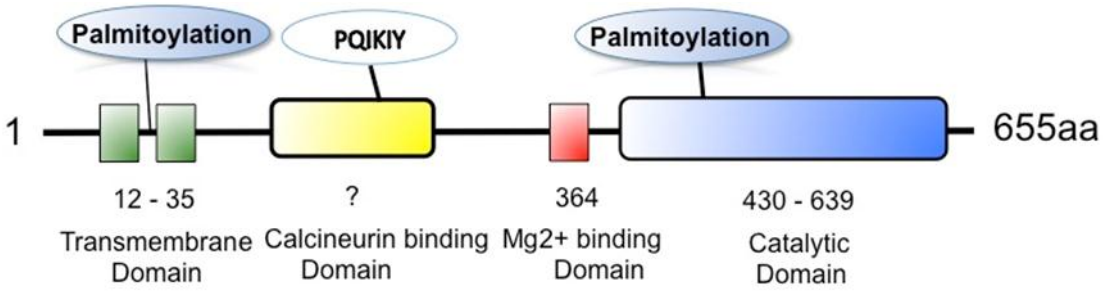

Figure 7. Domain architecture of neutral sphingomyelinase.
Catalytic domain, blue; Hydrophobic segments 1 and 2, green; Calcineurin binding motif, yellow; and palmitoylation sites are indicated. Numbers indicate the amino acid residues involved in the designated domains. Adapted from Wu et al., 2017.

The Nsm hydrolyzes the phosphocholine head group of sphingomyelin explicitly, thereby generating ceramide. Hofmann et al. showed that both neutral pH and divalent cations (Mg^{2+} or Mn^{2+}) are necessary for the activity of the Nsm. However, the deacylated form of sphingomyelin, sphingosylphosphocholine, can be hydrolyzed by Nsm without detergent (Miura et al., 2004).

Unlike the Asm, the Nsm is believed to reside in the cytosolic leaflet of either Golgi bodies or the plasma membrane, and its association with the plasma membrane depends on the palmitoylation of the enzyme on its cysteine residues (Tani and Hannun, 2007). The phosphorylation of the Nsm upon stimulation with H_2O_2 occurs on five conserved serine residues located near the calcineurin binding site. To de-phosphorylate Nsm, calcineurin binds a PQIKIY motif (Figure 7) (Filosto et al., 2012;

Shamseddine et al., 2015). Also, yeast two-hybrid interaction mapping suggested that polycomb protein embryonic ectoderm development (EED) is a binding partner of the Nsm via its C-terminus (Philipp et al., 2010).

1.7 Sphingomyelinases and infection

1.7.1 Asm and infection

Over the last decades, dozens of studies have been describing the role of the Asm/ceramide system in infection with several pathogens, such as *N. gonorrhoeae*, *S. aureus*, *P. aeruginosa*, *Listeria monocytogenes (L. monocytogenes)*, *Salmonella enterica* serovar typhimurium (*S. tryphimurium*), *Escherichia coli (E. coli),* and pathogenic mycobacteria (Table 2) (Avota et al., 2011; Becker et al., 2012; Dreschers et al., 2007; Esen et al., 2001; Falcone et al., 2004; Gassert et al., 2009; Gluschko et al., 2018; Grassme et al., 1997; Grassme et al., 2017; Grassme et al., 2003; Grassme et al., 2005; Hauck et al., 2000; Hedlund et al., 1998; Li et al., 2017; Luisoni et al., 2015; Ma et al., 2017; McCollister et al., 2007; Miller et al., 2012; Nakatsuji et al., 2011; Peng et al., 2015; Roca and Ramakrishnan, 2013; Schramm et al., 2008; Simonis et al., 2014; Teichgraber et al., 2008; Utermohlen et al., 2008; Utermohlen et al., 2003; Vazquez et al., 2016; Yu et al., 2009; Zhang et al., 2008; Zhang et al., 2010).

The first study to report a role of Asm/ceramide in infection was performed with *N. gonorrhoeae*-infected epithelial cells. This study revealed that Asm is crucial for the invasion of the pathogen into epithelial cells and fibroblasts (Grassme et al., 1997). Pharmacological inhibition of the Asm by imipramine prevented the invasion of *N. gonorrhoeae* into epithelial cells. Additionally, Asm-deficient fibroblasts obtained from patients with Niemann-Pick disease type A, who lack acid sphingomyelinase did not internalize gonococci. Transfection of Asm restored the uptake of *N. gonorrhoeae* by these fibroblasts (Grassme et al., 1997; Simonis et al., 2014). Another study demonstrated that the ASM/ceramide system is necessary for the uptake of *N. gonorrhoeae* into human phagocytes (Hauck et al., 2000). Pharmacological inhibition of the ASM prevents not only the bacterial internalization but also subsequent signaling activations, i.e., the Src-like tyrosine kinases and JNK (Hauck et al., 2000).

P. aeruginosa is one of the best-investigated pathogens in the context of the interaction between Asm and microorganisms. In infected epithelial cells and fibroblasts, the Asm is activated and translocated to the extracellular leaflet of the plasma membrane and stimulates the formation of ceramide-enriched platforms. The ceramide platforms promote bacterial internalization and killing, the induction of death of infected cells, and the controlled release of cytokines (Grassme et al., 2003; Teichgraber et al., 2008; Yu et al., 2009; Zhang et al., 2008; Zhang et al., 2010). Furthermore, a recent study shows that ceramide accumulation leads to downregulation of acid ceramidase and subsequent, depletion of sphingosine, thereby enhancing the bacteria susceptibility of cystic fibrosis mice to *P. aeuginosa* (Grassme et al., 2017).

Asm deficient mice have been shown to be highly susceptible to infection with *S. typhimurium*. Several investigators found that constitutive expression of Asm is important for the killing of *S. typhimurium* by macrophages, as indicated by the finding that Asm deficient macrophages were much less able to kill *S. typhimurium* than wild-type macrophages. These studies reveal that Asm deficient cells have a defect in the NADPH-mediated release of ROS (McCollister et al., 2007; Utermohlen et al., 2003). Additionally, Asm deficiency highly impairs the bactericidal ability of mice challenged with *L. monocytogenes* as well (Utermohlen et al., 2003). Recently, the same group showed that the Asm is linked to LC3B-associated phagocytosis upon *L. monocytogenes* infection (Gluschko et al., 2018).

For *S. aureus*, it has been shown, that the induction of endothelial cell apoptosis involved the activation of the Asm and a subsequent release of ceramide, which mediates the stimulation of cellular caspases and JNK and triggers the release of cytochrome C from mitochondria to the cytosol. Recent studies have shown that the Asm is also involved in inflammation induced by *Propionibacterium acnes* and several more pathogens (Ma et al., 2017; Nakatsuji et al., 2011). Studies investigating the Asm/ceramide system and pathogens are listed in Table 2 (Wu et al., 2017).

1.7.2 Nsm and infection

Nsm has been reported to be important in various cellular and pathological processes, such as circulatory and cardiac pathophysiology, neuropathology, Alzheimer disease, cancer, and bone development (Shamseddine et al., 2015). However, the role of Nsm in pathogen-host interactions has been barely studied.

Faulstich et al. showed that Nsm is necessary for PorB-dependent invasion of *N. gonorrhoeae* into epithelial cells (Faulstich et al., 2015). The invasion involves the Nsm-dependent recruitment of phosphatidylinositol-3-kinase (PI3K) to caveolin, thereby activating signaling events that mediate the invasion of bacteria (Faulstich et al., 2015). The Nsm/ceramide system, along with the Asm/ceramide system, has been reported to play a role in the uptake of measles viruses by DCs and as a microbial sensor (Avota et al., 2011). After binding the carbohydrate structures on the pathogen ligands to a specific dendritic adhesion molecule, both Asm and Nsm are transiently activated within several minutes (Avota et al., 2011) (Table 2) (Wu et al., 2017). Li et al. demonstrated that Nsm plays an important role in *M. bovis* BCG infection, both in macrophages and *in vivo* (Li et al., 2016) (see section 1.8).

Table 2. Pathogens and the acid or neutral sphingomyelinase/ceramide system.

Bacteria	References	Asm/ceramide or Nsm/ceramide-related mechanisms
Adenovirus	(Luisoni et al., 2015)	Asm is required for adenoviral endocytosis and escape of viruses from endosome to the cytoplasm.
Escherichia coli	(Falcone et al., 2004)	Asm plays a central role in *E. coli*-induced dendritic cells apoptosis.
	(Hedlund et al., 1998)	The binding of P-fimbriated *E. coli* to uroepithelial cells causes the activation of the ceramide signaling pathway and cytokine response in the epithelial cells.
Listeria mono-cytogenes	(Schramm et al., 2008)	Asm is required for the proper fusion of late phagosomes with lysosomes during infection with *L. monocytogenes*.
	(Utermohlen et al., 2003)	Asm is necessary for the intracellular control of *L. monocytogenes* in macrophages and granulocytes by nonoxidative mechanisms.
	(Utermohlen et al., 2008)	The phagolysosomal fusion in macrophages infected with *L. monocytogenes* requires the activity of the Asm.
	(Gluschko et al., 2018)	Asm is required for inducing LC3B associated phagocytosis in *L. monocytogenes* infected macrophages
Mycobacterium avium	(Utermohlen et al., 2008)	Asm is essential for the generation of multinucleated giant cells in granuloma of mice infected with *M. avium*.
Mycobacterium bovis BCG	(Li et al., 2016)	Inhibition of the Nsm increases autophagy expression upon BCG infection and thereby protects mice from BCG infection.
Mycobacterium marinum	(Roca and Ramakrishnan, 2013)	TNF-induced necroptosis occurs through Asm-mediated ceramide production in *M. marinum* infected zebrafish.
Mycobacterium tuberculosis	(Vazquez et al., 2016)	Phagosomal association of sortilin is critical for the delivery of Asm and required for efficient maturation of phagosome in *M. tuberculosis*-infected macrophages.
Measles virus	(Gassert et al., 2009)	MV causes ceramide accumulation in human T cells in a Nsm and Asm-dependent manner
	(Avota et al., 2011)	Nsm and Asm activation is important in promoting DC-SIGN signaling, but also for enhancement of MV uptake into dendritic cells.
Neisseria gonorrhoeae	(Hauck et al., 2000)	Phagocytosis of Opa-expressing *N. gonorrhoeae* by human granulocytes results in rapid activation of Asm.

	(Grassme et al., 1997)	The activation of Asm is an essential requirement for the entry of *N. gonorrhoeae* into human epithelial cells and fibroblasts.
	(Faulstich et al., 2015)	Nsm is necessary for PorB-dependent invasion of *N. gonorrhoeae* into epithelial cells
Neisseria meningitidis	(Simonis et al., 2014)	*N. meningitidis* causes transient activation of Asm followed by ceramide release in brain endothelial cells.
Pseudomonas aeruginosa	(Grassme et al., 2003)	*P. aeruginosa* infection triggers activation of the Asm and the release of ceramide in sphingolipid-rich rafts which are required to internalize *P. aeruginosa*, induce apoptosis and regulate the cytokine response in infected cells.
	(Zhang et al., 2008)	Ceramide-enriched membrane platforms are essential for amplification of Asm-mediated redox signaling, which mediates JNK activation and thereby apoptosis upon *P. aeruginosa* infection.
	(Zhang et al., 2010)	*Cftr*-deficient macrophages fail to respond to acute infection with *P. aeruginosa* by activation of the Asm-ceramide system, clustering of NADPH oxidase, release of ROS and killing of bacteria.
	(Yu et al., 2009)	The Asm pathway in CF is important for regulation of IL-8 release after infection of bronchial epithelial cells by *P. aeruginosa*.
	(Teichgraber et al., 2008)	Ceramide accumulates in bronchial and tracheal epithelial cells of *Cftr*-deficient mice and contributes to pulmonary inflammation and high susceptibility to *P. aeruginosa* infections.
	(Becker et al., 2012)	Increased ceramide concentrations in airways of *Cftr*-deficient mice results in upregulation and activation of CD95.
	(Grassme et al., 2017)	Increased ceramide in cystic fibrosis mice results in depletion of sphingosine and thereby high susceptibility to *P. aeruginosa* infection.
Propionibacterium acnes	(Nakatsuji et al., 2011)	*P. acnes* CAMP factor hijacks host Asm to amplify bacterial virulence.
Rhinovirus	(Dreschers et al., 2007)	Asm induced formation of ceramide-enriched membrane platforms mediates attachment and uptake of human rhinovirus into human cells.
	(Grassme et al., 2005)	Asm and ceramide are critical molecules for rhinoviral uptake into human cells.
	(Miller et al., 2012)	Asm activity and sphingomyelin presence are necessary for efficient infection of cells by Ebolavirus.
Staphylococcus aureus	(Esen et al., 2001)	Infection of human endothelial cells with *S. aureus* results in Asm-activation and subsequent apoptosis.
	(Peng et al., 2015)	The Asm/ceramide system triggers *S. aureus*-induced lung edema in mice. Inhibition of the Asm protects mice from lethal *S. aureus* sepsis.
	(Li et al., 2017)	The binding of CD44 and *S. aureus* stimulates Asm/ceramide, thus resulting in cytoskeleton rearrangement and bacterial internalization.
S. aureus α-toxin	(Ma et al., 2017)	Asm induces inflammation upon *S. aureus* toxin stimulation.
Salmonella typhimurium	(McCollister et al., 2007)	Functional Asm is essential for the killing activity of macrophages against *S. typhimurium.*
	(Utermohlen et al., 2003)	Asm-deficient mice are highly susceptible to infection with *S. typhimurium*.

Abbreviations: Asm, acid sphingomyelinase; Nsm, neutral sphingomyelinase; BCG, Bacillus Calmette-Guérin; LC3B, microtubule-associated protein 1 light chain 3 beta;

TNF, tumor necrosis factor; DC-SIGN, Dendritic Cell-Specific Intercellular adhesion molecule-3-Grabbing Non-integrin; MV, *Measles virus*; JNK, c-Jun N-terminal kinases; ROS, reactive oxygen species; NADPH, nicotinamide adenine dinucleotide phosphate; CF, cystic fibrosis; CD, Cluster of differentiation. Modified from Wu et al., 2017.

1.8 Sphingomyelinases and mycobacteria

Anes et al. first reported that ceramide, sphingomyelin, sphingosine, and S1P are involved in actin nucleation on phagosomes, thereby initiating the fusion of phagosomes with lysosomes to activate antimicrobial factors that kill mycobacteria (Anes et al., 2003). This work highlighted the importance of the sphingolipids metabolism in regulating phagosome-lysosome fusion during mycobacterial infection, but the interactions between these lipids and how they orchestrate these processes remain unknown.

Later on, another group describe, that the formation of multinucleated giant cells via cell-cell fusion in *M. avium* infection is dependent on Asm, and provide an innate immuno-escape niche for the replication of *M. avium* (Utermohlen et al., 2008). The authors hypothesize that the Asm-mediated hydrolysis of the lipid sphingomyelin into phosphorylcholine and the generation of cone-shaped ceramide alter the biological properties of the lipid layer and the fluidity of the plasma membrane. They suggest that the cone-shape ceramide induces membrane bending and curvatures, thereby regulating fusion of phagosomes and lysosomes or fusion of macrophages into giant cells.

Zebrafish infected with *M. marinum* was used as a model to describe a survival strategy involving inhibiting the Asm (Roca and Ramakrishnan, 2013). The authors described TNF-mediated receptor-interacting serine-threonine kinases 1 and 3 (RIP1 and RIP3) dependent necroptosis resulted in replication of pathogens. This necroptosis is induced by the Asm/ceramide system and mitochondrial cyclophilin D. Upon *M. marinum* infection in zebrafish; mitochondrial ROS are rapidly produced in infected macrophages due to increased TNF expression. The elevated ROS initially increase the microbicidal activity in phagosomes. However, it rapidly induces programmed necrosis (necroptosis) via Asm-mediated production of ceramide and mitochondrial cyclophilin D, finally leading to the release of mycobacteria into the growth-permissive extracellular milieu and a subsequently higher burden of bacteria in the fish (Roca and Ramakrishnan, 2013). The combined genetic blockade of Asm and cyclophilin D

prevent the macrophage necrosis and increase microbicidal activity (Roca and Ramakrishnan, 2013).

A typical survival strategy used by mycobacteria is to arrest phagosome maturation. Thus, studies regarding mechanisms and dynamics of phagosome maturation may provide new perspectives about mycobacterial infection. A recent study suggested that Asm-mediated maturation of phagosomes is important to control mycobacterial infection (Vázquez et al., 2016). Sortilin 1 (encoded by gene *Sort1*) is a transmembrane receptor that transports lysosomal proteins from the trans-Golgi network into lysosomes. Sortilin 1 has been reported to be upregulated during mycobacterial infection in macrophages and is necessary for the delivery of both prosaposin and Asm from the Golgi complex to phagosomes (Wähe et al., 2010; Gutierrez et al., 2008). Vázquez et al. showed that sortilin 1 is required for the transport of Asm to phagosomes containing mycobacteria and thereby restricting bacterial growth. The association of the Asm with phagosomes was significantly reduced in mycobacteria-containing phagosomes of *Sort1*-deficient cells (Vazquez et al., 2016). The decreased association of the Asm and phagosomes is accompanied by the uncontrolled growth of BCG and *M. tuberculosis* in macrophages as well as a high bacterial burden in the lungs of *Sort1*-deficient mice (Vazquez et al., 2016). However, how Asm-associated phagosomes mature and manipulate bacterial killing remains to be elucidated.

So far, insights into the role of Nsm in mycobacterial infections have been only reported once (Li et al., 2016). Upon BCG infection, murine RAW 264.7 macrophages exhibit rapid activation of Nsm, followed by massive production of ROS. Authors showed that the excessive production of ROS inhibits autophagy. The genetic knockdown of Nsm, both *in vitro* and *in vivo*, leads to reduced ROS production, increased autophagy and thereby bacterial killing (Li et al., 2016). Interestingly, a case-control study in a Moroccan population identified the NSM activation-associated factor (NSMAF) as a candidate gene for TB susceptibility (Qrafli et al., 2017). They observed that genetic variations in the *NSMAF* gene modulate the risk of pulmonary TB in a Moroccan population. Also, a negative form of NSMAF has been shown to reduce caspase activation and cytochrome c release from mitochondria, thereby inhibiting TNF-triggered apoptosis in human fibroblasts (Segui et al., 2001).

Taken together, these studies provide evidence that sphingomyelinases play diverse roles in mycobacterial infections (Figure 8) (Wu et al., 2018). Asm, on the one hand, induces lysosomal activities or fusogenic properties of bacteria-containing phagosomes, on the other hand, Asm-derived ceramide from lysosomes promotes host cell death. Nsm triggers the release of ROS which subsequently suppresses autophagy and thereby leads to enhanced survival of mycobacteria.

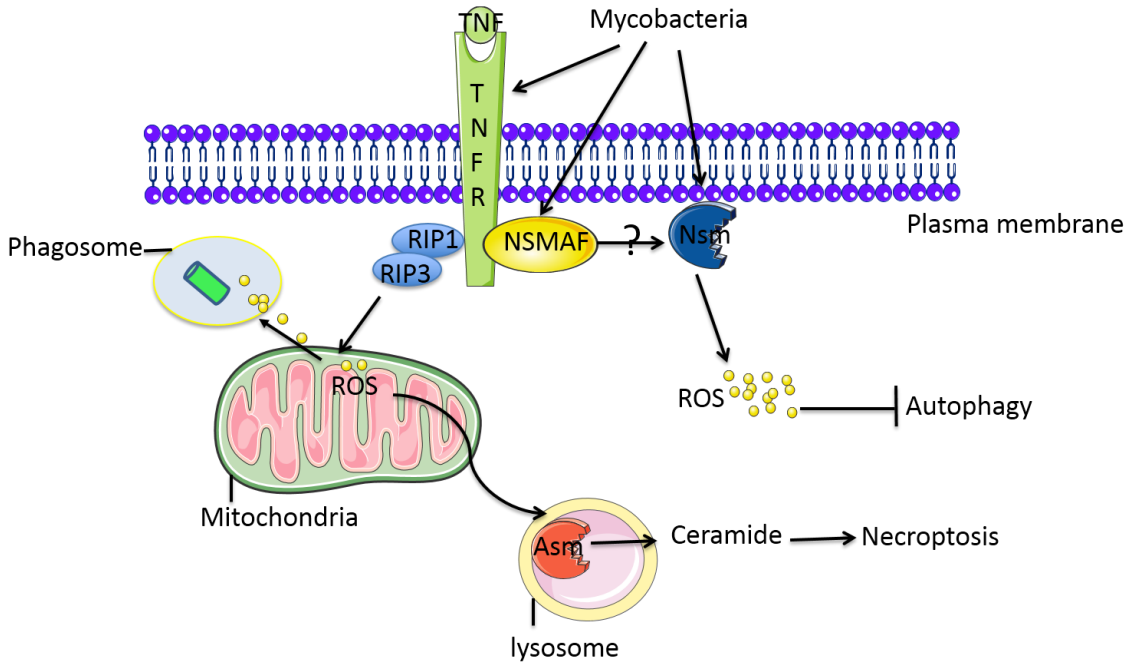

Figure 8. Model of the role of sphingomyelinases in mycobacterial infection.
Mycobacterium avium infections activate tumor necrosis factor (TNF)/TNF-receptor (TNF-R) and RIP1/RIP3 necrosome and lead to the release of reactive oxygen species (ROS). This activates the acid sphingomyelinase (Asm) and Asm-released ceramide results in necroptosis (Roca and Ramakrishnan, 2013). *Mycobacterium bovis* Bacillus Calmette-Guérin (BCG) activates neutral sphingomyelinase (Nsm) and induces ROS, which inhibits autophagy (Li et al., 2016). A TNF-R-associated protein, neutral sphingomyelinase activation-associated factor (NSMAF), modulates the risk of TB development in human (Qrafli et al., 2017). However, whether NSMAF is related to Nsm activation upon mycobacterial infections is unknown. Adapted from Wu et al., 2018.

1.9 Aim of the study

M. tuberculosis is the causative pathogen of TB, an airborne infectious disease which remains a significant cause of mortality and morbidity worldwide, particularly in low-

income and middle-income countries. With the development of new TB diagnostics, BCG vaccine, and antibiotics, TB has been under control in the last century. However, the globalization and the appearance of drug-resistant mycobacteria lead to less effective vaccines and antibiotics in controlling the global TB epidemic. Thus, the researches of mycobacterial infections again gain attention and are being increasingly funded to develop new vaccines and better therapeutic strategies.

The sphingomyelinase/ceramide system has been reported to be involved in several infectious diseases, especially in pulmonary infections caused by pathogens, such as *P. aeruginosa*, *S. aureus*, as well as mycobacteria. The overall goal of this study is to elucidate the role of the acid and neutral sphingomyelinases in mycobacterial infections with BCG as a model for mycobacteria.

To identify the role of the Nsm in BCG-infection, the current study focused on the mechanism of Nsm regulated granuloma, the hallmark of mycobacterial infection. The present study is based on previous work (Li et al., 2016) demonstrating that the *in vivo* infection of Wt mice with BCG leads to higher bacterial burden and bacterial aggregates compared to Nsm heterozygous ($Nsm^{+/-}$) mice. Their study showed that genetic downregulation of the Nsm protects mice against BCG infection (Li et al., 2016). The authors focused on the role of autophagy as host defense mechanisms and demonstrated that ROS and autophagy are controlled by the Nsm and affect the survival of BCG in mice.

For *in vitro* study on the role of the Nsm in granuloma formation in present work, bone marrow-derived macrophages (BMDMs) from Wt and $Nsm^{+/-}$ mice were isolated to monitor migration and clustering of macrophages and related downstream signaling events upon BCG infection. For *in vivo* study, Wt and $Nsm^{+/-}$ mice were used to investigate the role of the Nsm for mechanical function in granuloma formation upon infection with BCG.

To identify the role of the Asm in BCG infection, the present study focuses mainly on bacterial control and early events of phagocytosis upon BCG infection. The Asm has been shown to induce fusogenic properties of bacteria-containing phagosomes and lysosomes, which serve as a microbicidal environment for mycobacteria (Utermohlen et al., 2008). The *in vivo* study in the thesis focused on the bacterial burden and used Wt mice and Asm deficient ($Asm^{-/-}$) mice. *In vitro* examinations, which aim to elucidate

underlying mechanisms of Asm-dependent phagocytosis, were performed with BMDMs from both genotypes.

2 Materials

2.1 Chemicals

Acetic acid (100 %)	Merck KGaA, Darmstadt, Germany
Acrylamide	Carl-Roth GmbH & Co, Karlsruhe, Germany
Ammonium persulfate (APS)	Carl-Roth GmbH & Co, Karlsruhe, Germany
Aprotinin	Roche Deutschland Holding GmbH, Freiburg, Germany
BODIPY™ FL C12-Sphingomyelin	Thermo Fisher Scientific, Waltham, MA, USA
Bovine serum albumin (BSA)	Sigma-Aldrich Chemie GmbH, Steinheim, Germany
Bradford Protein Dye Reagent	Biorad Laboratories GmbH, München, Germany
Bromphenol blue	Sigma-Aldrich Chemie GmbH, Steinheim, Germany
Calcium chloride (≥ 99 %)	Carl-Roth GmbH & Co, Karlsruhe, Germany
CDP-Star substrate	Perkin Elmer, Rodgau, Germany
Chloroform	AppliChem GmbH, Darmstadt, Germany
CMH (1-Hydroxy-3-methoxycarbonyl-2,2,5,5-tetramethylpyrrolidine)	Noxygen Science Transfer & Diagnostics, Elzach, Germany
Complete protease inhibitor cocktail	Roche Deutschland Holding GmbH, Freiburg, Germany
Dabco	Thermo Fisher Scientific, Waltham, MA, USA
deferoxamine	Sigma-Aldrich Chemie GmbH, Steinheim, Germany
dietheyldithiocarbamate	Sigma-Aldrich Chemie GmbH, Steinheim, Germany
Dimethylsulfoxid (DMSO)	Sigma-Aldrich Chemie GmbH, Steinheim
Di-potassium hydrogen phosphate	Carl-Roth GmbH & Co, Karlsruhe, Germany
Di-sodium hydrogen phosphate	Merck KGaA, Darmstadt, Germany
Eosin	Carl-Roth GmbH & Co, Karlsruhe, Germany
Ethanol (absolute, anhydrous)	Diagonal GmbH & Co. KG, Münster, Germany
Ethyl acetate	Diagonal GmbH & Co. KG, Münster, Germany

Fluorescent Dye 555-I Phalloidin	Abnova Corporation, Taiwan, China
Glucose	Sigma-Aldrich Chemie GmbH, Steinheim, Germany
Glycerol (≥ 99 %)	Carl-Roth GmbH & Co, Karlsruhe, Germany
Hematoxylin	Carl-Roth GmbH & Co, Karlsruhe, Germany
HEPES	Carl-Roth GmbH & Co, Karlsruhe, Germany
Hydrochloric acid (37 %)	Sigma-Aldrich Chemie GmbH, Steinheim, Germany
Isoflurane (Isothesia)	Henry Schein Vet GmbH, Hamburg, Germany
Leupeptin	Becton Dickinson GmbH, Heidelberg, Germany
Liposomes (clodronate liposomes and PBS control liposomes)	Liposoma B.V., Amsterdam, The Netherlands
Liquid Nitrogen	AIR LIQUIDE Medical GmbH, Düsseldorf, Germany
Magnesium chloride hexyhydrate (≥ 99 %)	Carl-Roth GmbH & Co, Karlsruhe, Germany
Magnesium sulfate heptahydrate (≥ 99 %)	Sigma-Aldrich Chemie GmbH, Steinheim, Germany
Manganese chloride	Sigma-Aldrich Chemie GmbH, Steinheim, Germany
Methanol (≥ 99.8 %)	Diagonal GmbH & Co. KG, Münster, Germany
Middlebrook 7H10 agar plates	Becton Dickinson GmbH, Heidelberg, Germany
Middlebrook 7H9 Broth with Glycerol	Becton Dickinson GmbH, Heidelberg, Germany
Mowiol	Kuraray Specialities Europe GmbH, Frankfurt, Germany
NBD-ceramide	Thermo Fisher Scientific, Waltham, MA, USA
NP-40 (Igepal)	Sigma-Aldrich Chemie GmbH, Steinheim, Germany
Paraformaldehyde (powder, 95 %)	Sigma-Aldrich Chemie GmbH, Steinheim, Germany
Phalloidin CruzFlour™ 647 conjugate	Santa Cruz Biotechnology, Inc., Dallas, Texas, USA

Polyoxyethylene glycol sorbitan monolaurate (Tween20)	Sigma-Aldrich Chemie GmbH, Steinheim, Germany
Potassium chloride (≥ 99 %)	Carl-Roth GmbH & Co KG, Karlsruhe, Germany
Propidium iodide (95-98 %)	Sigma-Aldrich Chemie GmbH, Steinheim, Germany
saponin	Serva Electrophoresis GmbH, Heidelberg, Germany
Sodium chloride (≥ 99,5 %)	Carl-Roth GmbH & Co KG, Karlsruhe, Germany
Sodium citrate (tribasic, dehydrate)	Sigma-Aldrich Chemie GmbH, Steinheim, Germany
Superoxide dismutase (SOD)	Sigma-Aldrich Chemie GmbH, Steinheim, Germany
β-Mercaptoethanol	Sigma-Aldrich Chemie GmbH, Steinheim, Germany
Starting Block TBS Blocking Solution	Thermo Fisher Scientific, Waltham, MA, USA
Tissue-Tec	Sakura Finetek, USA, Torrance, CA, USA
Trypan blue (0.4% w/v in PBS)	Corning Inc., NY, USA
Xylene (a mixture of isomers)	Diagonal GmbH & Co. KG, Münster, Germany

2.2 Antibodies

anti-mouse CD16/32, Fcγ block	Biolegend, Inc., San Diego, CA, USA
anti-β actin antibody (HRP)	Santa Cruz Biotechnology, Inc., Dallas, Texas, USA
APC anti-mouse F4/80 (clone BM8)	Biolegend, Inc., San Diego, CA, USA
Brilliant Violet 711 anti-mouse CD115 (clone AFS98)	Biolegend, Inc., San Diego, CA, USA
Fluorescent secondary antibodies	Jackson ImmunoResearch Europe Ltd., Cambridgeshire, UK
Goat anti-mouse cathepsin D (AF1029)	R&D Systems, Inc., Minneapolis, USA
Isotype control (R35-95, Rat anti-mouse IgG_{2a}, κ)	Becton Dickinson GmbH, Heidelberg, Germany

Mouse anti-gp91^{phox}	Becton Dickinson GmbH, Heidelberg, Germany
Mouse anti-p67^{phox}	Becton Dickinson GmbH, Heidelberg, Germany
Mouse anti-Rac1	Cytoskeleton Inc., Denver, CO, USA
Pacific Blue anti-mouse CD11b (clone M1/70)	Biolegend, Inc., San Diego, CA, USA
PE anti-mouse Gr-1 (Ly6G/C; clone RB6-8C5)	Biolegend, Inc., San Diego, CA, USA
PE/Cy7 anti-mouse NK1.1 (clone PK136)	Biolegend, Inc., San Diego, CA, USA
PerCP anti-mouse CD3 (clone 145-2C11)	Biolegend, Inc., San Diego, CA, USA
PerCP anti-mouse CD45R/B220 (clone RA3-6B2)	Biolegend, Inc., San Diego, CA, USA
PerCP anti-mouse Ter119 (clone TER-119)	Biolegend, Inc., San Diego, CA, USA
Rabbit anti-mouse p47^{phox}	Merck Chemicals GmbH, Darmstadt, Germany
Rabbit anti-phospho-p38 MAPK (Thr180/Tyr182)	Cell Signaling Technology, USA
Rabbit anti-phospho-SAPK/JNK (Thr183/Tyr185)	Cell Signaling Technology, USA
Anti-β1-Integrin, activated (9EG7, Rat anti-mouse IgG_{2a}, κ)	Becton Dickinson GmbH, Heidelberg, Germany
Anti-β-actin	Santa Cruz Biotechnology, Inc., Dallas, Texas, USA

2.3 Inhibitors

Apocynin (NADPH oxidase inhibitor)	Abcam PLC, Cambridge, UK
NSC23766 (Rac1 inhibitor)	Bio-Techne GmbH,Wiesbaden-Nordenstadt, Germany

Pepstatin A (cathepsin D inhibitor)	Sigma-Aldrich Chemie GmbH, Steinheim, Germany
SB239063 (p38K inhibitor)	Sigma-Aldrich Chemie GmbH, Steinheim, Germany
SKI-I (sphingosine kinase inhibitor)	Abcam PLC, Cambridge, UK
SP600125 (JNK inhibitor)	Sigma-Aldrich Chemie GmbH, Steinheim, Germany

2.4 Kits

Cellular ROS detection assy kit (Deep red fluorescence)	Abcam PLC, Cambridge, UK
ECL prime system	GE Healthcare Europe GmbH, Freiburg, Germany
Oil Red O staining kit	Abcam PLC, Cambridge, UK
Truant TB Fluorescent stain kit	Becton Dickinson GmbH, Franklin Lakes, NJ, USA
Rac1 pulldown kit	Cytoskeleton Inc., Denver, CO, USA

2.5 Tissue culture materials

MEM	Thermo Fisher Scientific, Waltham, MA, USA
DMEM	Thermo Fisher Scientific, Waltham, MA, USA
FBS	Thermo Fisher Scientific, Waltham, MA, USA
L-Glutamine	Thermo Fisher Scientific, Waltham, MA, USA
Non-essential amino acids	Thermo Fisher Scientific, Waltham, MA, USA
PenStrep	Thermo Fisher Scientific, Waltham, MA, USA
Sodium pyruvate	Thermo Fisher Scientific, Waltham, MA, USA

2.6 Prepared buffers and solution

Ac/Asm/Nsm assay buffer	250 mM sodium acetate (Ac, Asm) or 100 mM HEPES (Nsm) 0.1 % NP-40

	pH 4.5 (Ac) or pH 5.0 (Asm) or pH 7.0 (Nsm)
Ac/Asm/Nsm lysis buffer	250 mM sodium acetate (Ac, Asm) or 100 mM HEPES (Nsm) 1 % NP-40 pH 4.5 (Ac) or pH 5.0 (Asm) or pH 7.0 (Nsm)
Ac substrate solution	1 µl NBD-Ceramide 27.2 mL Ac assay buffer
Asm/Nsm substrate solution	0.5 µl BODIPY-Sphingomyelin 1 mL Asm/Nsm assay buffer
HEPES/Saline (H/S) (10x)	200 mM HEPES 1.32 M NaCl 10 M $CaCl_2$ 7 mM $MgCl_2$ 8 mM $MgSO_4$ 54 mM KCl
Mowiol	20-25 % Mowiol-488 2.5 % Dabco
Paraformaldehyde (PFA), 4%	4 % PFA 1 x PBS pH 7.2 – 7.4 adjusted with HCl and NaOH
Phosphate buffered saline (PBS), pH7.4	137 mM NaCl 2.7 mM KCl 10 mM $Na_2HPO_4 \cdot 2\ H_2O$ 2.0 mM KH_2PO_4 pH adjusted with HCl and NaOH
Reducing SDS sample buffer (5x)	250 mM Tris pH 6.8 20 % Glycerine 4 % SDS 8 % ß-mercaptoethanol 0.2 % bromphenol blue
0.1 % SDS lysis buffer	25 mM HEPES, pH 7.3 0.1 % sodium dodecyl sulfate 0.5 % sodium deoxycholate

	1 % Triton-X-100
	125 mM NaCl
	10 mM NaF
	10 mM $Na_2P_2O_7$
	20 mM Na_3VO_4
	10 mM ethylenediaminetetraacetic acid
	10 µg/ml aprotinin
	10 µg/ml leupeptin
	1 x Roche Complete protease inhibitor cocktail
SDS Running buffer	25 mM Tris
	192 mM glycine
	0.1 % SDS
Transfer buffer	25 mM Tris
	192 mM Glycine
	10 % Methanol
Trypsin	0.25% Trypsin
	5 mM Glucose
	1.3 mM EDTA
TN3 lysis buffer	125 mM NaCl
	10 mM ethylenediaminetetraacetic acid (EDTA)
	25 mM Tris (pH 7.4)
	10 mM sodium pyrophosphate
	3% NP-40
	10 µg/mL aprotinin/leupeptin

2.7 Consumables

Cell culture flasks	Sarstedt AG & Co, Nümbrecht, Germany
Cell culture, 6, 24 and 96 well plate	Corning Inc., NY, USA
Cell strainer (70 µm, 100 µm)	Corning Inc., New York, NY, USA
Centrifuge tubes (15 mL, 50 mL)	Greiner Bio-One GmbH, Frickenhausen, Germany
Coverglass (18 x 18 mm)	Engelbrecht GmbH, Wien, Austria

Coverslips (Ø 12 mm)	Carl-Roth GmbH & Co, Karlsruhe, Germany
Cuvettes	Sarstedt AG & Co, Nümbrecht, Germany
Hybond ECL nitrocellulose membrane	GE Healthcare Europe GmbH, Freiburg, Germany
Hypodermic needle	Becton Dickinson GmbH, Heidelberg, Germany
Microscopic slides	Langenbringen Labor- und Medizintechnik, Emmendingen, Germany
Microtiter plates	Sarstedt AG & Co, Nümbrecht, Germany
Needles (different gauges)	Becton Dickinson GmbH, Heidelberg, Germany
Parafilm	Peckiney, Chicago, IL, USA
Pipettes (5 mL, 10 mL, 25 mL)	Greiner Bio-One, Frickenhausen, Germany
Reaction tubes, 1.5 mL	Sarstedt AG & Co, Nümbrecht, Germany
Reaction tubes, 2 mL	Eppendorf AG, Hamburg, Germany
Syringes	
-Insulin syringe (1ml)	Becton Dickinson GmbH, Heidelberg, Germany
-syringes (5ml, 10ml, 20ml)	Becton Dickinson GmbH, Heidelberg, Germany
Thin layer chromatography (TLC) Silica G60 plates	Merck KGaA, Darmstadt, Germany

2.8 Equipment

Attune NxT Flow Cytometer	Thermo Fisher Scientific, Waltham, MA, USA
Centrifuges	
- 5417 R	Eppendorf AG, Hamburg, Germany
- Heraeus 3SR+ multifuge	Thermo Fisher Scientific, Waltham, MA, USA
Clean bench (biological safety cabinet class II)	NuArie, Plymouth, MN, USA
Cryotome (CM1850 UV)	Leica Mikrosysteme Vertrieb GmbH, Wetzlar, Germany
Microscopes	
- confocal fluorescence (TCS-SP5)	Leica Mikrosysteme Vertrieb GmbH, Wetzlar, Germany
-inverted fluorescence microscope (DMIRE2)	Leica Mikrosysteme Vertrieb GmbH, Wetzlar, Germany

Developer machine	Thermo Fisher Scientific, Waltham, MA, USA
Digital caliper	Mitutoyo UK Ltd., Andover, UK
Freezers	
- 80 °C, ultra low MDF-U54V	Sanyo Electric Co, Osaka, Japan
- 20 °C, Premium NoFrost	Liebherr-International Deutschland GmbH, Biberach, Deuschland
Fridge, 4 °C, Premium BioFresh	Liebherr-International Deutschland GmbH, Biberach, Germany
Glasswares (beakers, cylinders, flasks)	DURAN Group GmbH, Wertheim, Germany
Incubator	Binder GmbH, Tuttlingen, Germany
Magnetic stirrer (M21)	Intern. Laborat. App GmbH, Dottingen, Germany
Mass spectrometer (6530/6490)	Agilent Technologies, Waldbronn, Germany
Mechanical shaker (Rotamax120)	Heidolph Instruments GmbH & Co. KG, Schwabach, Germany
Microplate reader (SpectraMax Gemini EM)	Molecular Devices GmbH, Biberach an der Riß, Germany
pH Meter (HI9025)	Hanna instruments, Woonsocket, RI, USA
Pipettes (different sizes)	Nichiryo CO., Ltd., Saitama, Japan
Pipettus (pipetus-akku)	Hirschmann Laborgeräte GmbH und Co. KG, Eberstadt, Germany
Sonicator	Bandelin Electronic, Berlin, Germany
Spectrophotometer	Eppendorf AG, Hamburg, Germany
SpeedVac	Thermo Fisher Scientific, Waltham, MA, USA
SpotChem EZ chemistry analyser	Scil animal care company GmbH, Viernheim, Deutschland
Thermomixer	Eppendorf AG, Hamburg, Germany
Typhoon FLA 9500	GE Healthcare Europe GmbH, Freiburg, Germany
Ultrasonic bath (sonorex RK 102 H)	BANDELIN electronic GmbH & Co. KG, Berlin, Germany
Vacuum concentrator (SpeedVac)	Bachofer GmbH, Reutlingen, Germany
Vortexer (Reax 2000)	Heidolph Instruments GmbH & Co. KG, Schwabach, Germany

Water bath (1o12)	GFL Gesellschaft für Labortechnik mbH, Burgwedel, Germany

2.9 Software

FlowJo (v10)	LLC, Ashland, OR, USA
GraphPad Prism 6	GraphPad Software, La Jolla, CA, USA
ImageQuant	GE Healthcare Europe GmbH, Freiburg, Germany
Leica advanced Fluorescence – Application Suite (2.61)	Leica Mikrosysteme Vertrieb GmbH, Wetzlar, Germany
MassHunter Software	Agilent Technologies, Waldbronn, Germany
Microsoft Office (2016)	Microsoft Corporation, Redmond, WA, USA
ImageJ (Fiji)	Image J

3 Methods

3.1 Mice

Mice heterozygous for Nsm2 ($Nsm^{+/-}$, sphingomyelin phosphodiesterase 3 heterozygote, *Smpd3*) and syngenic wild-type (Wt) littermates were purchased from the European Mouse Mutant Archive (EMMA; Consiglio Nazionale delle Ricerche, France) and maintained on the 129sv genetic background. $Nsm2^{+/-}$ mice were used in this study but not knock out mice for the Nsm2, because of the severe phenotype of the complete knock-out and ethical reasons. $Nsm2^{+/-}$ mice showed a reduction of the Nsm2-activity of about 30% (unpublished results) but do not develop any obvious spontaneous phenotype and also do not show any severe bone disease. In the following experiments and results, $Nsm^{+/-}$ is referred to $Nsm2^{+/-}$.

Asm-deficient ($Asm^{-/-}$) mice and Wt littermates (Horinouchi et al., 1995) (sphingomyelin phosphodiesterase 1 knockout; $Smpd1^{-/-}$) were maintained on a C57BL/6J background. $Asm^{-/-}$ mice, and Wt littermates were used only aged from 6 to 8 weeks to avoid sphingomyelin accumulation (Niemann-Pick Type A disease).

Mice were housed in the animal facility of the University of Duisburg-Essen under pathogen-free conditions according to the criteria of the Federation of Laboratory Animal Science. The genotype was verified by polymerase chain reaction (PCR) analysis before experimentation. *In vivo* infections were approved by the Landesamt für Natur, Umwelt und Verbraucherschutz (LANUV).

3.2 Cells

The *in vitro* experiments were performed with bone marrow-derived macrophages (BMDMs). The culture of BMDMs has been previously described in detail (Zhang et al., 2008). Briefly, femurs and tibias from donor mice were flushed with minimum essential medium (MEM; Thermo Fisher Scientific, Waltham, MA, USA) supplemented with 10% fetal bovine serum (FBS) (Thermo Fisher Scientific), 10 mM HEPES (Roth GmbH, Karlsruhe, Germany; pH 7.4), 2 mM L-glutamine, 1 mM sodium pyruvate, 100 µM nonessential amino acids, 100 U/mL penicillin, and 100 µg/mL streptomycin

(Thermo Fisher Scientific). Isolated cells were passed through a 23-G needle for obtaining single cells which were cultured for 24 hrs in small tissue-culture flasks. Cells were washed, and $3x10^4$ or $1.2x10^5$ non-adherent cells were cultured in 24- or 6-well plates in MEM with 20% L-cell supernatant as a source of macrophage colony-stimulating factor (M-CSF). Fresh MEM/L-cell supernatant medium was applied after 4 days of culture. Macrophages matured within the next 6 days and were used on day 10 of culture.

3.3 Infection experiments

All *in vivo* and *in vitro* infections were performed with green fluorescent protein (GFP)-expressing BCG (GFP-BCG). The GFP-BCG strain was constructed by transforming BCG with the dual reporter plasmid pSMT3LxEGFP (Humphreys et al., 2006). For infection experiments, bacteria were shaken at 120 rpm at 37°C in Erlenmeyer flasks with 10 ml Middlebrook 7H9 Broth with Glycerol (BD Biosciences, Heidelberg, Germany), supplemented with 50 µg/ml hygromycin B for maintaining GFP in plasmids. Bacteria were used for infection experiments after 5 to 7 days of culture. Bacteria were collected by centrifugation at 2000 rpm for 10 min. The bacterial pellet was resuspended in HEPES/saline buffer (H/S) and was vortexed for 5 min. Samples were bath-sonicated for 5 min at 4°C and were passed 10 times through a syringe with a needle 0.8 mm in diameter. Clumps of bacteria were removed by centrifugation for 2 min at 1000 rpm. The supernatant containing single cells of GFP-BCG was carefully collected. The bacterial number was calculated with a 100×oil lens and an inverted fluorescence microscope (DMIRE2; Leica, Heidelberg, Germany).

For *in vitro* assays, BMDMs were left uninfected or were infected with GFP-BCG in MEM/10 mM HEPES at a bacteria-to-host cell ratio (multiplicity of infection, MOI) of 5:1 to 10:1 for the indicated time. For *in vitro* granuloma formation, 1 µg/ml anti-β1-integrin antibody (Becton Dickinson GmbH, Heidelberg, Germany) was added 1 hr before infection and then every 5 hrs until 25 hrs after infection. If indicated, 100 µM NSC23766 (Bio-Techne GmbH, Wiesbaden-Nordenstadt, Germany) was added 1 hr before infection. For measuring mechanism of β1-integrin activation, 10 µM p38 inhibitor (SB239063) (Sigma-Aldrich Chemie GmbH, Steinheim, Germany), 10 µM JNK inhibitor (SP600125) (Sigma-Aldrich Chemie GmbH), or an equal amount of

dimethylsulfoxide (DMSO, Sigma-Aldrich Chemie GmbH) was added 1 hr before infection. For measuring mechanism of Asm in BCG infection, 1 µM or 5 µM SphK inhibitor (SKI-I) (Abcam PLC, Cambridge, UK), 10 µM pepstatin A (Sigma-Aldrich Chemie GmbH) or 10 µM apocynin (Abcam) was added 1 hr before infection. Synchronous infection conditions and enhanced interactions between bacteria and host cells were achieved by centrifugation (500 rpm) of the bacteria onto the cells for 8 min. The end of the centrifugation was defined as the starting point of infection. The infection was terminated by fixation or lysis, as described below.

For *in vivo* infections, bacteria were prepared as described above and then pelleted at 3200 rpm for 10 min. BCG bacteria were resuspended in 0.9% NaCl, and 200 µl of $1x10^7$ CFU bacteria were intravenously injected into mice. For the study the role of Nsm in mycobacterial infection, mice were left untreated or treated with anti-β1-integrin antibody (9EG7) or isotype control (Becton Dickinson GmbH) intraperitoneally at a dose of 30 µg every 2 to 3 days during infection (3 times a week after infection, in total 9 times). After 3 weeks, the animals were sacrificed by cervical dislocation. To study the role of Asm in mycobacterial infection, mice were left untreated or injected with 200µl clodronate liposomes (Liposoma B.V., Amsterdam, The Netherlands). 24 hours after depletion, mice were reconstituted intravenously with 5×10^6 BMDMs either from Wt or $Asm^{-/-}$ mice. Mice were injected with BCG 24 hours after transplantation and sacrificed 1 day till 3 weeks after infection.

Livers and spleens were obtained for further processing. The collected tissues were homogenized into tiny pieces and lysed with 5 mg/mL saponin in PBS. Total numbers of bacteria were determined two weeks after growth at 37°C on Middlebrook 7H10 agar plates enriched with oleic acid, albumin, dextrose, and catalase (OADC; Becton Dickinson GmbH). The counts represent the number of bacteria in whole-liver or spleen samples.

3.4 Determination of Nsm, Asm and Ac activity

Nsm, Asm or Ac activity was determined as recently described (Mühle and Kornhuber 2017) with green fluorescent BODIPY FL C_{12}-sphingomyelin (Thermo Fisher Scientific) or NBD-ceramide (Thermo Fisher Scientific) as a substrate. Briefly, cells were infected

or left uninfected, harvested, and lysed in Nsm, Asm or Ac lysis buffer for 5 min on ice. Cells were sonicated for 10 min in an ice bath sonicator for further lysis (Bandelin Electronic, Berlin, Germany). The protein concentration was measured by Bradford protein assay (BioRad, München, Germany): 20 µg of protein for Nsm, or 0,5 µg for Asm, or 20 µg for Ac in 20 µL lysis buffer were used. Samples and the NBD-ceramide or BODIPY-sphingomyelin substrate solutions were sonicated in ice bath sonicator for 10 min to induce micelle formation. Sonicated 100 pmol/sample NBD-ceramide or 100 pmol/sample BODIPY-sphingomyelin were added to the sonicated samples. The samples were incubated at 37°C for 1 hr (Nsm and Asm) or 4 hr (Ac) with shaking at 300 rpm. The reaction was stopped by adding 200 µL chloroform: methanol (2:1, v/v). Samples were well mixed by vortexing and followed by centrifugation for 5 min at 14,000 rpm. The lower phase was dried in a SpeedVac Concentrator (Thermo Fisher Scientific) and resuspended in 20 µL of chloroform: methanol (2:1, v/v). The samples were spotted on a 20-cm thin-layer chromatography (TLC) plate (Merck, Darmstadt, Germany) in 3-µL steps. After all spots were dried, the samples were separated with chloroform: methanol (80: 20, v/v, Nsm and Asm) or ethyl acetate : acetic acid (100:1, v/v, Ac), scanned with a Typhoon FLA 9500 laser scanner (GE Healthcare Life Sciences, Freiburg, Germany), and analyzed with ImageQuant software (GE Healthcare Life Sciences).

3.5 Ceramide and sphingomyelin quantification

Ceramides, sphingomyelins, sphingosines, and S1Ps were quantified by Dr. Fabian Schumacher (University Duisburg-Essen and University Potsdam) by rapid resolution liquid chromatography/mass spectrometry as recently described (Gulbins et al., 2018). Briefly, cells were infected with BCG for indicated time periods, collected in methanol, and directly sent to Potsdam with dry ice or stored at -80ºC for further measurement. For extracting lipid, cell pellets were sonicated on ice for 15 min. For saponification, the samples were then incubated with 150 µL methanolic KOH (1 M) for 2 h at 37°C with gentle shaking. Samples were then neutralized with 12 µL glacial acetic acid and centrifuged at 2,200 x g for 10 min at 4°C. The organic phase was dried in a Savant SpeedVac concentrator (Thermo Fisher Scientific). The dried samples were reconstituted in 200 µL of acetonitrile/methanol/water (47.5: 47.5: 1, *v: v: v*) and

acidified with 0.1% formic acid. Samples were thoroughly vortexed for 10 min at 1,500 rpm and centrifuged at 2,200 x g for 10 min at 4°C for mass spectrometric sphingolipid quantification. Sphingomyelins and ceramides were analyzed using a 6530 mass spectrometer (Agilent Technologies, Waldbronn, Germany). Sphingosine and S1P were analyzed with a 6490 triple quadrupole mass spectrometer (Agilent Technologies). Both instruments were interfaced with an electrospray ion source operating in the positive ion mode (ESI+). Sphingomyelins, ceramides, sphingosine, and S1P were analyzed in MS/MS mode utilizing the fragmentation of the precursor ions into the production *m/z* 184.07 (for all sphingomyelins), *m/z* 264.3 (for S1P and all ceramides) or *m/z* 282.3 (for sphingosine). Quantification was performed using the MassHunter software (Agilent Technologies).

3.6 Western blots and pull-down assay

BMDMs were left uninfected or were infected for the indicated time, washed in cold H/S buffer, and lysed for 5 min on ice in TN3 or 0.1% SDS lysis buffer. Cells lysates were pelleted by centrifugation for 10 min at 14,000 rpm. The supernatants were added to 5 x sodium dodecyl sulfate (SDS) sample buffer; samples were boiled for 5 min and separated by 7.5% to 12.5% SDS polyacrylamide gel electrophoresis (SDS-PAGE). Samples were blotted on nitrocellulose membranes (Amersham Protran Premium 0.2 µm, GE Healthcare) for 2 hrs at 4°C (80 V). For detection of proteins, blots were washed with PBS and blocked for 1 hr at room temperature in Starting Block Tris-buffered saline (TBS) buffer (Thermo Fisher Scientific). After two additional washes in PBS, membranes were incubated with specific primary antibodies against phosphorylated p38 (1:1000), phosphorylated JNK (1:1000), $p47^{phox}$ (1:1000), $gp91^{phox}$ (1:1000), $p67^{phox}$ (1:1000), Rac1 (1:500), cathepsin D (1:1000), or HRP-conjugated β-actin (1: 50,000) overnight at 4°C or 1 hr at room temperature in Starting Block TBS buffer. After 6 washes in TBS/Tween, blots were incubated for 1 hr at room temperature in TBS/Tween with alkaline phosphatase (AP)-conjugated secondary antibodies (Santa Cruz Biotechnology, Inc., Dallas, Texas, USA) or directly for further development. Samples were washed extensively and developed with CDP-Star substrate (Perkin Elmer, Rodgau, Germany) or HRP substrate.

Rho family GTPase activity was detected with the Rac1 Activation Assay Combo Biochem Kit (Cytoskeleton Inc., Denver, CO, USA) according to the manufacturer's instructions. Briefly, cells were infected and lysed in supplied lysis buffer and additional proteinase inhibitors. Equivalent amounts of protein were added to a predetermined concentration of p21-activated protein kinase (PAK)-p21-binding domain (PBD) (PAK-PBD) beads and incubated at 4°C on a rotator for 1 hr. Beads were washed with supplied washing buffer. Finally, 20 µL of Laemmli sample buffer was added to each sample. Samples were centrifuged, and the supernatants were separated on a 10% SDS-PAGE gel and transferred to a nitrocellulose membrane. Blots were incubated with monoclonal anti-Rac1 (ARC03; antibodies from Cytoskeleton Inc.) according to the vendor's instructions and were developed as described above.

3.7 β1-integrin immunoprecipitation

To demonstrate activation of β1-integrin on the surface of BMDMs, we infected cells for various time periods, removed the medium, and incubated macrophages on ice for 30 min with 1 µg of anti-β1-integrin antibodies, clone 9EG7. The samples were washed extensively and lysed in TN3 lysis buffer for 5 min at 4°C. They were then centrifuged at 14,000 rpm. The immunocomplexes were immobilized with protein A/G agarose (Santa Cruz Biotechnology) for 45 min, washed 6 times in lysis buffer, resuspended in 1xSDS Laemmli Sample buffer, and boiled for 5 min at 95°C. Proteins were separated on 8.5% SDS-PAGE gels, blotted with β1-integrin antibody clone MB1.2, and developed with an AP-coupled secondary antibody and a chemiluminescence system (Thermo Fisher Scientific).

3.8 Measurement of production of ROS and superoxide

Superoxide production was measured by electron spin resonance (ESR) by Dr. Yang Zhang (University of Houston, College of Pharmacy, USA), as previously described (Abais et al., 2014). 10^6 cells were infected with GFP-BCG for the indicated time. Cells were scraped in 20 mM HEPES (pH 7.5), 1 mM EDTA, and 255 mM sucrose. The samples were directly sent to the USA with dry ice or shock-frozen in liquid nitrogen

for later measurement. Proteins were isolated and resuspended with modified Krebs-HEPES buffer containing deferoxamine (100 µM, Sigma-Aldrich) and diethyldithiocarbamate (5 µM, Sigma-Aldrich). The samples were added with or without of manganese-dependent superoxide dismutase (SOD, 200 U/mL; Sigma-Aldrich) and then added with a spin trap, CMH (1-hydroxy-3-methoxycarbonyl-2,2,5,5-tetramethyl pyrrolidine, Noxygen Science Transfer & Diagnostics, Elzach, Germany; 1 mM final concentration). The mixture was analyzed for the kinetics of O_2 in glass capillaries for 10 min. To calibrate the system, the SOD-inhibited fraction of the signal was used. The strength of the ESR signal was recorded in arbitrary units (a.u.), and the final results of strength were shown as the fold changes from control (Xu et al., 2013).

ROS were measured by using the Cellular Reactive Oxygen Species Detection Assay Kit (Deep Red Fluorescence, Abcam) according to the manufacturer's instructions. Briefly, 10^4 cells were seeded in 96-well plate and infected with BCG for the indicated time. Cells were then washed with PBS, incubated with ROS deep red dye for 30 min and analyzed with a microplate reader at Ex/Em = 650/675 nm (cut off 665 nm) (SpectraMax Gemini EM, Molecular Devices GmbH, Biberach an der Riß, Germany).

3.9 Immunocytochemistry

Cells were grown on coverslips and were infected or left uninfected. They were then fixed in 1% paraformaldehyde (PFA; Sigma-Aldrich); washed in PBS and buffered in PBS (pH 7.2-7.4) for further staining. Fixed cells were permeabilized with 0.1% Triton X-100 (Sigma-Aldrich) in PBS (pH 7.4) for 10 min at room temperature, washed once with H/S and once with H/S with 0.05% Tween-20 (Sigma-Aldrich), and blocked for 45 min in H/S supplemented with 5% fetal calf serum (FCS; Thermo Fisher Scientific). Cells were washed three times in H/S with 0.05% Tween-20 and incubated for 45 min with Rac1 (Santa Cruz Biotechnology), Alexa Fluor 647-conjugated phalloidin or 555-phalloidin, cathepsin D (R&D Systems, Inc., Minneapolis, USA) or p47phox (Millipore) in H/S supplemented with 1% FCS. Cells were washed three times in H/S with 0.05% Tween-20 and were incubated with secondary antibodies corresponding to the primary antibodies for an additional 45 min (all antibodies from Jackson ImmunoResearch; final concentration of all antibodies, 1.5 µg/mL; diluted in 5% FCS/PBS). To confirm the

specificity of fluorescent staining, samples were incubated with secondary antibody controls. After three washes in H/S with 0.05% Tween-20 and a final wash with H/S, cells were mounted on glass microscope slides with Mowiol (Kuraray Specialities Europe GmbH, Frankfurt, Germany). Cells were examined with a Leica TCS SP5 confocal microscope (Leica Microsystems, Wetzlar, Germany).

3.10 Determination of bacterial binding and internalization

BMDMs were left uninfected or were infected with BCG-GFP for the indicated time, washed in cold PBS buffer and incubated with cold PBS on ice for 15min. Cells were harvested and either fixed with 4% PFA for 10min at room temperature or processed to quench adherent bacteria. For quenching the fluorescence of adherent bacteria, 500 µl trypan blue (0.4% w/v in PBS, Corning Inc., NY, USA) was added after the first acquisition and 1 min before the second acquisition. Quenching with trypan blue reduced the FITC fluorescence of adherent bacteria by excitation energy transfer (Hed, 1986; Szollosi et al., 1984). Attune NxT flow cytometry (Thermo Fisher Scientific) analyzed cells with bound or internalized bacteria (without trypan blue treatment) and cells with internalized bacteria (with trypan blue treatment).

3.11 Histopathologic assessment

Mice livers and spleens were collected, embedded in Tissue-Tec (Sakura Finetek USA, Torrance, CA, USA), and shock-frozen in liquid nitrogen. 6 µm-thick sections were cut with a cryotome (CM1850 UV, Leica Microsystems). For staining, sections were air-dried for at least 15 min and fixed in ice-cold acetone for 10 min. After a washing step with PBS, tissues were air-dried for 20 min, stained with the Truant TB Fluorescent Stain Kit (Becton Dickinson) as described above. The fluorescent staining of mycobacteria (Truant) was performed according to the manufacturer's instructions. For evaluation of bacterial numbers in granulomas, single bacteria were counted in serial sections. Samples were analyzed with an inverted fluorescence microscope or a confocal microscope (DMIRE2; Leica Microsystems).

For hematoxylin and eosin (H&E) staining, liver and spleen sections were prepared as above and stained for 20 min with Mayer's hematoxylin solution (hematoxylin, Roth). Samples were washed in water for 15 min, stained for an additional 2 min with 1% eosin solution, washed with water, dehydrated in ethanol, embedded in Eukitt mounting medium (Sigma-Aldrich), and analyzed on a Leica DMIRE2 microscope. The bacterial number was calculated with a 100×oil lens and an inverted fluorescence microscope.

Oil Red O staining was performed according to the manufacturer's instruction. Briefly, liver sections were fixed with 4% paraformaldehyde for 15 min. Slides were washed, incubated in 85% Propylene Glycol for 2 min, stained with 0.5% Oil red O (Abcam, Cambridge, UK) for 1 hr at room temperature, differentiated in 85% propylene glycol for 1min, counterstained with Mayer´s hematoxylin solution to stain nuclei for 30 sec and imaged by Leica DMIRE2 microscope with a ×100 objective lens.

3.12 Quantification of bacterial numbers

To count BCG colony forming units (CFUs) in tissue, liver, and spleen from infected mice were collected, added 5 mg/mL saponin (Serva Electrophoresis GmbH, Heidelberg, Germany) in H/S, and homogenized. The homogenates were incubated for 30 min at 37°C for the release of intracellular bacteria. Samples were centrifuged for 2 min at 1000 rpm; the supernatant was diluted in PBS and plated on Middlebrook 7H10 agar plates enriched with OADC (Becton Dickinson). For CFU assays *in vitro*, infected cells were washed once with HEPES after various infection times to remove non-adherent bacteria and were then lysed in 3 mg/mL saponin for 30 min at 37°C. 100 µL aliquots were plated, and bacteria were counted after 2 weeks incubation in a humidified 37°C atmosphere.

3.13 Depletion and reconstitution of macrophages in mice

Liposomes (Liposoma B.V) were stored at 4 °C and calibrate to room temperature 2hrs before injection. For macrophages depletion, clodronate or PBS liposomes (200 µL) were injected intravenously. For reconstitution, macrophages were generated by

culturing bone marrow cells as described before in section 3.2. 24 hrs after depletion, mice were left untreated or intravenously injected with 10^6, 5×10^6 or 10^7 BMDMs. Mice were sacrificed indicated days after BMDMs transplantation. Liver, spleen, and bone marrow were collected for detection of macrophages by Attune NxT flow cytometer (ThermoFisher scientific).

3.14 Flow cytometry

Cells suspension were harvested from the bone marrow, liver, and spleen and adjusted to the concentration of $1x10^6$ cells/ 50 μL in PBS. Cells were incubated for 30 min at 4°C with anti-mouse CD16/32 antibody to block Fcγ receptors followed by incubation with primary antibodies for 45 min at 4°C. After washing 2 times with PBS, cells were re-suspended in PBS and acquired with Attune NxT flow cytometer.

Fluorochrome-conjugated mAbs specific to mouse PE-Gr-1 (Ly6G/C; clone RB6-8C5), Brilliant Violet-CD115 (clone AFS98), Pacific Blue-CD11b (clone M1/70), PerCP-CD3 (clone 145-2C11), PerCP-CD45R/B220 (clone RA3-6B2), PerCP-Ter119 (clone TER-119), APC-F4/80 (clone BM8), PE/Cy7-NK1.1 (clone PK136), were purchased from Biolegend. Multiparameter analyses of stained cell suspensions were performed on and analyzed with FlowJo software v10 (LLC, Ashland, Oregon).

3.15 Statistical analysis

Data are expressed as arithmetic means ± standard deviation (SD) unless otherwise indicated. Statistical analysis was performed with Student's *t*-test for single comparisons or with analysis of variance (ANOVA) for multiple comparisons. Statistical significance was set at the level of $p \leq 0.05$. All data were obtained from independent measurements. The GraphPad Prism statistical software program (GraphPad Software, La Jolla, CA, USA) was used for analysis.

4 Results

4.1 Role of the Nsm in mycobacterial infection

4.1.1 BCG infection of macrophages leads to rapid activation of the Nsm and migration/clustering of macrophages

A previous study shows an important role of the Nsm in mycobacteria infection via negatively regulating autophagy (Li et al., 2016), while the role of Nsm in mediating granuloma, a hallmark in mycobacterial infection, is mostly unknown.

To identify the initial events of Nsm-dependent granuloma formation, BMDMs from Wt mice and mice heterozygous for Nsm ($Nsm^{+/-}$) were isolated. BMDMs were left uninfected or were infected with BCG for the indicated time periods.

Upon BCG infection, rapid activation of Nsm was observed in Wt BMDMs; it was approximately two-fold higher in infected cells than that in uninfected BMDMs. Nsm activity in Wt BMDMs rapidly reached a peak at 5 min post infection (mpi) and subsequently returned to baseline levels (Figure 9A). In contrast, Nsm activity remained at basal levels in $Nsm^{+/-}$ BMDMs upon BCG infection (Figure 9A).

Interactions of mycobacteria-containing macrophages initiate granuloma formation (Davis et al., 2002). Therefore, macrophages clusters were investigated 10 to 30 hrs after the initiation of infection (Figure 9B and 9C). Macrophage clusters were observed 10 hours post infection (hpi) in both genotypes of BMDMs, while approximately 1.5 fold more clusters were induced in Wt BMDMs compared to in $Nsm^{+/-}$ BMDMs. The numbers of macrophage clusters increased rapidly in Wt BMDMs but were nearly absent in $Nsm^{+/-}$ BMDMs at 20 hpi and 25 hpi (Figure 9C). Besides, Wt BMDMs formed multiple large clusters upon BCG infection, whereas $Nsm^{+/-}$ BMDMs formed clusters which were markedly reduced in both size and number (Figure 8B and 8C). At 25 hpi, the number of BMDM clusters reached the peak in both Wt, and $Nsm^{+/-}$ BMDMs, but Wt BMDMs generated approximately twice more macrophage clusters compared to $Nsm^{+/-}$ BMDMs after infection with BCG at this time point (Figure 9C).

To assess the contribution of Nsm in modulating the mycobactericidal activity of macrophages, the numbers of intracellular bacteria in macrophages were determined

by CFU assay after 25 hrs of infection, which is the peak time for cluster formation. The results shown in Figure 9D revealed that BMDMs from Wt mice exhibited a higher bacterial burden than Nsm$^{+/-}$ BMDMs (Figure 9D).

Taken together, these results indicate that the Nsm plays an important role in macrophage clustering and reducing bacterial burden in macrophages upon BCG infection.

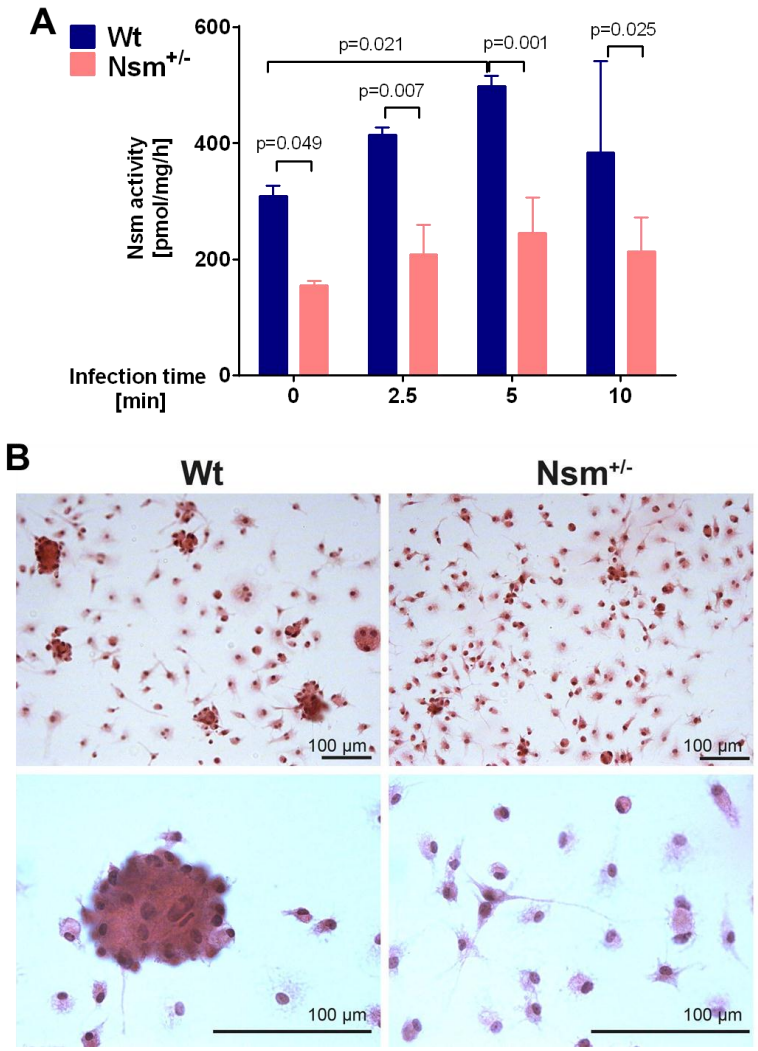

Figure 9. Nsm is activated and mediates macrophage clustering upon BCG infection in vitro.

(A) BMDMs were infected and lysed, and the activity of Nsm was determined by the consumption of BODIPY FL C_{12}-sphingomyelin. Samples were extracted and separated on TLC plates, which were then scanned with a Typhoon laser scanner. Shown are the means ± standard deviation (SD) of 3 independent experiments, the p-value is given as determined by ANOVA followed by Bonferroni's multiple comparisons test. **(B)** BMDMs were infected for 25 hrs, fixed, and stained with hematoxylin and eosin (H&E). Macrophage clusters were observed with a 40x lens by light microscopy. The scale bar represents 100 µm. The pictures represent the results of 4 independent experiments.

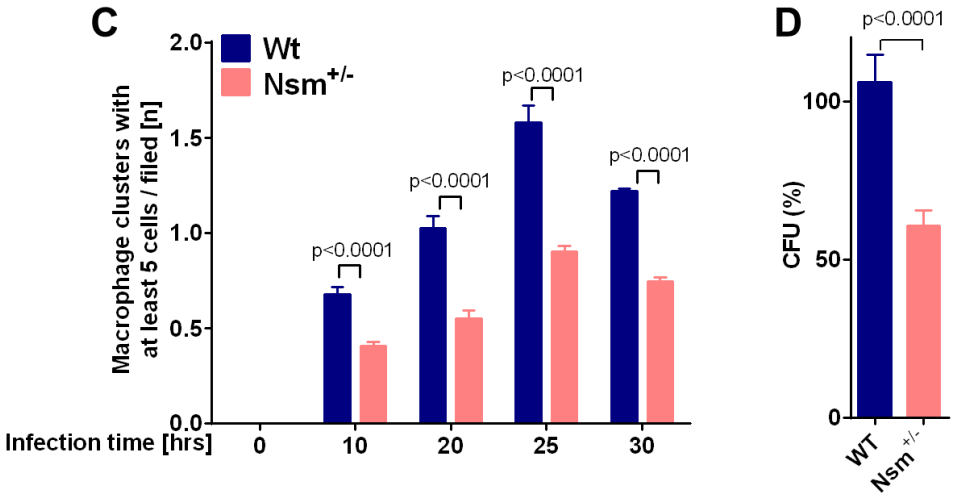

Figure 9C-D. Nsm is activated and mediates macrophage clustering upon BCG infection *in vitro*.

(C) Macrophage clustering was quantified by counting clusters in 100 fields per sample by light microscopy (40x lens). Shown are the means ± SD of 4 independent experiments. The exact p-values are determined by ANOVA followed by Bonferroni's multiple comparisons test. **(D)** Wt or Nsm$^{+/-}$ BMDMs were infected with BCG for 25 hrs, and the number of colony-forming units (CFUs) was determined after 2 weeks of culture. Shown are the means ± SD of the CFUs from 4 independent experiments. The quantitative analysis was performed with GraphPad and analyzed with t-test, an exact p-value is given.

4.1.2 Nsm dependent cytoskeleton redistribution orchestrates the migration /clustering of macrophages

Actin cytoskeleton dynamics play a crucial part in most cell movement processes, mediating the formation of cellular structures such as lamellipodia, filopodia, stress fibers, and focal adhesions (Bailly and Condeelis, 2002; Lee and Dominguez, 2010; Parsons et al., 2010). These findings led to the question whether the increase in macrophage cluster formation is linked to a redistribution of the cytoskeleton in macrophages after BCG infection.

Actin architecture in BMDMs isolated from Wt and $Nsm^{+/-}$ mice was first studied by staining F-actin with Alexa Fluor 647or 555-labeled phalloidin (Figure 10A). In Wt BMDMs, F-actin was enriched in extended broad lamellipodia 1 hr after BCG infection. However, infected $Nsm^{+/-}$ BMDMs exhibited a striking reduction in actin stress fiber formation, with an accentuated cortical localization, and minimal lamellipodia (Figure 10A). After 6 hrs of infection, Wt BMDMs showed remarkable F-actin lamellipodia and elongated filopodia (see arrows), which induced cellular recruitment. This effect was abolished entirely in $Nsm^{+/-}$ BMDMs. After 25 hrs of infection, actin depolymerized and formed cellular aggregates in both Wt and $Nsm^{+/-}$ BMDMs (Figure 10A).

Rac1 has been shown to interact with and regulate the actin cytoskeleton (Etoc et al., 2013; Guo et al., 2006). The results here revealed that BCG induced a marked activation of Rac1 as early as 30 min after infection in Wt BMDMs but not in $Nsm^{+/-}$ BMDMs (Figure 10B). Likewise, immunofluorescence studies showed that at 25 hpi Rac1 was strongly expressed upon BCG infection at 25 hpi in Wt BMDMs, while almost absent in $Nsm^{+/-}$ mice (Figure 10C). These findings indicated that BCG activated Rac1 in an Nsm-dependent manner.

To investigate whether the cytoskeleton redistribution and Rac1 activation are related to the formation of macrophage clusters, macrophage migration was determined upon pretreating BMDMs with an inhibitor of Rac1 (NSC23766) for 1 hr before infection with BCG (Figure 10D). Microscopic examinations revealed that the formation of clusters at 25 hpi in Wt BMDMs was decreased after Rac1 inhibitor treatment.

Taken together, both early and late events of the Nsm-dependent cytoskeleton reorganization are involved in lamellipodia extension and filopodia protrusion during cell migration and lead to the formation of macrophage clusters.

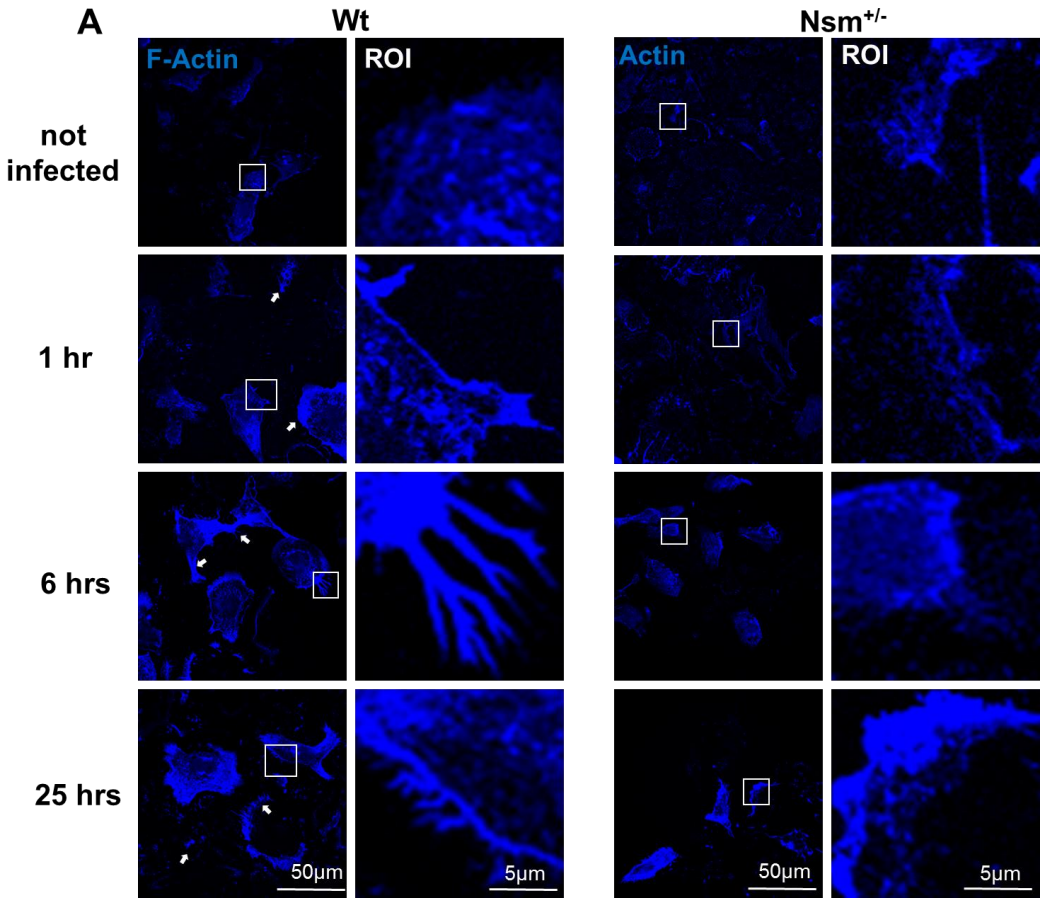

Figure 10. Nsm regulates cytoskeleton rearrangement in BMDMs after infection. **(A)** BMDMs were left uninfected or infected with BCG for 1 hr, 6 hrs, or 25 hrs. Cells were then fixed and stained with Alexa Fluor 555 phalloidin. The samples were analyzed by confocal microscopy. Shown are representative pictures of four independent studies. The scale bar is 50 µm, for the region of interest (ROI) 5 µm.

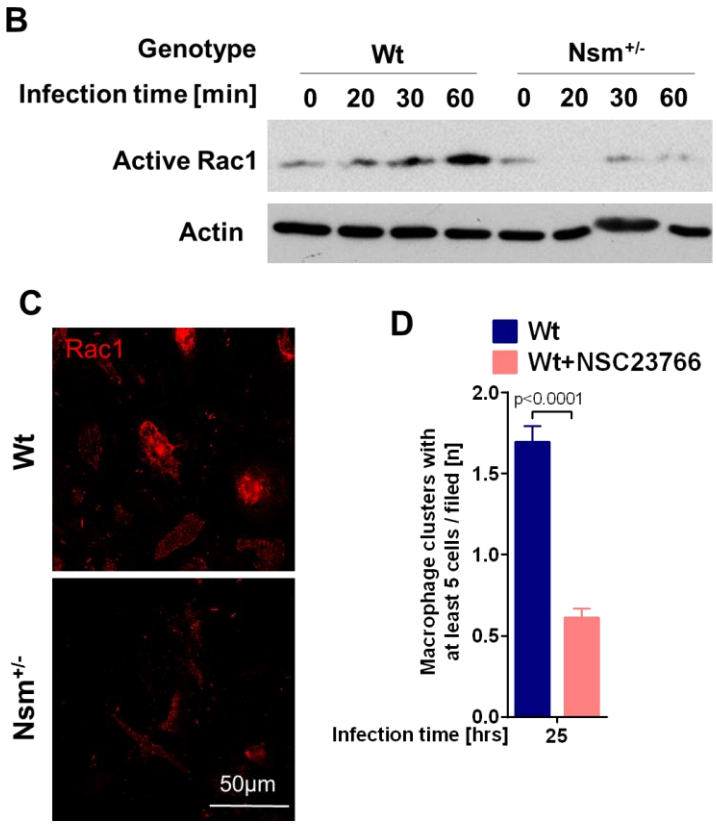

Figure 10B-D. Nsm regulates cytoskeleton rearrangement and Rac1 activity in BMDMs upon BCG infection.

(B) Rac1 activation was determined for indicated times by pull-down assays from lysates obtained from BCG-infected or non-infected BMDMs. Shown are representative results of 3 independent studies. **(C)** BMDMs were infected with BCG for 60 min and stained with Cy3-coupled Rac1. The samples were analyzed by confocal microscopy. Shown are representative microscopic images of 3 independent studies. The scale bar is 50 µm. **(D)** BMDMs from Wt mice were left untreated or pretreated with the Rac1 inhibitor NSC23766 for 1 hr and were infected for 25 hrs, fixed, and stained with hematoxylin and eosin (H&E). Macrophage migration/clustering was quantified by counting macrophage clusters in 100 fields. Shown are the means ± SD of 3 independent experiments, the p-value was determined by *t*-test.

4.1.3 Nsm-dependent migration/clustering of infected macrophages is mediated by a signaling cascade from p38K and JNK via β1-integrin to Rac1 and actin

Previous studies of human TB granulomas revealed that active β1-integrin controls granuloma formation and that the Asm/ceramide system leads to the activation and clustering of β1-integrin in melanoma cells and the upper-airway epithelial cells from mice and humans with cystic fibrosis (CF) (Carpinteiro et al., 2015; Grassme et al., 2017; Puissegur et al., 2007). These findings led to the hypothesis that active β1-integrin is involved in Nsm-dependent granuloma formation upon BCG infection.

Therefore, active surface β1-integrin was measured by immunoprecipitation at several time points upon BCG infection. Integrin activation was detected as early as 30 min after BCG infection in Wt BMDMs. In sharp contrast, integrin activation was almost completely absent in $Nsm^{+/-}$ BMDMs after bacterial infection (Figure 11A and B).

To determine whether active β1-integrin orchestrates cell movement and macrophage clusters, the effect of active β1-integrin on actin cytoskeleton organization and Rac1 activity was investigated, To this end, surface β1-integrin of infected macrophages were blocked by using anti-β1-integrin antibodies. The F-actin in untreated Wt BMDMs was enriched in extended lamellipodia 1 and 6 hrs after BCG infection, while the actin architecture in Wt BMDMs, which were pretreated with anti-β1-integrin antibodies, was largely organized into cytoplasmic structures and disappeared from sites of cell-cell contact (Figure 11 C) which is similar to $Nsm^{+/-}$ BMDMs (Figure 11A). In parallel, Rac1 activity in Wt cells upon 30 or 60 min infection was dramatically reduced after the blockade of active integrin (Figure 11 D).

These findings indicate that activation of β1-integrin is necessary for the formation of actin stress fibers and the activation of Rac1 in BMDMs upon BCG infection.

To investigate the function of active β1-integrin in macrophage migration and clustering upon BCG infection, BMDMs were infected for 25 hrs, and β1-integrins on cells were neutralized by treating them with anti-β1-integrin antibodies every 5 hrs after initiation of the infection (for a total of 5 times). The neutralization of β1-integrin substantially reduced the size and number of macrophage clusters formed by Wt BMDMs, whereas it did not affect macrophage clusters formed by $Nsm^{+/-}$ BMDMs (Figure 11 E).

Upon mycobacterial infection, mitogen-activated protein kinases (MAPKs) orchestrate the signaling pathways in macrophages, especially p38 mitogen-activated protein kinase (p38K), extracellular signal-regulated kinase (ERK), and c-Jun NH2-terminal kinase (JNK) (Bonay et al., 2015; Schorey and Cooper, 2003; Shin et al., 2010).

To identify further signaling events that link Nsm activation with macrophage migration/clustering after infection with BCG, the phosphorylation of p38K and JNK at various time points after infection were monitored (Figure 11F-H). The results revealed significant phosphorylation of p38K and JNK in Wt BMDMs after 30 or 60 min, whereas the levels of phosphorylated p38K and JNK were much lower in $Nsm^{+/-}$ BMDMs upon BCG infection (Figure 11F-H). Measurement of the phosphorylated extracellular regulated kinase (pERK) showed no difference between Wt and $Nsm^{+/-}$ BMDMs upon BCG infection (results not shown).

To investigate whether Nsm-dependent activation of p38K/JNK is connected to β1-integrin stimulation or macrophage migration, Wt BMDMs were pretreated for 1 hr with anti-β1-integrin antibodies and then infected with BCG for various time periods. These experiments revealed that the blockade of active β1-integrin on cells did not change the phosphorylation level of either p38K or JNK (data not shown). In contrast, pretreatment of macrophages with specific inhibitors of JNK (SP600125) or p38K (SB203580) for 1 hr prior infection with BCG prevented BCG-induced β1-integrin activation, whereas, the solvent dimethyl sulfoxide (DMSO) was without effect on β1-integrin activation by BCG (Figure 11I-J). These findings indicated that p38K and JNK are upstream of β1-integrin activation.

Taken together, these findings suggest that BCG modulates macrophage migration/clustering through Nsm-dependent p38K/JNK phosphorylation and subsequent β1-integrin activation.

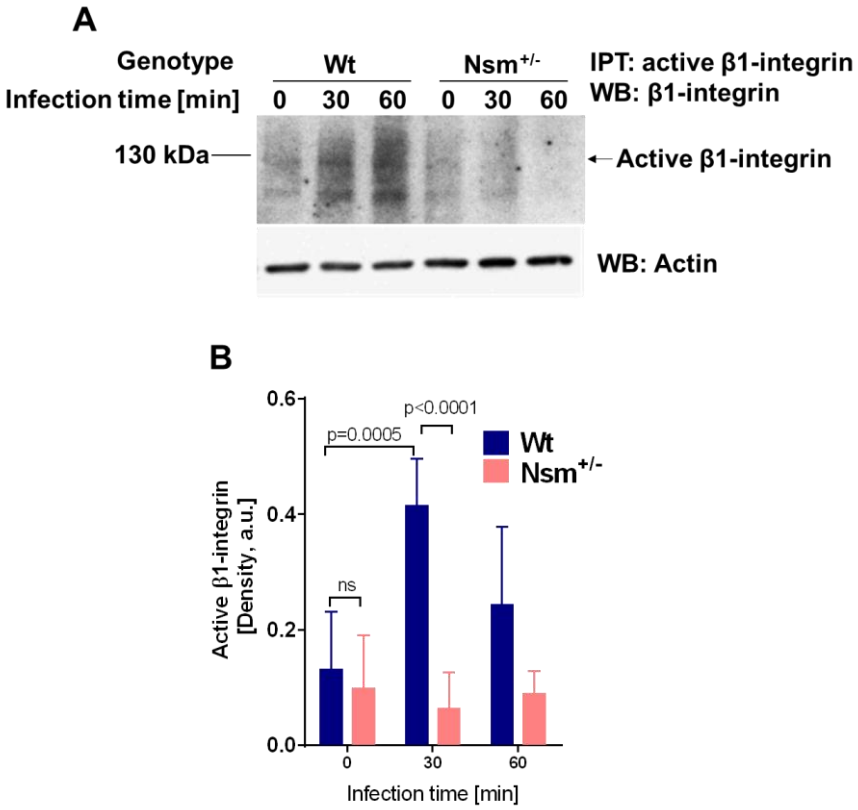

Figure 11. Nsm-dependent migration and cytoskeleton redistribution of BCG-infected macrophages is mediated by β1-integrin and regulated by p38K and JNK. (**A**) Active β1-integrin expression on the surface of wild-type (Wt) and neutral sphingomyelinase heterozygous ($Nsm^{+/-}$) bone marrow-derived macrophages (BMDMs) was determined after Bacillus Calmette–Guérin (BCG) infection for 30 or 60 min by immunoprecipitation. Shown is a representative result from 4 independent experiments. (**B**) Quantitative analysis of activation of β1-integrin immunoprecipitation. Shown is the mean ± SD, n = 4, of the density of the western blots as determined by ImageJ, given in arbitrary units (a.u.). P-values were determined by ANOVA followed by Bonferroni's multiple comparisons test.

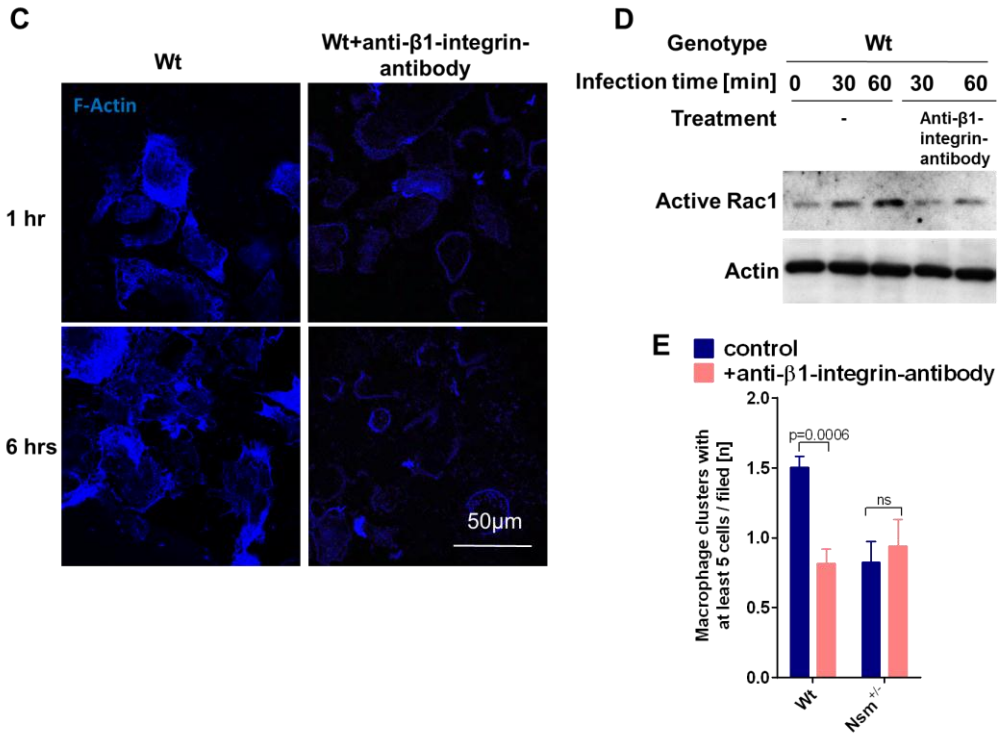

Figure 11C-E. Nsm-dependent migration and cytoskeleton redistribution of BCG-infected macrophages is mediated by β1-integrin and regulated by p38K and JNK. **(C)** Wt bone marrow-derived macrophages (BMDMs) were left untreated or pretreated with anti–β1-integrin-antibody 9EG7 for 1 hr and were then infected with BCG for 1 or 6 hrs, fixed and stained with Alexa Fluor 647-labeled phalloidin. The samples were analyzed by confocal microscopy. Shown is a picture representing 4 independent studies. The scale bar is 50 µm. **(D)** Wt BMDMs were left untreated or pretreated with anti-β1-integrin-antibody 9EG7 for 1 hr and were then left uninfected or infected with BCG for the indicated time. Rac1 activity was detected with a Rac1 pull-down assay. **(E)** Wt or $Nsm^{+/-}$ BMDMs were infected with BCG for 25 hrs and either left untreated or treated with anti–β1-integrin-antibody 9EG7 every 5 hrs after initiation of infection, for a total of 5 times. The samples were stained with hematoxylin and eosin (H&E), and the number of macrophage clusters was counted in 100 fields per infection experiment (total of 300 fields were counted). Given is the mean ± SD of three independent experiments. P-values were determined by ANOVA followed by Bonferroni's multiple comparisons test.

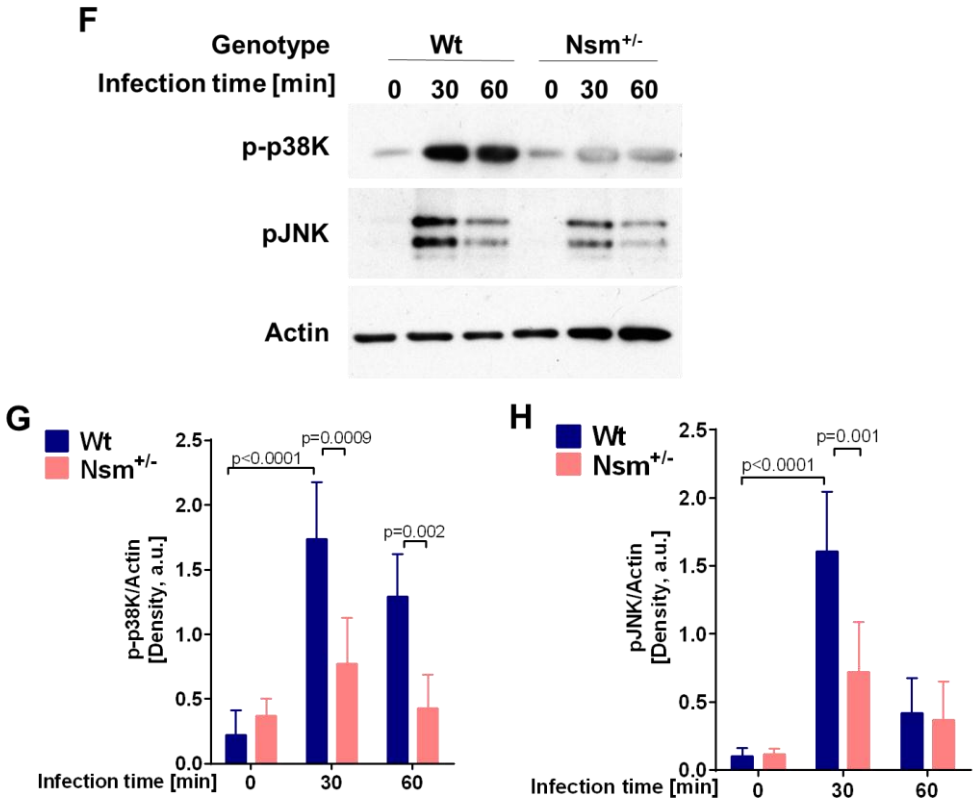

Figure 11F-H. Nsm-dependent migration and cytoskeleton redistribution of BCG-infected macrophages is mediated by β1-integrin and regulated by p38K and JNK. (**F-H**) Wt or Nsm$^{+/-}$ BMDMs were infected with BCG for the indicated periods of time and were then subjected to Western blot analysis using antibodies of p-p38K, p-c-Jun NH2 terminal kinase (p-JNK), and β-actin (**F**). The western blot is representative of 4 independent experiments. Panel **G** and **H** displays the quantification of the phosphorylation of p38K and JNK performed using ImageJ, given in arbitrary units (a.u.). Shown is the mean ± SD of four experiments, p-values were calculated by ANOVA followed by Bonferroni's multiple comparisons test.

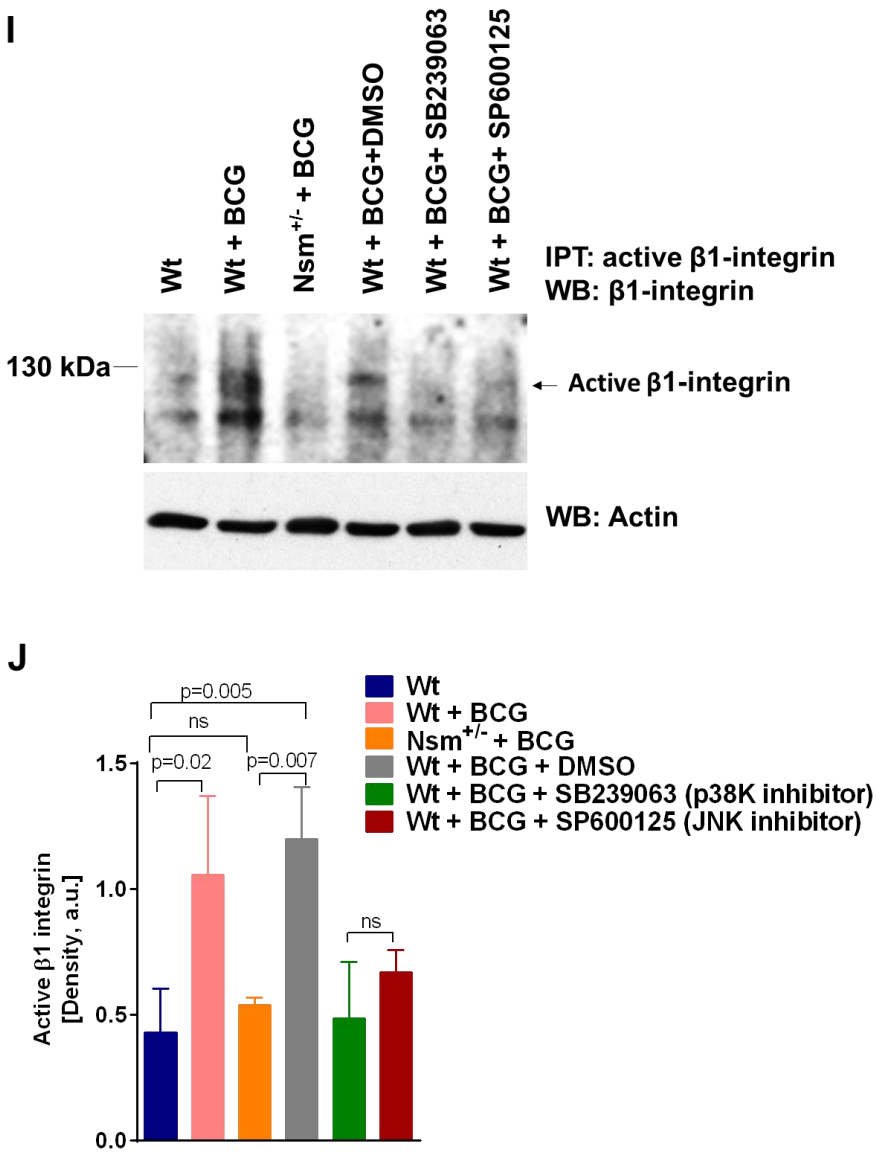

Figure 11I-J. Nsm-dependent migration and cytoskeleton redistribution of BCG-infected macrophages is mediated by β1-integrin and regulated by p38K and JNK. (**I, J**) Expression of active β1-integrin on the cell surface of Wt BMDMs after BCG infection for 30 min was measured after pretreatment with SB239063 (10 µM), SP600125 (10 µM), or DMSO for 1 hr. (**I**) Shown is a representative western blot results of three independent experiments. (**J**) The quantification of the western blots performed using ImageJ, given in arbitrary units (a.u.), shown are the means ± SD. The exact p-values were given as determined by ANOVA followed by Bonferroni's multiple comparisons test.

4.1.4 Nsm is necessary for granuloma formation in mice upon BCG infection

To find out if the described *in vitro* findings are also relevant *in vivo*, Wt and $Nsm^{+/-}$ mice were intravenously infected with $1x10^7$ bacteria for various periods of time, and the role of Nsm in granuloma formation was investigated.

First, granuloma formation in livers from Wt and $Nsm^{+/-}$ mice was monitored after infection by H&E staining (Figure 12A). The results revealed that *in vivo* intravenous infection with BCG for one week induced only the formation of a small number of liver granulomas both in Wt mice and in $Nsm^{+/-}$ mice. Instead, three weeks after infection, the liver of Wt mice exhibited larger and more-mature granulomas than that of $Nsm^{+/-}$ mice. In fact, the liver of $Nsm^{+/-}$ mice exhibited 2-fold fewer granulomas after three weeks of infection than that of Wt mice (Figure 12A-B). Also, at this infection time point, three weeks after infection most granulomas in Wt mice contained a small fatty center surrounded by lymphocytes; this fatty center was not found in $Nsm^{+/-}$ liver granulomas indicating that granulomas in $Nsm^{+/-}$ mice were less mature than in Wt mice (Figure 12C).

After 6 weeks of BCG infection, number and size of granuloma in the livers of Wt mice was still impressive but slightly reduced in comparison to 3 weeks' infection, whereas almost no granulomas were found in the livers of $Nsm^{+/-}$ mice at this time point (Figure 12A-B). Granulomas were almost completely cleared from both Wt and $Nsm^{+/-}$ livers, 12 weeks after infection (Figure 12A-B).

Lipid droplets accumulation is considered to be the sole carbon source for mycobacteria making it essential for their survival and growth within granuloma (Peyron et al., 2008; Russell et al., 2009). Therefore, the appearance of lipid droplets was investigated by Oil Red O lipid staining in uninfected and infected liver sections from Wt and $Nsm^{+/-}$ mice. Light microscopy examination showed that no lipid droplets in uninfected livers but impressive lipid droplets in Wt mice after 3 weeks of infection, whereas the lesions from $Nsm^{+/-}$ mice had fewer lipid droplets compared to Wt mice (Figure 12D-E).

These findings indicate that the Nsm controls the formation of granulomas *in vivo*.

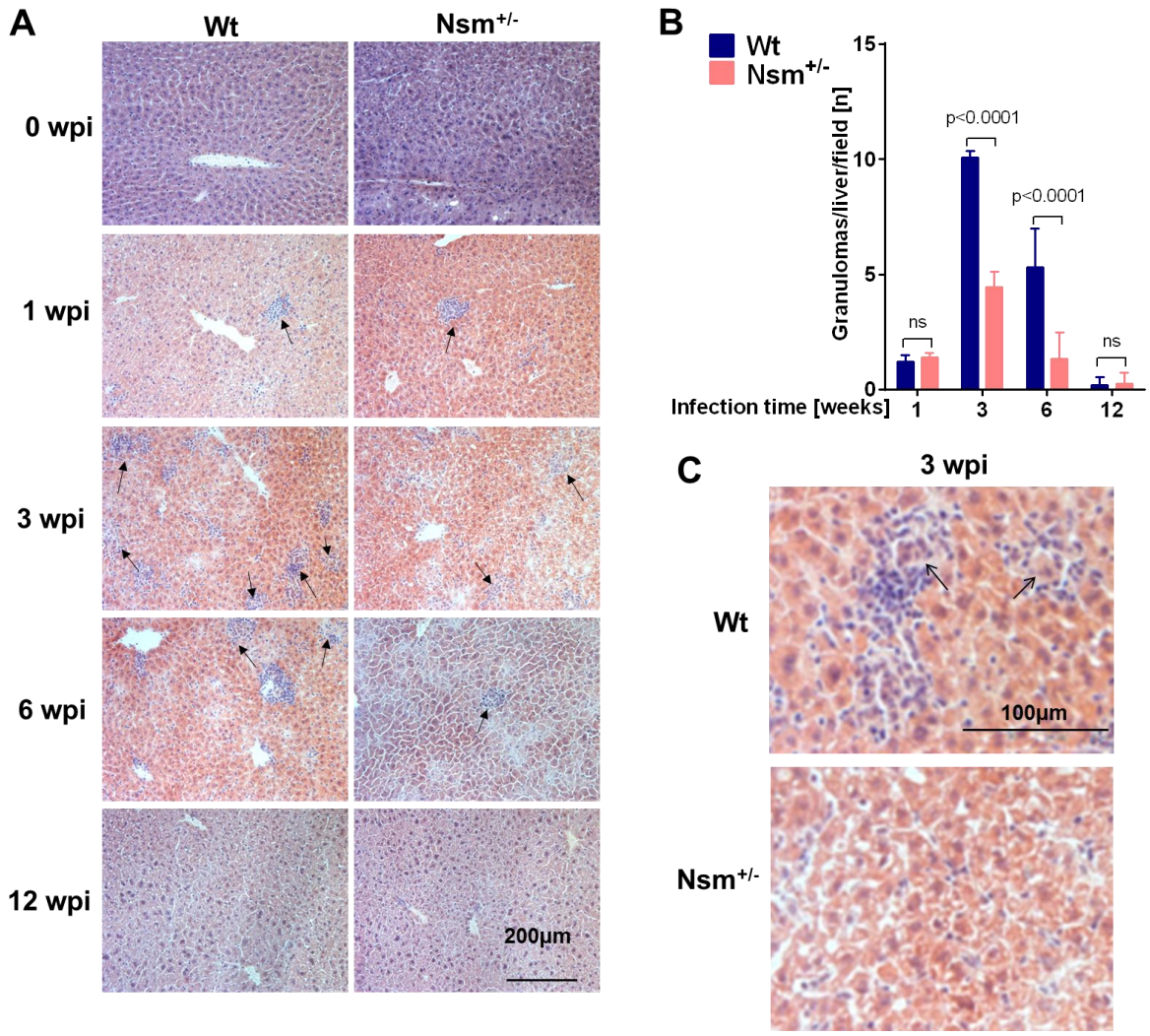

Figure 12. Nsm modulates granuloma formation in mice upon BCG infection.
(**A**) Wt or Nsm$^{+/-}$ mice were left uninfected (0 week post-infection, wpi) or infected with 10^7 BCG per mouse for 1 to 12 weeks (1-12 wpi). Cryosections of liver tissue were stained with hematoxylin and eosin (H&E) and analyzed by light microscopy with a 20x lens. Arrowheads indicate granulomas with a rather large core. Shown are pictures representative of four independent experiments. The scale bar represents 200 µm. (**B**) The number of granulomas from 1 to 12 wpi in murine liver tissue was determined by counting granulomas in 10 serial sections. Shown are the means ± SD of 3 independent experiments (a total of 30 sections was counted), ANOVA followed by Bonferroni's multiple comparisons test. **(C)** Granulomas in Wt liver were visualized by H&E staining. Shown are representative pictures of four independent experiments. The scale bar is 100 µm.

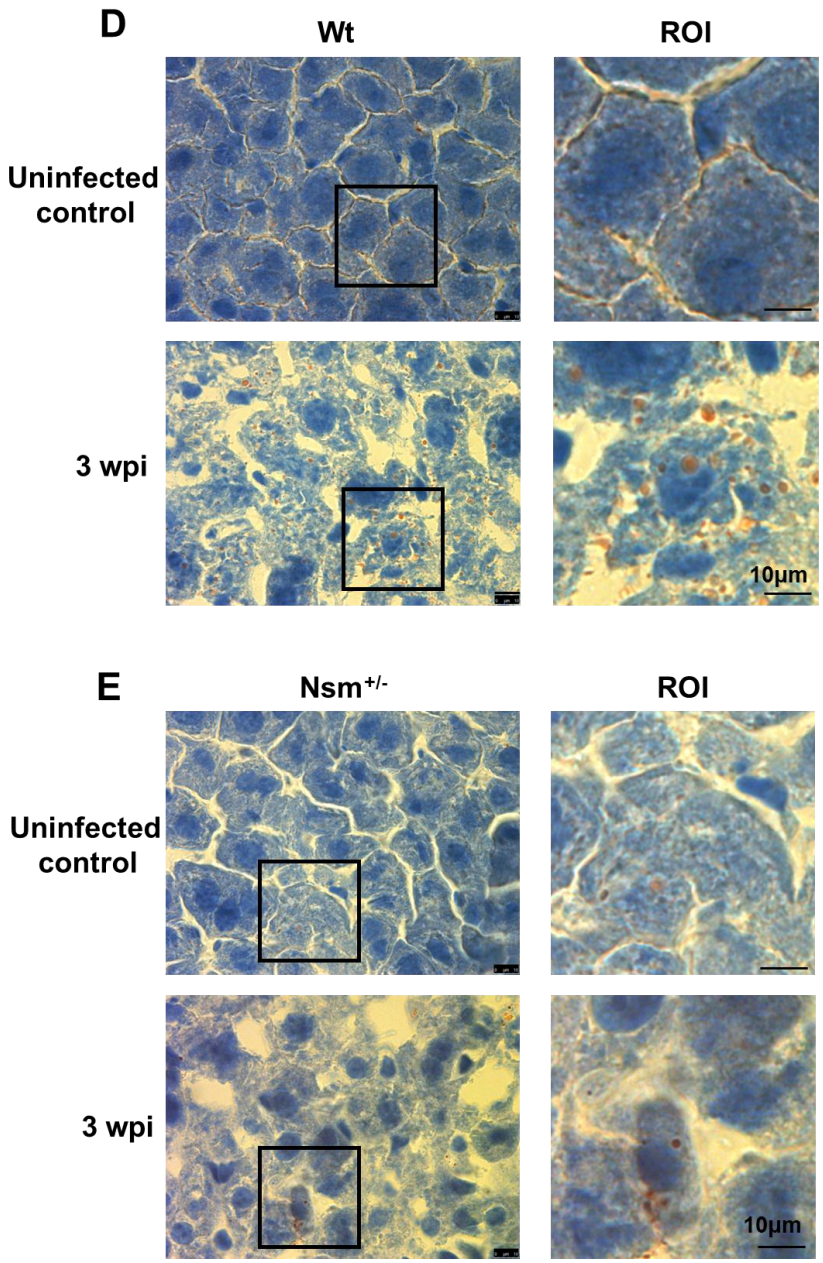

Figure 12 D-E. Nsm modulates granuloma formation in mice upon BCG infection. (D and E) Lipid droplets in liver sections from uninfected or 3 weeks infected (3 weeks post-infection, wpi) Wt **(D)** and Nsm$^{+/-}$ **(E)** mice were visualized with Oil Red staining and analyzed by light microscopy with a 20x lens. Shown are representative pictures of four independent experiments. The scale bars in overview and region of interest (ROI) pictures are 10 µm.

4.1.5 Blockade of Nsm-dependent β1-integrin activation reduces granuloma formation and improves host outcome upon BCG infection *in vivo*

To investigate the functional outcome of *in vivo* granuloma formation regulated by active β1-integrin, and to clarify whether these granulomas protect the host or serve as a favorable niche for bacteria, active β1-integrin was neutralized in vivo. Therefore, mice were first infected with 10^7 BCG, and then BCG-infected mice were treated with either anti-β1-integrin antibody or an isotype control antibody (3 times per week during the 3 weeks' infection period, a total of 9 times).

To determine the bacterial burden in the liver and spleen of Wt mice, which were left untreated or treated with anti-β1-integrin antibodies or isotype control antibodies, CFU assays were performed, and BCG in the tissues were stained with Truant dye. The results demonstrated that the bacterial numbers in livers and spleens were 40%-50% lower in Wt mice treated with anti-β1-integrin antibodies than in untreated Wt mice or mice treated with isotype control antibodies (Figure 13 A-C).

Consistent with the decreased bacterial burden, the results show that anti-β1-integrin antibodies treated Wt mice exhibited 40%- 60% fewer granulomas in the liver than untreated control mice or isotype control treated animals (Figure 13D). Furthermore, these granulomas were less organized and devoid of a large center (Figure 13E). Moreover, injection of anti-β1-integrin antibodies to Wt mice reduced the number of hepatic bacteria in granulomas compared to untreated mice or isotype control treated mice (Figure 13F).

Furthermore, Red Oil O staining revealed, that anti-β1-integrin antibodies treated Wt mice had dramatically reduced (but not absent) lipid droplet accumulations after 3 weeks of infection with BCG, compared to untreated or isotype control antibodies treated mice (Figure 13G).

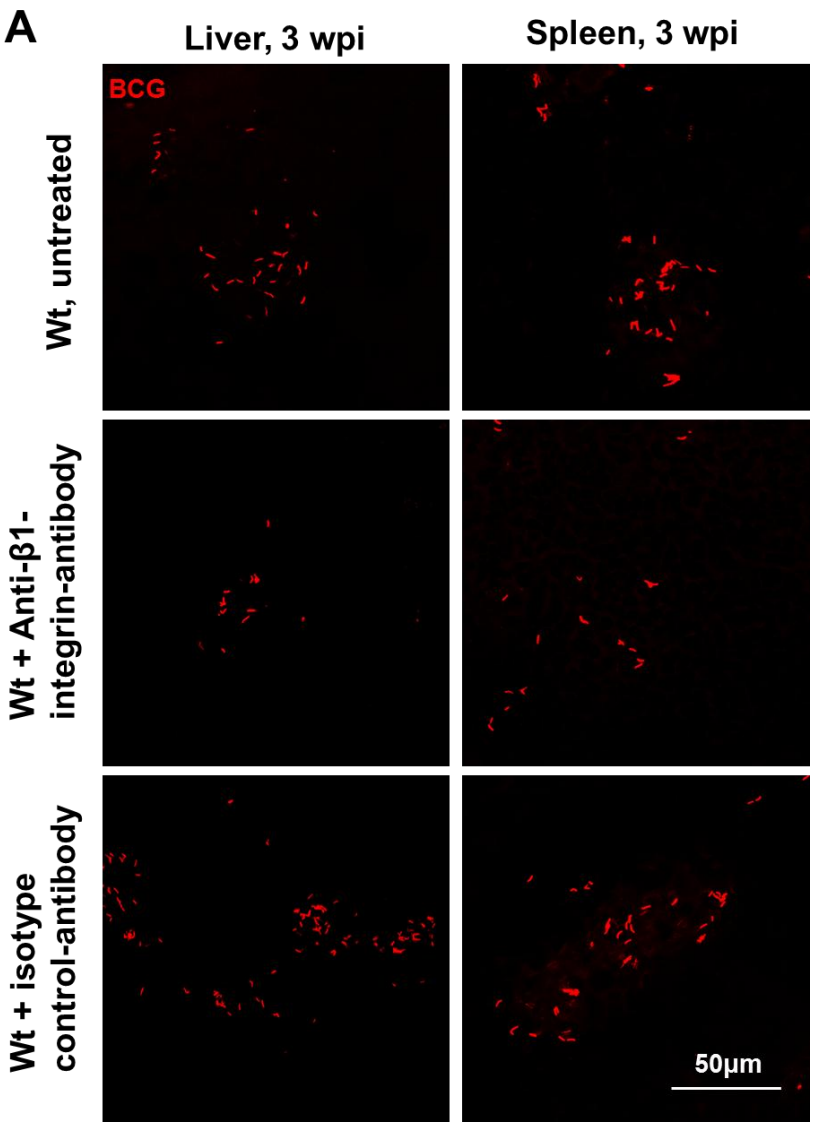

Figure 13. Blockade of β1-integrin leads to the increased killing of BCG and reduces granuloma formation *in vivo*.

(**A**) Wt or Nsm$^{+/-}$ mice were infected with BCG for 3 weeks with or without treatment with anti-β1 integrin antibodies (anti-β1-integrin-Abs) or its isotype control antibodies (isotype control-Abs) 3 times per week. Liver and spleens of those mice were stained with Truant dye for visualization of mycobacteria and analyzed by fluorescence microscopy. Shown are representative pictures of three independent experiments. The scale bar is 50 µm.

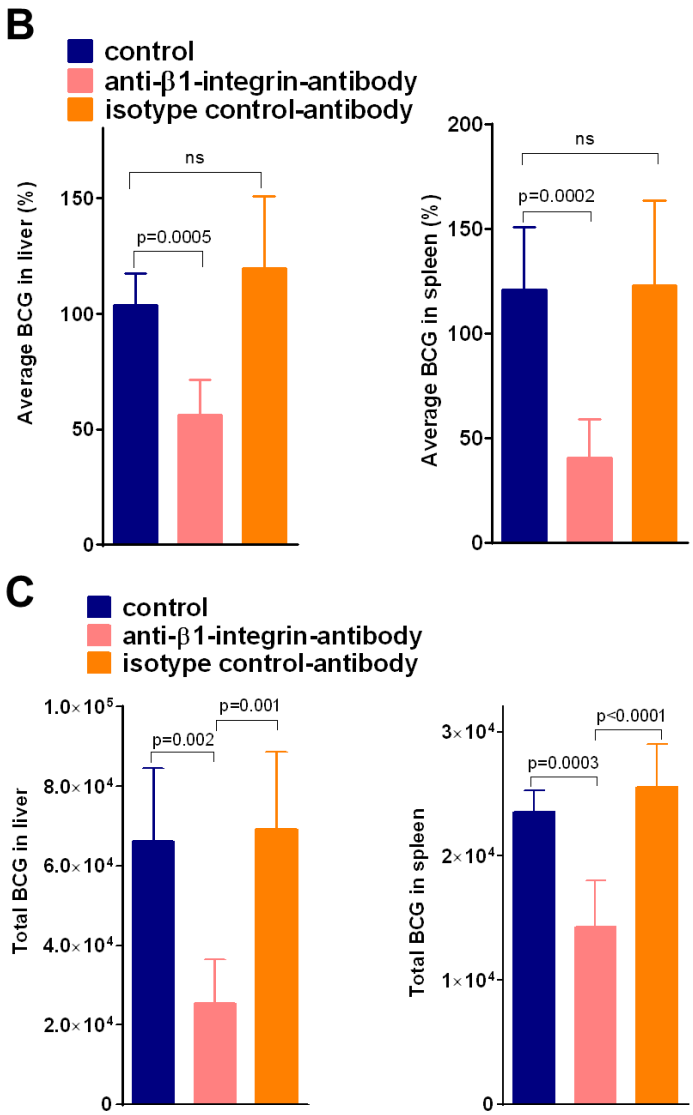

Figure 13B-C. Blockade of β1-integrin leads to the increased killing of BCG and reduces granuloma formation *in vivo*.

(**B**) Quantitative analysis of 10 serial sections/experiment was performed by fluorescence microscopy after Truant staining of the liver (left) and spleen (right) of 3 weeks infected untreated mice (control), and isotype or β1-integrin antibodies treated mice. Experiments were repeated 3 times. Shown are the means ± SD (in percent of control) of the number of bacteria in a total of 30 sections, the exact p-value is given as determined by ANOVA followed by Tukey's multiple comparisons test. (**C**) The total number of BCG in tissues homogenates of 3 weeks of infected untreated mice (control), and isotype or β1-integrin antibodies treated mice was determined by colony-forming unit (CFU) assays. Shown are the means ± SD of the numbers of BCG in liver (left) and spleen (right) tissue of at least 6 independent experiments, ANOVA followed by a Bonferroni's multiple comparisons test.

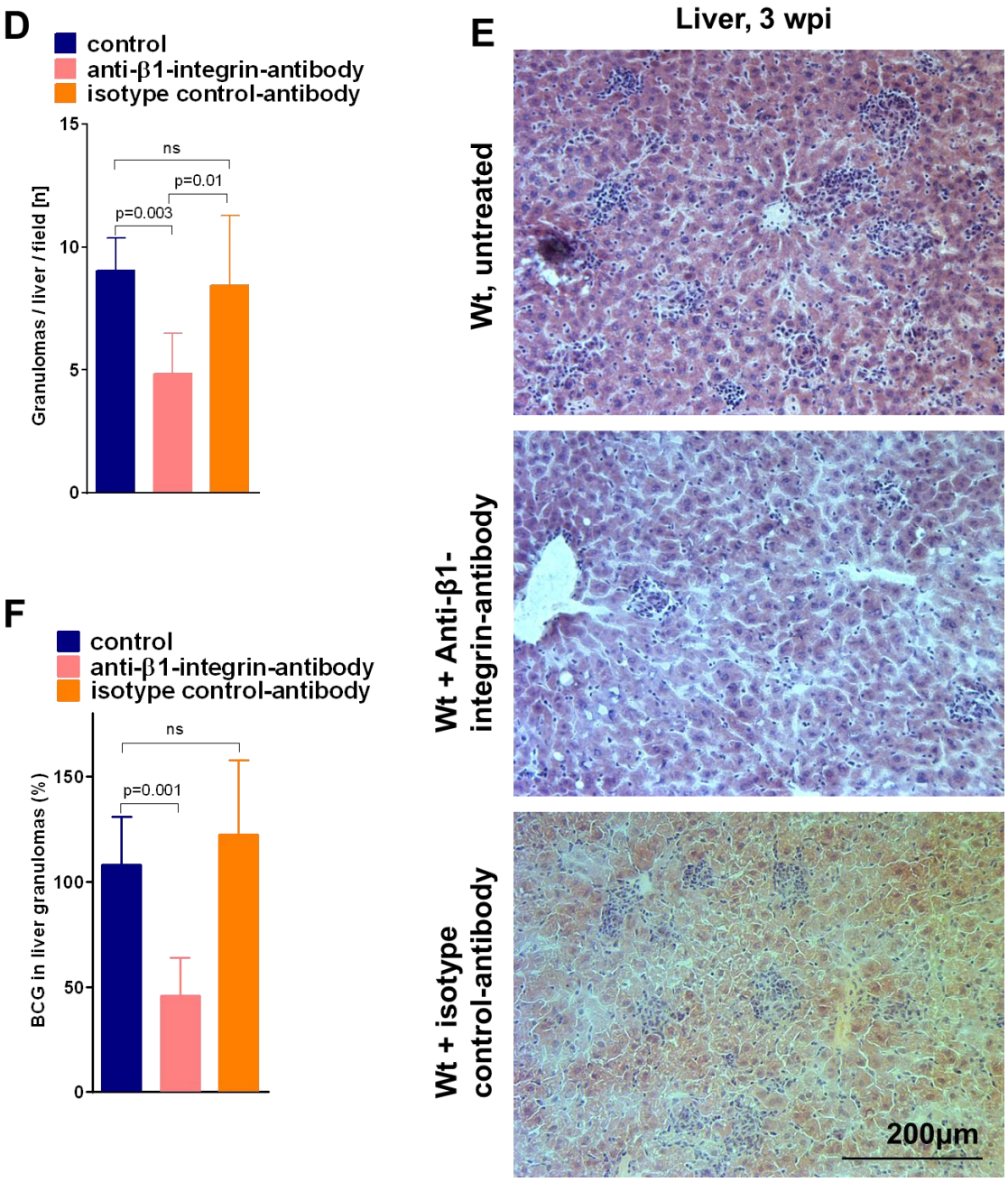

Figure 13D-F. Blockade of β1-integrin leads to the increased killing of BCG and reduces granuloma formation *in vivo*.

(**D**) The numbers of granulomas in the livers of 3 weeks infected untreated mice (control), and isotype control or β1-integrin antibodies treated mice were determined by counting in a total of 30 serial sections (10 sections per mouse tissue) by hematoxylin and eosin (H&E) staining. Shown are the means ± SD from 3 independent experiments, p-values were determined by ANOVA followed Tukey's multiple comparison tests. (**E**) Granulomas in the livers of untreated, isotype control or β1-integrin antibodies-treated mice were visualized by H&E staining. Shown are representative pictures of three independent experiments. (**F**) The number of BCG in granuloma from untreated mice (control) and isotype control or β1-integrin antibodies-treated mice were determined by counting 10 serial sections of Truant staining of liver tissues of 3 mice (total of 30 serial sections). Shown are the means ± SD, p-values were determined by ANOVA followed by Bonferroni's multiple comparisons test.

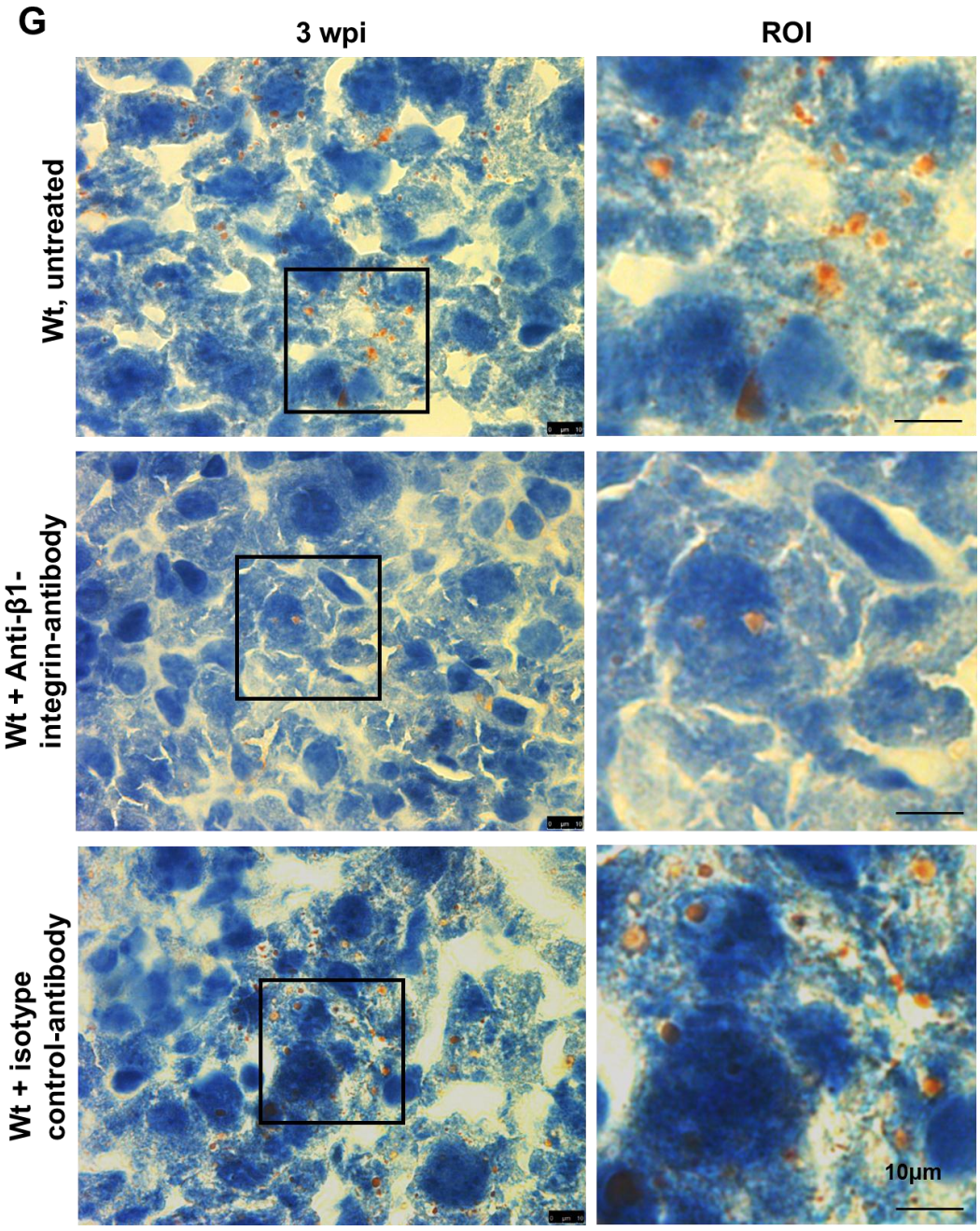

Figure 13G. Blockade of β1-integrin leads to the increased killing of BCG and reduces granuloma formation in vivo.

(**G**) Accumulation of lipid drops in infected liver sections of 3 weeks infected untreated mice and isotype control or β1-integrin antibodies-treated mice were visualized with Oil Red stain and analyzed by light microscopy with a 20x lens. Shown are representative pictures of 4 independent experiments. Scale bars in overview and region of interest (ROI) are 10 µm.

4.2 Role of Asm in mycobacterial infection

4.2.1 Asm deficient mice are more susceptible to BCG infection

To determine whether Asm plays a role in BCG infections *in vivo*, Wt and Asm deficient ($Asm^{-/-}$) mice were intravenously infected with 10^7 BCG.

These results revealed that CFUs in the livers of Wt mice were significantly reduced compared to $Asm^{-/-}$ at 1-day post-infection (dpi). Bacterial burden was 2 fold higher in $Asm^{-/-}$ livers than in Wt livers (Figure 14A). In comparison to 1dpi, the hepatic bacterial burden at 3 dpi was decreased by 80% in Wt mice and 70% in $Asm^{-/-}$ mice (Figure 14A). However, absolute hepatic bacterial numbers remained 60% higher in $Asm^{-/-}$ mice than Wt mice at 3 dpi (Figure 14A).

In spleen tissues, CFUs showed a similar result as in liver tissues at 1dpi. The bacterial burden in $Asm^{-/-}$ spleens was 1.5-2 fold higher than in Wt spleens after 1 day of infection (Figure 14B). Compared to 1 dpi, the splenic bacterial burden was reduced by 80% and 90% at 3 dpi in Wt and $Asm^{-/-}$ mice, respectively. In contrast to the difference in hepatic CFUs, splenic CFUs did not show a significant difference between Wt and $Asm^{-/-}$ at 3 dpi (Figure 14B). These data suggest a rapid control of bacterial infection in Wt mice in the early stages and indicate a less efficient bacterial killing in $Asm^{-/-}$ mice.

The numbers of granulomas and bacterial aggregates were monitored from 1 week to 3 weeks after infection (Figure 14C-F). Histological analysis showed that granulomas in livers were generated 3 weeks after infection (Figure 14C). The number of hepatic granulomas was 2-3 folds higher in Wt mice than in $Asm^{-/-}$ mice after 3 weeks of BCG infection (Figure 14D).

As granulomas cannot reflect the bacterial load *in vivo*, the bacterial burden was determined by CFU assay after 1 week and 3 weeks of infection. Wt mice showed a significantly lower hepatic bacterial burden compared to $Asm^{-/-}$ after 1 week and 3 weeks of infection (Figure 14E). Consistent with the results of CFUs in spleens observed at 3 dpi, no significant differences of splenic bacterial numbers were observed between Wt and $Asm^{-/-}$ mice at 1 wpi and 3 wpi (Figure 14F).

These data suggest that Asm, especially in the liver, regulates the immune response to BCG, limits the bacterial replication and potentially regulates granuloma formation.

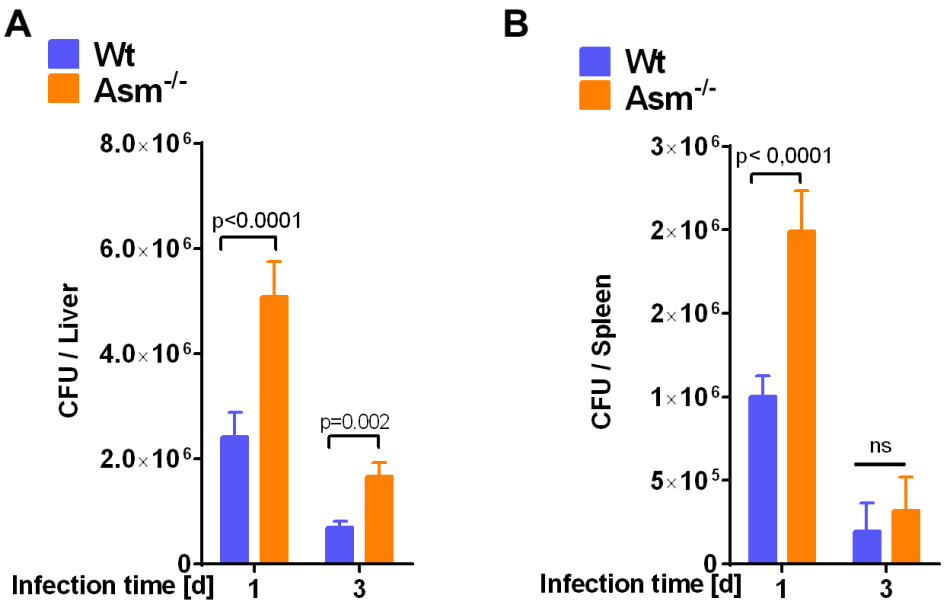

Figure 14. Acid sphingomyelinase deficiency enhances BCG infection *in vivo*.
(A-B) Wt or Asm$^{-/-}$ mice were infected with 10^7 BCG per mouse for 1 day or 3 days. The total number of BCG in liver **(A)** and spleen **(B)** tissue homogenates were determined by CFU assays. Shown are means ± SD of the numbers of bacteria in 6 independent experiments, p-values are given by ANOVA followed by Bonferroni's multiple comparisons test.

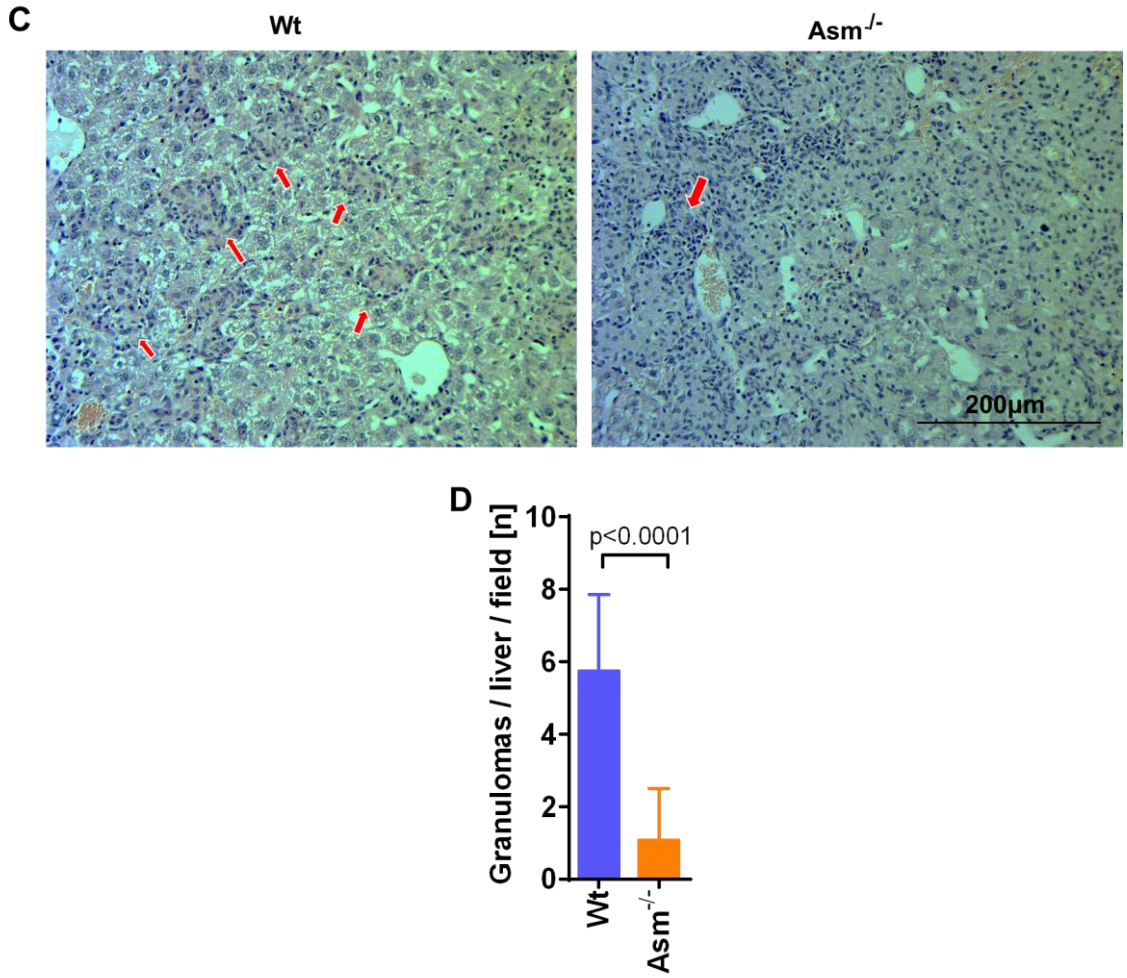

Figure 14C-E. Acid sphingomyelinase deficiency enhances BCG infection *in vivo*. **(C-D)** Wt or Asm$^{-/-}$ mice were infected with 10^7 BCG per mouse for 1 week or 3 weeks. **(C)** Cryosections of liver tissues 3 wpi were stained with H&E and analyzed by light microscopy with a 20 x lens. Arrows indicate granulomas. Shown are representative pictures of 3 independent experiments. **(D)** The number of granulomas in liver tissue (3 wpi) was determined by counting them after H&E staining in a total of 10 serial sections (3-4 sections per mouse liver). Shown are the means ± SD from, n = 6, *t-test*.

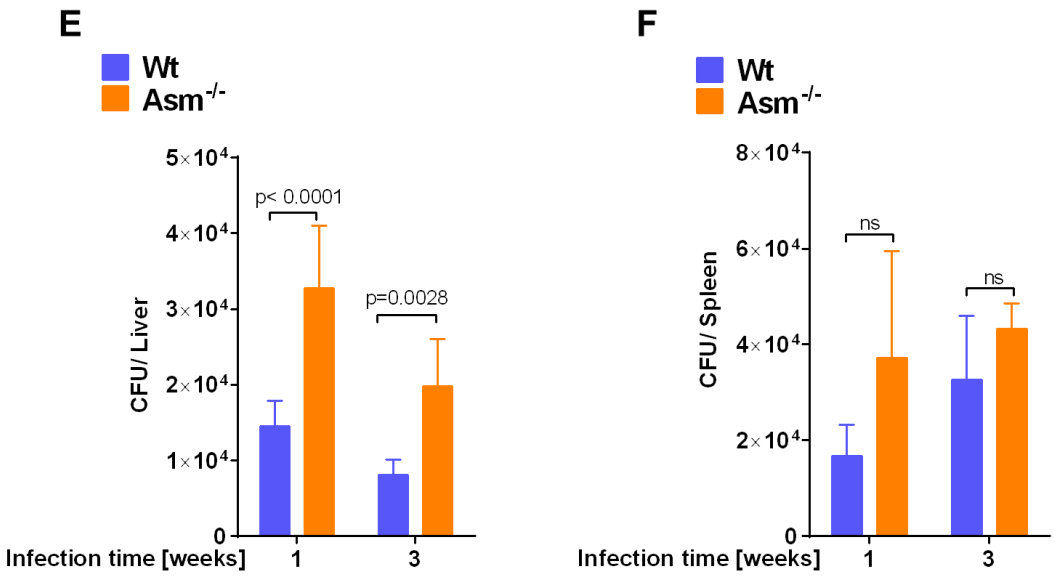

Figure 14E-F. Acid sphingomyelinase deficiency enhances BCG infection *in vivo*. **(E-F)** The total number of BCG in liver **(E)** and spleen **(F)** tissue homogenates was determined by CFU assays at 1 wpi and 3 wpi. Shown are means ± SD of bacterial numbers of 6 independent experiments, p-values are given by ANOVA followed by Bonferroni's multiple comparisons test.

4.2.2. Asm deficiency leads to enhanced bacterial load without affecting bacterial internalization in macrophages

The rapid Asm-dependent BCG control in Wt mice, versus the inability of an early BCG clearance in Asm-deficient mice *in vivo*, suggests the involvement of phagocytes. As professional phagocytes, macrophages are the first line of defense in bacterial infection (Weiss and Schaible, 2015). Therefore, BMDMs from Wt and $Asm^{-/-}$ mice were isolated and infected with BCG to investigate the importance of Asm in dealing with BCG infection at the early stages.

The determination of bacterial numbers in the CFU assays revealed that the bacterial burden was decreased at 48 hpi compared to that at 24 hpi only in Wt BMDMs, but bacterial burden remained constant in $Asm^{-/-}$ BMDMs (Figure 15A). Wt BMDMs contained 30%-40% less intracellular bacteria than $Asm^{-/-}$ BMDMs during this time (Figure 15A). These results suggest that Wt BMDMs can eliminate BCG while $Asm^{-/-}$ BMDMs allow bacterial survival, which is consistent with the *in vivo* data presented above.

To investigate whether the higher bacterial load in $Asm^{-/-}$ BMDMs was caused by defective BCG-internalization by macrophages, BMDMs were infected by GFP-BCG. Bacterial internalization by BMDMs was examined by analyzing the GFP signal in infected cells via FACS. To avoid signals from GFP-BCG which only bound to cells but not internalized, trypan blue quenching was applied. Trypan blue absorbs the fluorescence emitted by green-emission fluorochromes or fluorescent proteins (i.e., GFP), and it is widely used to quench green fluorescence in microscopy and flow cytometry (Hed, 1986; Szollosi et al., 1984; Tschop et al., 2010). Therefore, trypan blue rapidly treated and fixed cells exhibited GFP signals only from internalized GFP-BCG as shown in Figure 15C (internalization), while cells without trypan blue treatment represented cells containing both adherent and internalized GFP-BCG as shown in Figure 15B (binding + internalization).

The FACS results suggested that neither bacterial binding nor internalization differed between Wt and $Asm^{-/-}$ BMDMs (Figure 15B-C). Around 40% of the cells were GFP positive in the first 30 min of infection, but only 20% of the cells remained GFP positive after trypan blue quenching in both Wt and $Asm^{-/-}$ BMDMs (Figure 15B-C). After 1 hr of infection, cells with trypan blue quenching showed similar GFP positive percentage

(about 40%) to cells without trypan blue treatment. This suggested that bacteria were all internalized into cells (Figure 15B-C). These results indicated that binding and internalization of BCG by BMDMs are independent of the Asm and that the higher bacterial burden in Asm$^{-/-}$ macrophages is not caused by enhanced binding and uptake of BCG.

Taken together, these results suggest that, Asm deficiency leads to higher susceptibility of macrophages to BCG infection *in vitro*, which is consistent with the *in vivo* results.

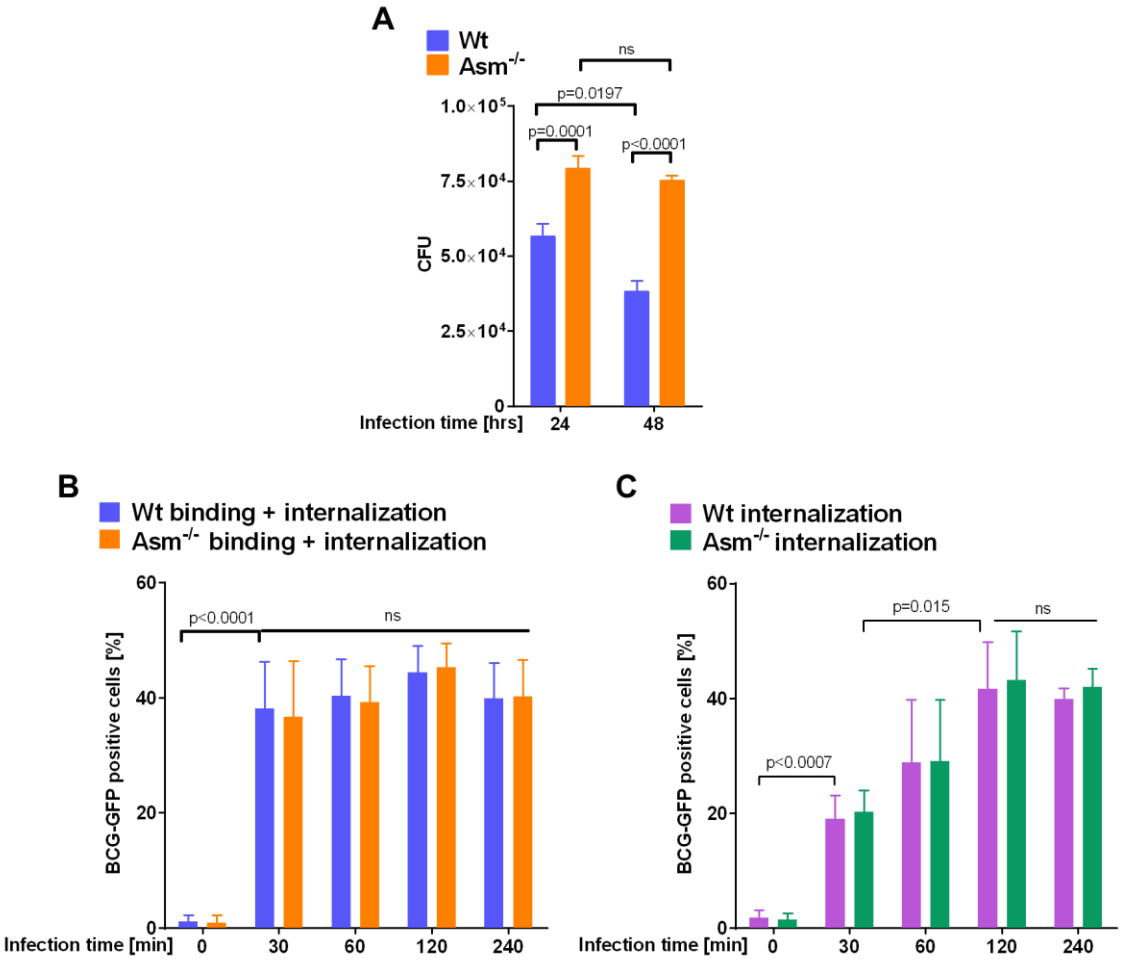

Figure 15. Bacterial overload in Asm deficient BMDMs is not due to enhanced internalization.

(A) Wt or Asm$^{-/-}$ BMDMs were infected with BCG for 24 hrs or 48 hrs, the CFUs were determined on agar plates. Shown are the means ± SD from 3 independent experiments. The quantitative analysis was performed with GraphPad and analyzed with two-way ANOVA followed by Bonferroni's multiple comparisons test. **(B-C)** Macrophages were infected with BCG-GFP for the indicated time, and bacterial binding **(B)** and internalization **(C)** was determined by analyzing GFP signals in cells without or with trypan blue quenching via FACS analysis of 10.000 cells/sample at BL1 channel.

Uninfected cells were used as a control. The results are representative of 3 independent studies.

4.2.3 Asm is essential for BCG degradation by cathepsin D

Maturation of phagosomes and the subsequent activation of cathepsins are important for degradation of bacteria and control of BCG infections (Deretic et al., 1997; Seto et al., 2011). The degradative activity or bactericidal capacity of the matured phagosome is achieved by hydrolytic enzymes, for example, cathepsins (Pauwels et al., 2017; Pires et al., 2016). To determine whether the Asm induces degradation of BCG, cathepsin D was investigated. Western blots for cathepsin D showed that this hydrolytic enzyme was degraded in $Asm^{-/-}$ macrophages upon BCG infection while it remained expressed in Wt at the level of uninfected cells (Figure 16A-B). Moreover, immunofluorescent stainings for cathepsin D showed a co-localization between cathepsin D and bacteria in infected Wt macrophages, whereas it was absent in infected $Asm^{-/-}$ macrophages (Figure 16C). These results suggest that Asm is important for phagosome-lysosome fusion and may induce interaction between BCG and cathepsin D. To assess whether the activated and colocalized cathepsin D in Wt cells functioned as a bactericidal factor, as it is described for *L. monocytogenens*, *Streptococcus pneumonia*, and *S. aureus* (Bewley et al., 2011; del Cerro-Vadillo et al., 2006; Thorne et al., 1976), an inhibitor of cathepsin D, pepstatin A, was used in the study. BMDMs from Wt and $Asm^{-/-}$ mice were left untreated or pretreated with pepstatin A 1 hr before infection, and the bacterial load was determined 24 hrs after infection (Figure 16D). The measurements revealed that pepstatin A treated Wt BMDMs showed significantly higher CFUs than untreated Wt BMDMs, whereas the inhibition did not lead to a higher bacterial burden in $Asm^{-/-}$ BMDMs.

Taken together, the results indicate that the Asm contributes to BCG killing in macrophages via cathepsin D.

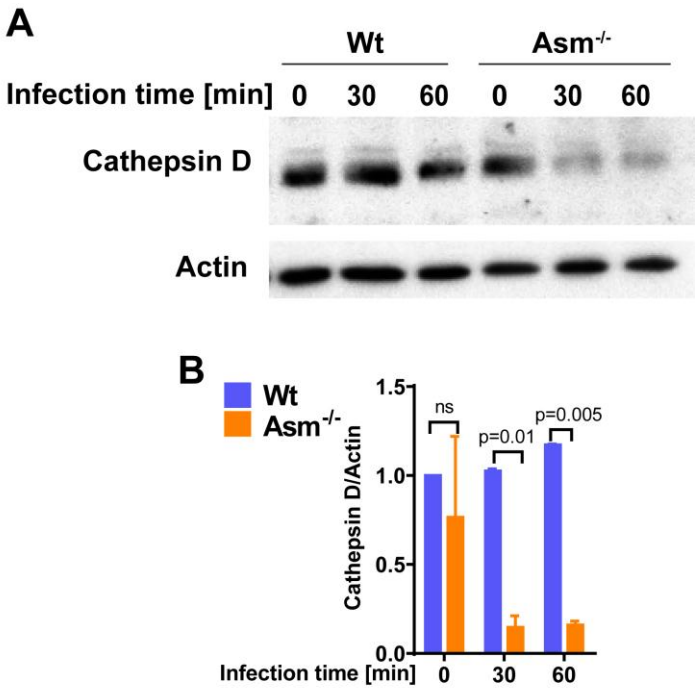

Figure 16. Asm is essential for BCG degradation by cathepsin D in macrophages. **(A-B)** BMDMs were infected with BCG for the indicated periods of time and were then subjected to Western blot analysis using antibodies of cathepsin D and β-actin. **(C)** The western blot is representative of 3 independent experiments. **(D)** The quantitation of the cathepsin D/Actin was performed using ImageJ. Displayed are the means ± SD of 3 experiments, p-values were calculated by ANOVA followed by Bonferroni's multiple comparisons test.

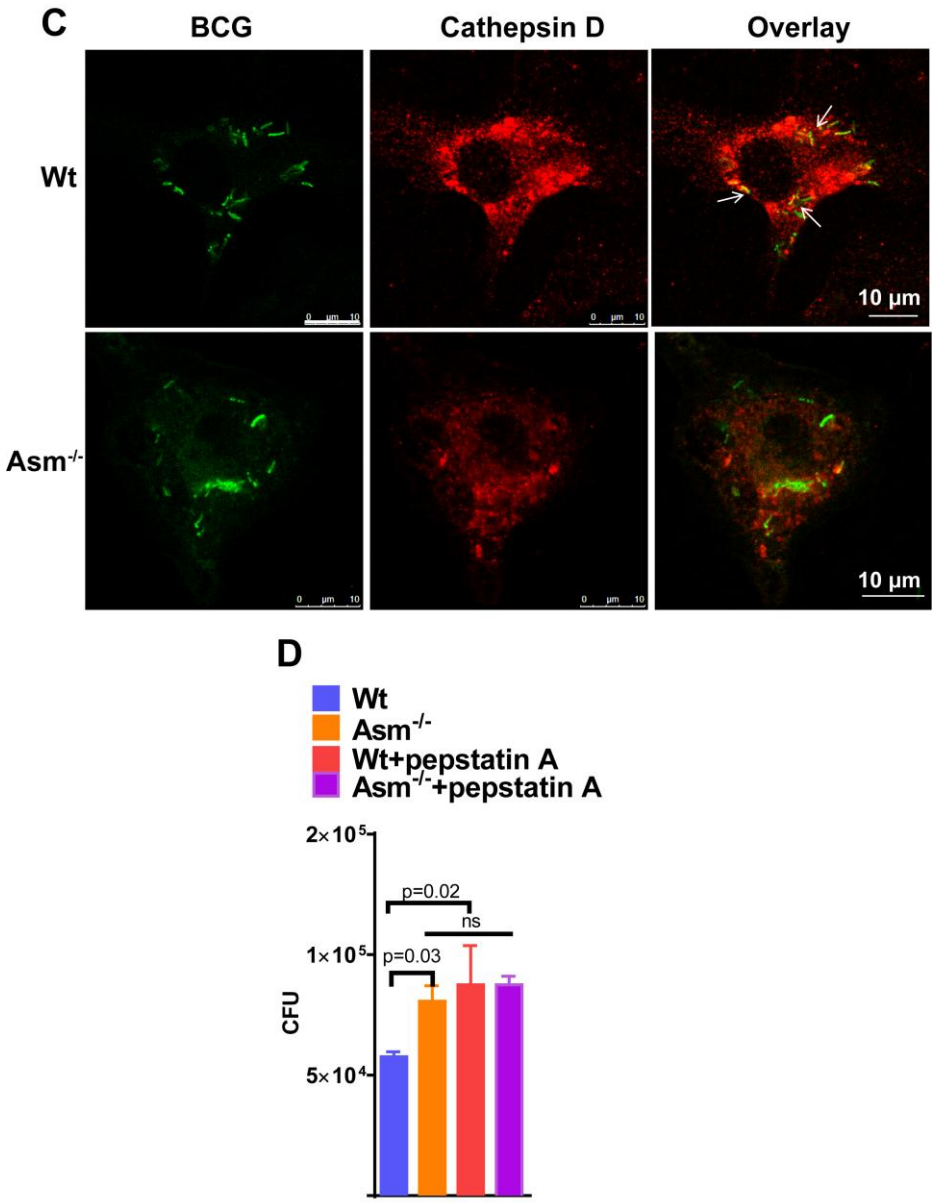

Figure 16C-D. Asm is essential for BCG degradation by cathepsin D in macrophages.

(C) Cells were left uninfected or infected with BCG for 60 min, then fixed and stained with Cy3-coupled cathepsin D. The samples were analyzed by confocal microscopy. Shown are pictures representing 3 independent studies. The scale bar is 10 µm. **(D)** BMDMs were left untreated or pretreated with 10 µM pepstatin A for 1hr and infected with BCG for 24 hrs. The number of BCG CFUs was determined after 2 weeks of culture. Shown are the means ± SD of the colony-forming units (CFUs) of 3 independent experiments. The quantitative analysis was performed with GraphPad and analyzed with two-way ANOVA followed by Bonferroni's multiple comparisons test.

4.2.4 Asm mediates cathepsin D activation via ROS

Reactive oxygen species (ROS) play an essential role in the microbicidal activity of the host (Bedard and Krause, 2007; Rybicka et al., 2010). This raises the question of whether ROS mediates the Asm-dependent bacterial degradation during BCG infection. To address this question, ROS production was investigated in BCG-infected BMDMs of Wt and $Asm^{-/-}$ mice. Within Wt BMDMs, ROS (Figure 17A) and superoxide levels (Figure 17 B) were rapidly elevated within 5 to 30 min after BCG infection. However, $Asm^{-/-}$ macrophages produced 20-30% less ROS after infection (Figure 17A-B).

To investigate the connection between ROS and cathepsin D upon BCG infection, the ROS inhibitor, apocynin, was used and the expression and distribution of cathepsin D were examined in those cells. For this purpose, macrophages from Wt and $Asm^{-/-}$ mice were left untreated or were pretreated with apocynin 60 min before infection. Subsequently, Western blots and immunofluorescent stainings for cathepsin D were performed. As shown in Figure 17C, the cathepsin D level in apocynin-treated Wt BMDMs was reduced after BCG infection for 30 min and 60 min compared to untreated Wt cells, while apocynin has no influence on cathepsin D expression level in $Asm^{-/-}$ macrophages (Figure 17C). Consistently, imaging results showed that the treatment with apocynin in Wt BMDMs reduced the co-localization between cathepsin D and BCG (Figure. 17D). These data indicate that Asm-mediated interactions between bacteria and cathepsin D are regulated via ROS.

ROS are produced by the activation of NADPH oxidase (NOX, mostly Nox2) via the binding of cytosolic subunits ($p47^{phox}$, $p40^{phox}$, $p67^{phox,}$ and Rac1 or Rac2) to transmembrane subunits (gp91 and p22) (Bedard and Krause, 2007). To figure out how Asm induces ROS production and whether Asm regulates Nox2 subunits, analysis of some involved proteins was performed by Western blot and immunofluorescent staining of infected BMDMs of Wt and $Asm^{-/-}$ mice. Only the expression of the Nox2 subunit $p47^{phox}$ was different upon infection and showed a higher level in Wt BMDMs than in $Asm^{-/-}$ BMDMs (Figure 17E). Other subunits, such as gp91, p22, $p67^{phox,}$ and active Rac1, showed no difference in expression between Wt and $Asm^{-/-}$ BMDMs after BCG infection (Figure 17E). Moreover, $p47^{phox}$ immunofluorescent staining showed not only a higher protein expression in Wt macrophages after 60 min of infection but also

an increased colocalization with BCG in Wt. This was absent in Asm$^{-/-}$ BMDMs (Figure 17E-F). These data suggest that Asm controls ROS production via regulation of Nox2 subunit p47^{phox}.

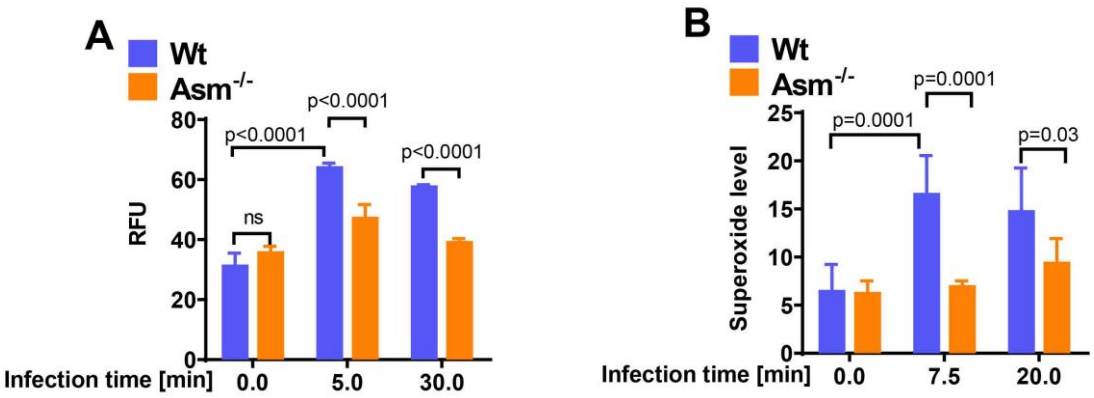

Figure 17. Asm regulates cathepsin D activation in BCG infected BMDMs via ROS. **(A-B)** Wt or Asm$^{-/-}$ BMDMs were infected with BCG for the indicated time, **(A)** To determine ROS burst, cells were incubated with a fluorescence probe, ROS deep red dye, and the fluorescence was determined by a fluorescence microplate reader at Ex/Em=650/675 nm (cut off 665 nm) after 30 min. Relative fluorescence unit (RFU) was used to represent the ROS release. **(B)** Superoxide production was measured by electron spin resonance. Shown are means ± SD of 3 independent experiments, p-values were calculated by ANOVA followed by Bonferroni's multiple comparisons test.

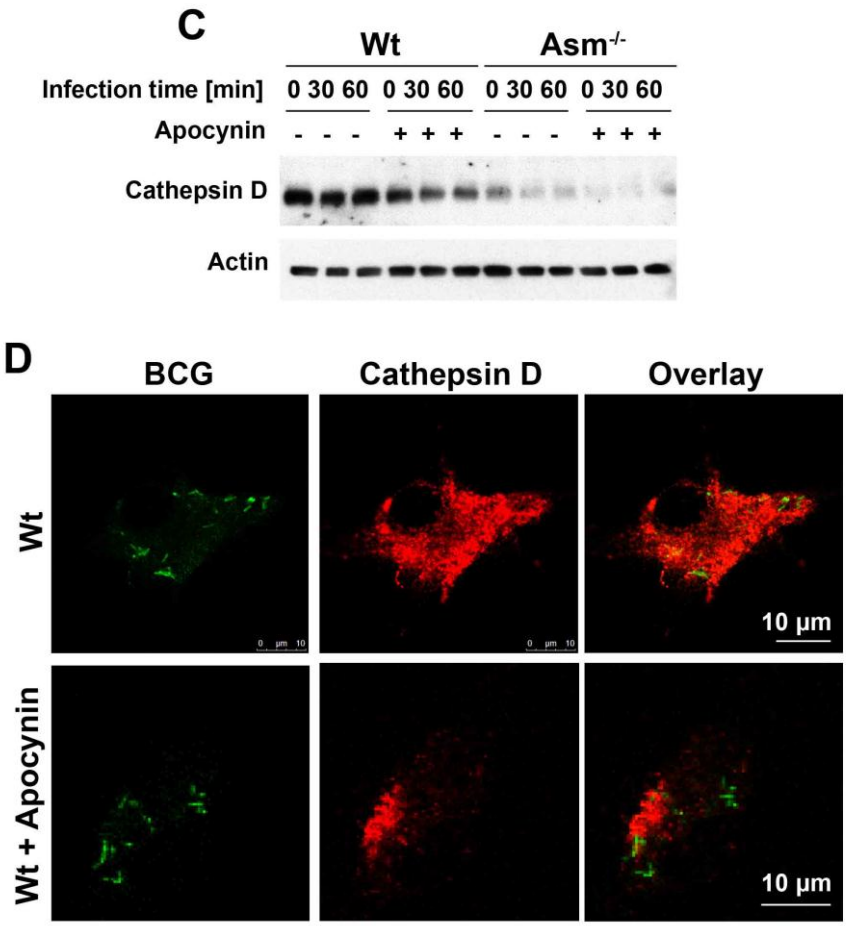

Figure 17C-D. Asm regulates cathepsin D activation in BCG infected BMDMs via ROS.

(C-D) BMDMs were left untreated or pretreated with 10µM apocynin for 1hr and infected with BCG for 1 hr. **(C)** After the indicated time of infection, cells were lysed and subjected to western blot to determine cathepsin D expression. Actin levels were used for normalization. **(D)** Cells were infected for 30 min, fixed and stained with Cy3-coupled cathepsin D. Representative confocal fluorescence and western blot images of 3 independent experiments are shown.

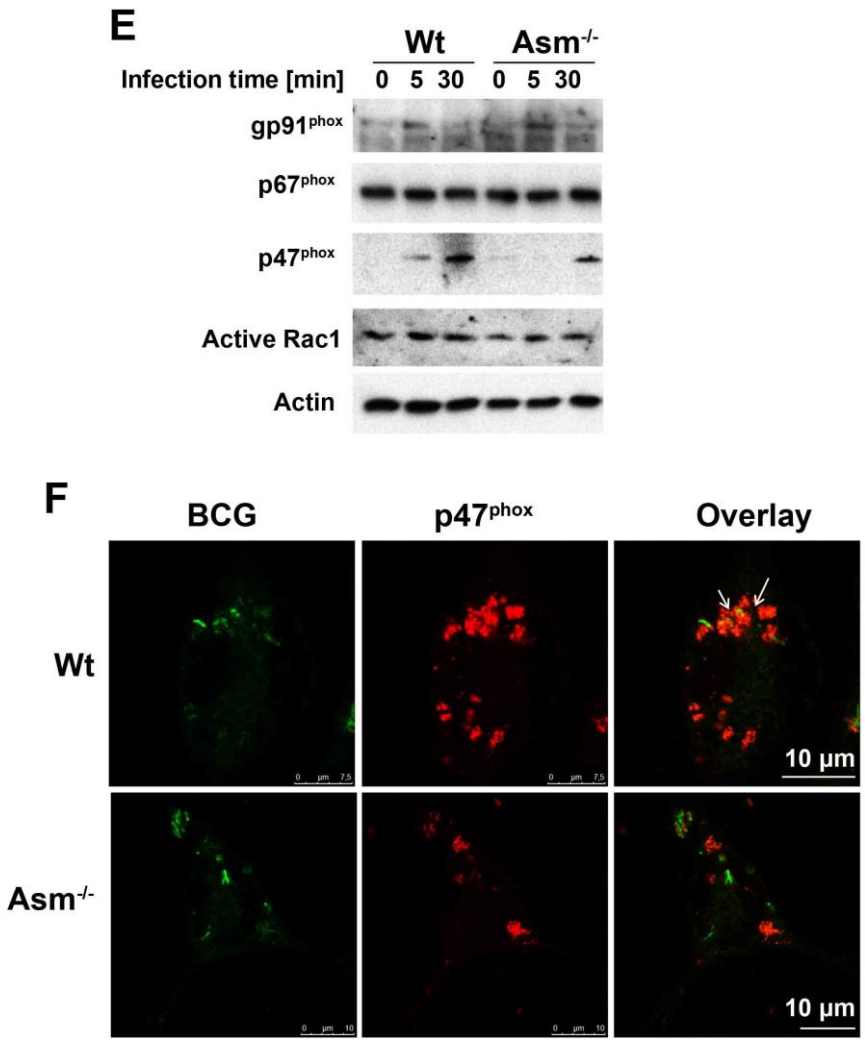

Figure 17E-F. Asm regulates cathepsin D activation in BCG infected BMDMs via ROS.

(E) BMDMs from Wt and Asm$^{-/-}$ mice were infected with BCG for the indicated time or left uninfected and then lysed. Western blot or immunoprecipitation was performed to determine the expression of Nox2 subunits, gp91^{phox}, p67^{phox}, p47^{phox} or the activation of Rac1. Shown are representative results from 3 independent studies. **(F)** Cells were left uninfected or infected with BCG for 30 min then fixed and stained with Cy3-coupled p47^{phox}. The samples were analyzed by confocal microscopy. Shown are representative pictures of 3 independent studies. The scale bars are 10 µm.

4.2.5 Asm regulates ROS via the Sphingosine kinase (SphK)/S1P

To better understand how Asm regulates the activation of NADPH oxidase and its enhancement of ROS, and which types of sphingolipids were influenced by the infection, conversion of sphingolipids upon BCG infection was measured. For this purpose, the Asm and Ac activities were measured in infected BMDMs of Wt and $Asm^{-/-}$ mice. In BCG-infected Wt BMDMs, Asm and also Ac activities were significantly increased upon BCG infection for 5 min until 2 hrs and reached for both enzymes a maximum after 30 min of infection (Figure 18A-B). In contrast, neither Asm nor Ac activity was significantly elevated in $Asm^{-/-}$ macrophages after infection (Figure 18A-B).

These results suggest a sphingolipid metabolism shift during BCG infection. Previous work has shown a bactericidal role of several sphingolipids. Some of them are also related to ROS release (Anes et al., 2003). Therefore, sphingolipids levels were investigated upon BCG infection. Mass spectrometry measurements of sphingolipids levels showed that sphingomyelin was accumulated in $Asm^{-/-}$ BMDMs after BCG infection whereas other sphingolipids, such as ceramide, sphingosine and S1P, were not affected upon BCG infection in this genotype (Figure 18C-F). The basal level of sphingomyelin in Wt BMDMs was lower in comparison to $Asm^{-/-}$ macrophages. In contrast to the levels in $Asm^{-/-}$ macrophages, sphingomyelin remained unchanged in Wt BMDMs during the infection. The basal levels of ceramide, sphingosine, and S1P in Wt cells were higher than in $Asm^{-/-}$ macrophages (Figure 18C-F). Neither ceramide nor sphingosine level was increased upon infection in Wt BMDMs, although both Asm and Ac were activated upon BCG infection (Figure. 18 C-E). Instead, S1P was significantly elevated in Wt BMDMs after BCG infection but not in $Asm^{-/-}$ BMDMs (Figure 18F). These data indicate that the activation of Asm upon BCG infection leads to the production of S1P. In addition, the determination of the individual ceramide species by mass spectrometry showed that certain ceramides (C16, C18, C20, C22) were not different between Wt and $Asm^{-/-}$ BMDMs (Figure 18G-J), whereas C24 and C24:1 ceramides were dependent on the expression of Asm (Figure 18K-L).

SphK produces S1P via phosphorylation of sphingosine. Both S1P and SphK have been shown to effectively control mycobacterial infection (Garg et al., 2004; Malik et al., 2003; Prakash et al., 2010; Yadav et al., 2006). S1P has also been shown to induce

ROS production (Catarzi et al., 2007). To examine these relationships with regard to mycobacterial infection, the SphK inhibitor, SKI-I was used, and expression of the Nox2 subunit, $p47^{phox}$ upon BCG infection was determined in Wt macrophages. Western blot and immunofluorescent stainings revealed that the inhibition of S1P by SKI-I reduced the expression of $p47^{phox}$ in Wt macrophages after 30 min of BCG infection (Figure 18 M) and diminished the co-localization of $p47^{phox}$ with mycobacteria (Figure 18N). Consistently, ROS production was downregulated upon SKI-I treatment after 30 min of BCG infection in Wt macrophages (Figure 18O). To assess whether Sphk/S1P was related to bactericidal function, the bacterial load in Wt and $Asm^{-/-}$ BMDMs under the influence of the inhibitor of SphK was detected. BMDMs were left untreated or pretreated with SKI-I for 1 hr before infection, and the bacterial burden was determined after 24 hrs of infection (Figure 18P). SKI-I treated Wt BMDMs contained significantly higher CFUs than untreated Wt BMDMs, whereas there was no significant change in $Asm^{-/-}$ BMDMs (Figure 18P).

Taken together, these data suggest that Asm controls ROS production and Nox2 subunit $p47^{phox}$ via the SphK/ S1P system and that SphK mediates bactericidal effects.

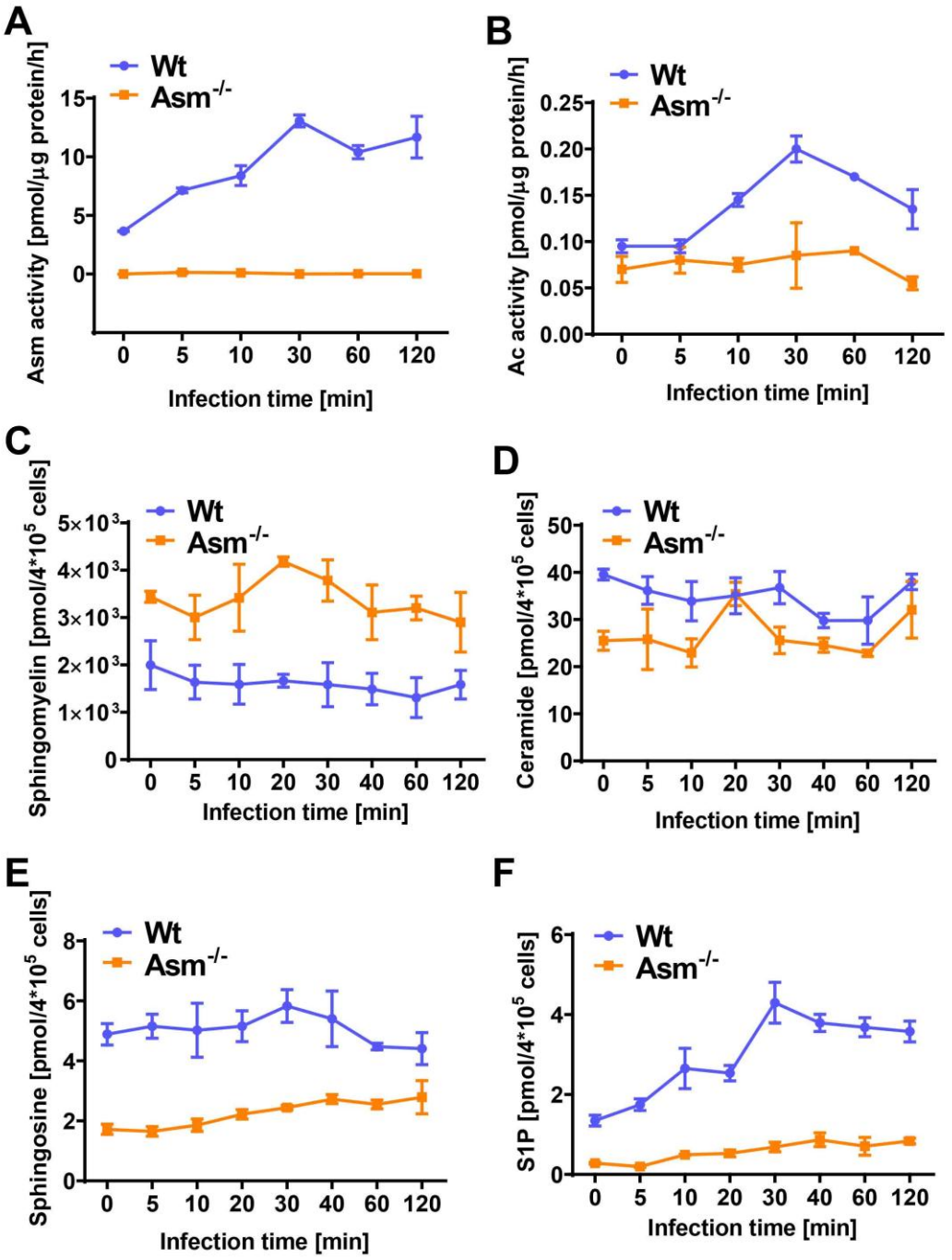

Figure 18. Asm regulates Nox2 subunit p47^{phox} in macrophages upon BCG infection via SphK/S1P.

(A-B) BMDMs were left uninfected or infected with BCG for the indicated time. Asm activity **(A)** and Ac activity **(B)** was assessed using, respectively, BODIPY-labeled sphingomyelin and NBD-labeled ceramide as a substrate. Given are the means ± SD of n = 3. **(C-F)** Wt or Asm deficient BMDMs were infected with BCG for the indicated times and the consumption of sphingomyelin **(C)**, ceramide **(D)**, sphingosine **(E)**, S1P **(F)** levels were measured by rapid resolution liquid chromatography/mass spectrometry. Displayed are the means ± SD of 3 experiments.

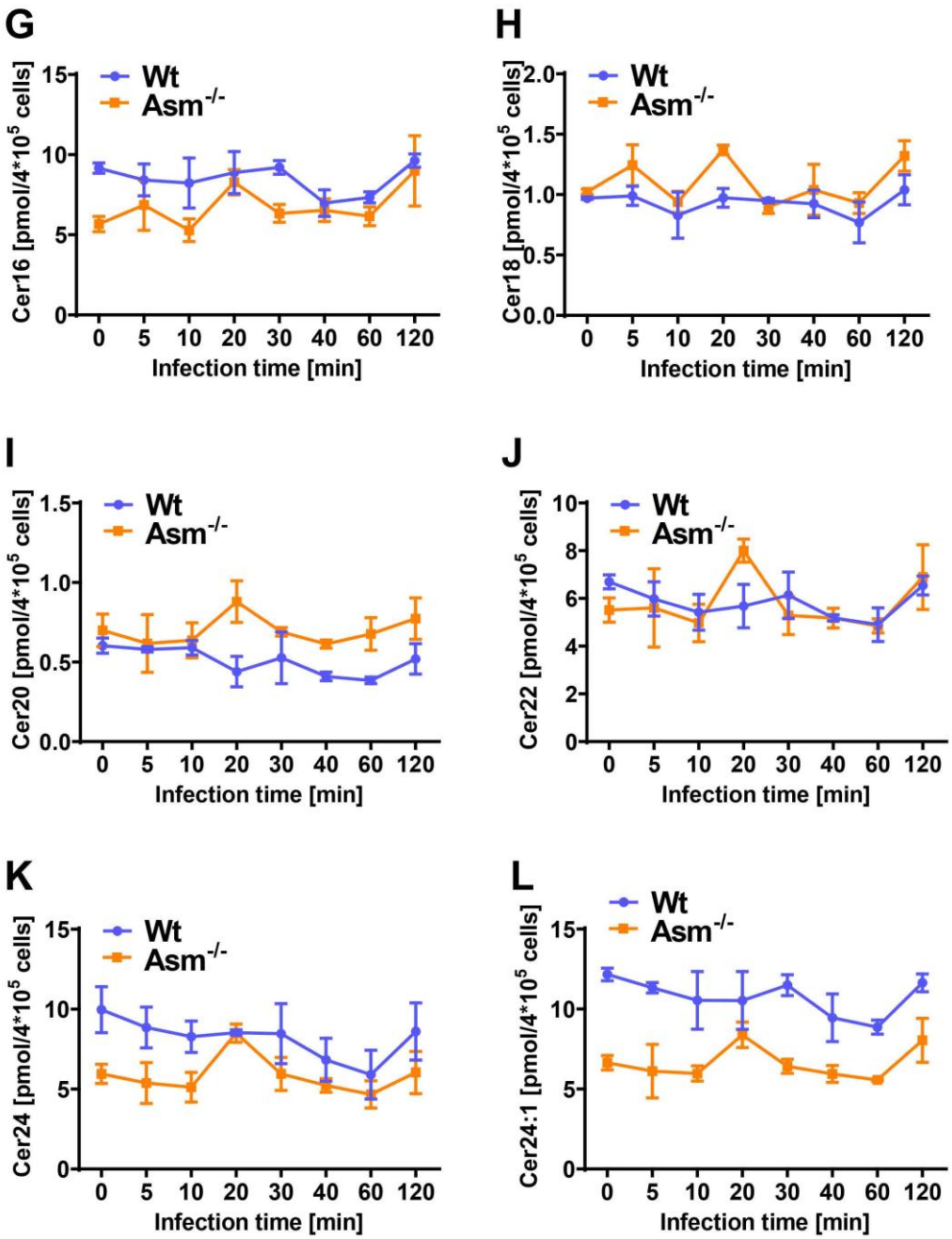

Figure 18G-L. Asm regulates Nox2 subunit p47^{phox} in macrophages upon BCG infection via SphK/S1P.

(G-L) Wt or Asm deficient BMDMs were infected with BCG for the indicated times and the consumption of ceramide species C16 **(G)**, C18 **(H)**, C20 **(I)**, C22 **(J)**, C24 **(K)**, C24:1 **(L)** levels were measured by rapid resolution liquid chromatography/mass spectrometry. Displayed are the means ± SD of 3 experiments.

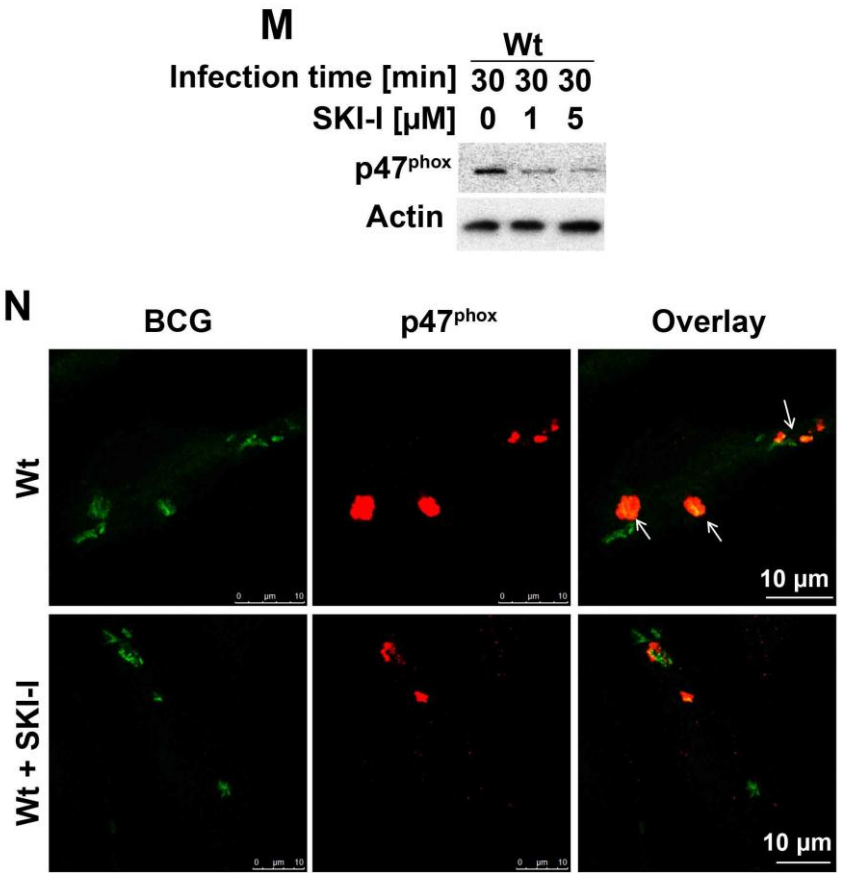

Figure 18M-N. Asm regulates Nox2 subunit p47^{phox} in macrophages upon BCG infection via SphK/S1P.

(M) Wt BMDMs were left untreated (0 µM) or pretreated with 1 µM or 5 µM SphK inhibitor (SKI-I) for 1 hr and infected with BCG for 30 min. Cells were lysed to determine p47^{phox} expression. Shown are representative results of 3 independent experiments. **(N)** Cells were left untreated or pretreated with 1 µM SphK inhibitor (SKI-I) for 1 hr. Cells were then infected with BCG for 30 min. Cells were fixed and stained with Cy3-coupled p47^{phox}. Shown are representative confocal fluorescence images of three independent experiments.

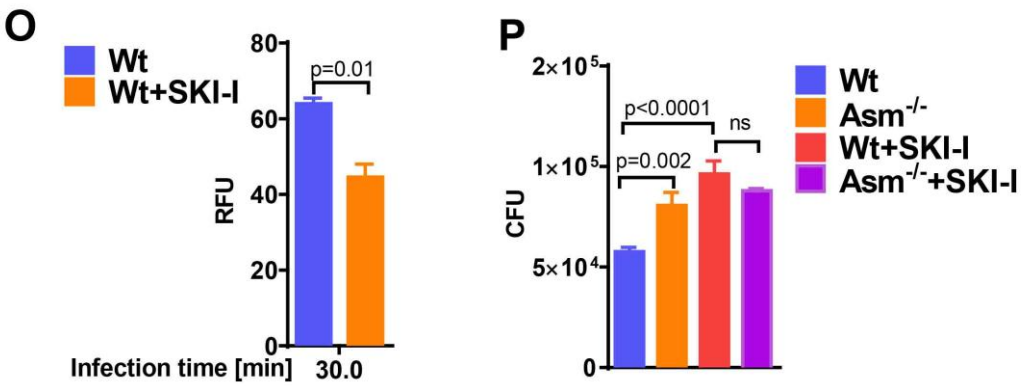

Figure 18O-P. Asm regulates Nox2 subunit p47phox in macrophages upon BCG infection via SphK/S1P.

(O) Wt BMDMs were left untreated or pretreated with 1μM SKI-I for 1 hr. Cells were then infected with BCG for 30 min. Cells were washed and incubated with a fluorescence probe, ROS deep red dye, and fluorescence was determined by a fluorescence microplate reader after 30 min. Relative fluorescence unit (RFU) was used to represent the ROS release. **(P)** Wt or Asm deficient BMDMs were left untreated or pretreated with 1 μM SKI-I for 1hr and then infected with BCG for 24 hrs. Cells were lysed, and bacterial numbers were counted on agar plates. Shown are the means ± SD of the CFUs of 3 independent experiments. The quantitative analysis was performed with GraphPad and analyzed with one-way ANOVA followed by Bonferroni's multiple comparisons test.

4.2.6 Transplantation of Wt BMDMs partially reverses susceptibility of Asm$^{-/-}$ mice to BCG infection

To further prove that the Asm is important for BCG infection *in vivo* and to clarify if macrophages are responsible for clearance of early BCG infection, *in vivo* transplantation experiments were performed. Therefore, Wt or Asm$^{-/-}$ mice were transplanted either with Wt or Asm$^{-/-}$ BMDMs.

To establish the protocol of macrophage depletion with clodronate liposomes and reconstitution, mice were transplanted with various numbers of macrophages and compared with non-transplanted or untreated mice. The percentages of macrophages from bone marrows, livers and spleens were measured by FACS (Figure 19A). The results showed that the depletion of macrophages with clodronate liposomes was quite efficient in all tested organs. In bone marrow and liver, macrophages were 90% depleted at day 2 (24 hrs), and the effect persisted for at least 2 weeks after a single depletion (indicated in the bars “clod d2” and “clod d14”). In the spleen, the depletion of macrophages was 50% after 2 weeks. The results of reconstitution with macrophages showed that 1 million cells were not sufficient for reconstitution of macrophages in mice (indicated in the bar “1m d2”). Both macrophages in liver and bone marrow were just recovered by 50% after the transplantation, while, transplantations with 5 million or 10 million macrophages were sufficient to reconstitute macrophages in all organs after 24 hours (indicated in the bars “5m d2” and “10m d2”). Therefore, for the following studies, mice macrophages were depleted once with clodronate liposomes for 24 hrs, and on the next day, mice were transplanted with 5 million BMDMs from Wt or Asm$^{-/-}$ mice. At day 3, mice were then infected with 10^7 BCG and monitored for an infection time of 1 day or 3 days. Bacterial burdens in the livers and spleens of transplanted mice were determined by CFUs.

Quantification of the bacterial burden after transplantation and infection revealed that bacterial burden in the liver of Asm$^{-/-}$ mice transplanted with Asm$^{-/-}$ BMDMs was significantly higher than that in Asm$^{-/-}$ mice transplanted with Wt BMDMs, both at 1dpi and 3dpi (Figure 19B-C). Surprisingly, Wt mice transplanted with Asm$^{-/-}$ BMDMs were not suffering a higher hepatic bacterial burden compared to those mice transplanted with Wt BMDMs (Figure 19B-C). These results indicate that Wt mice may have other complementing immune responses to prevent an uncontrolled infection.

However, the bacterial burden in the spleen was not significantly altered in Asm$^{-/-}$mice transplanted with Wt BMDMs compared to Asm$^{-/-}$ mice transplanted with Asm$^{-/-}$ BMDMs at 1dpi and 3dpi (Figure 19D-E). These results suggest a limited immune defense function of transplanted macrophages in the spleen.

Together, these results suggest that, at least in the liver, the susceptibility of Asm$^{-/-}$ mice to BCG infection is due to the impaired microbicidal effect of Asm$^{-/-}$ macrophages, and that the transplantation of Wt BMDMs can reverse this effect.

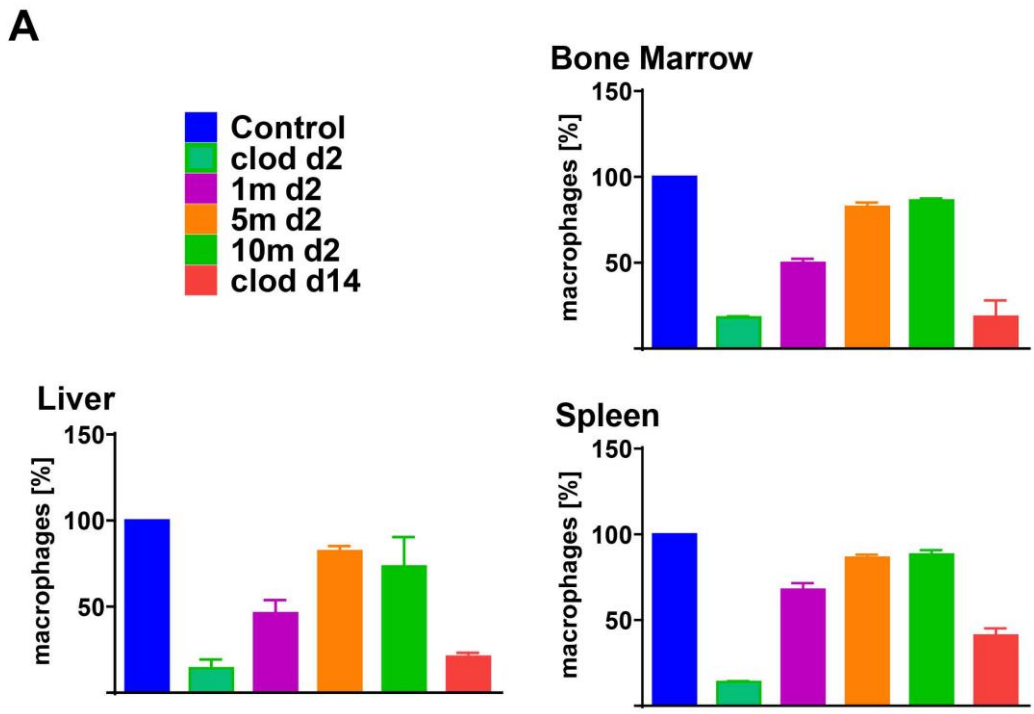

Figure 19. Transplantation of Wt macrophages partially reverses the bacterial burden in Asm$^{-/-}$ mice.

(A) To analyze the percentage of macrophages after depletion and reconstitution, mice were intravenously injected with clodronate liposomes or left untreated (control), and the depletion state was analyzed 24 hrs or 14 days after depletion (clod d2, clod d14). Mice were transplanted either with 1 million, 5 million or 10 million BMDMs (1m, 5m, 10m) 24hrs after depletion. The reconstitution was analyzed 24hrs after transplantation (1m d2, 5m d2, 10m d2) with FACS.

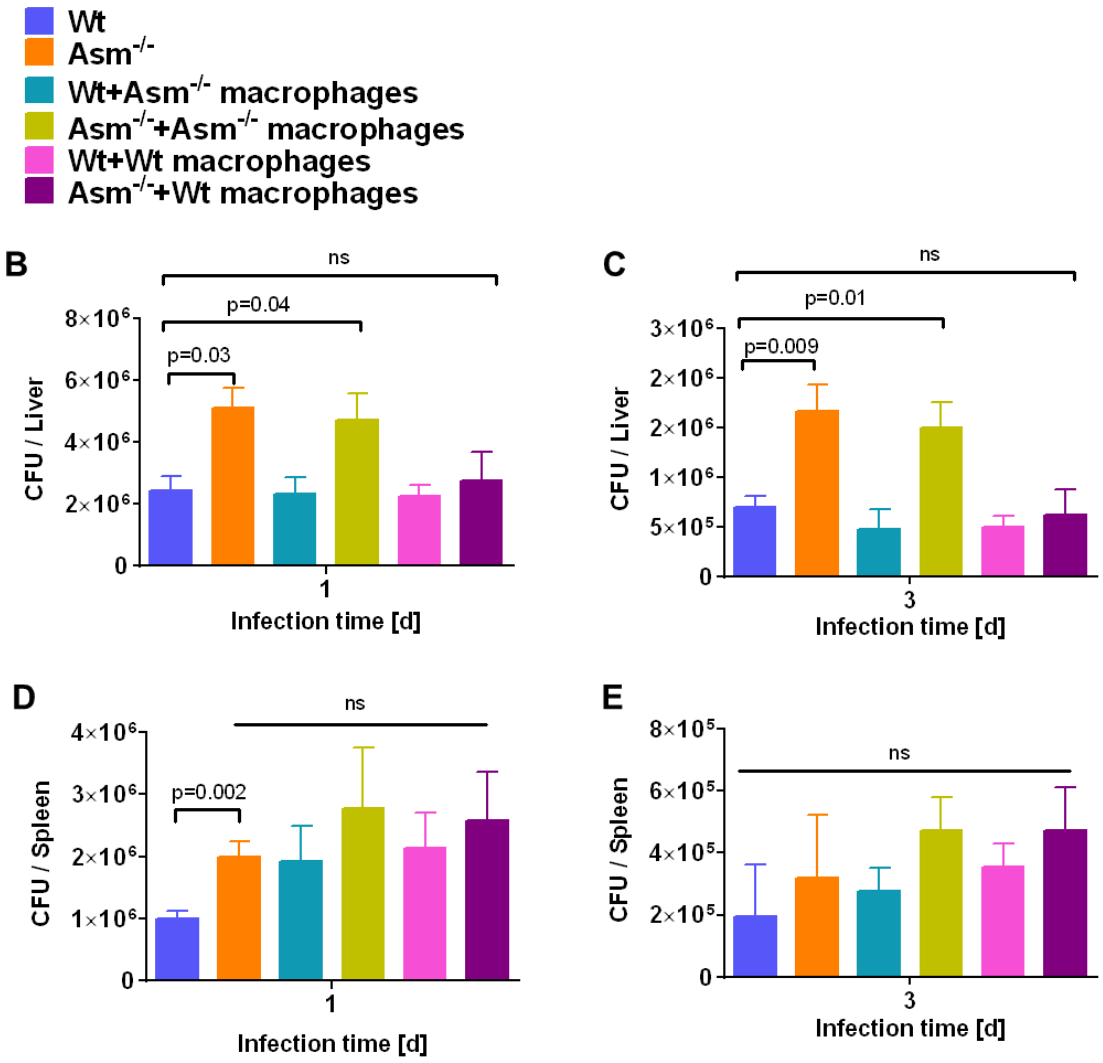

Figure 19B-E. Transplantation of Wt macrophages partially reverses the bacterial burden in Asm$^{-/-}$ mice.

(B-E) Wt or Asm$^{-/-}$ mice were intravenously injected with clodronate liposomes or untreated 2 days before infection and were transplanted with 5×10^6 Wt or Asm$^{-/-}$ BMDMs via intravenous injection 1 day before infection. Transplanted and control mice were infected with 10^7 BCG for 1 day or 3 days. The total numbers of BCG in liver homogenates were determined at 1 dpi **(B)** and 3 dpi **(C)**, in spleen homogenates at 1dpi **(D)** and 3dpi **(E)** by CFUs, p-values were determined by one-way ANOVA followed by Bonferroni's multiple comparisons test, n=6.

5 Discussion

5.1 The role of Nsm in mycobacterial infection

The results of this study show that neutral sphingomyelinase (Nsm) dependent activation of β1-integrin is a functional mediator of Bacillus Calmette-Guérin (BCG)-induced granuloma formation in mice.

Granulomas, a histopathological feature and a hallmark of TB have been described and studied for more than a century (Adams, 1976). Current results show that active β1-integrin is a novel mediator for the regulation of granulomas, which are a favorable niche for mycobacteria during infection.

Based on the present work, the following scenario is assumed (Figure 20): BCG infection activates Nsm in macrophages which results in activation and trapping of surface β1-integrin via the p38K/JNK pathway, Rac1 activation, and actin protrusion. The activation of Rac1 and the rearrangement of actin lead to the migration of macrophages and the formation of multiple granulomas *in vivo*, which seem to be a secure reservoir for mycobacteria. Infecting mice, which are heterozygous for Nsm ($Nsm^{+/-}$) or neutralizing active β1-integrin in wild-type (Wt) mice by administering corresponding antibodies disrupt the formation of granulomas and reduces the bacterial burden in infected hosts. This interrupts the trajectory of the BCG infection and protects the host from mycobacterial infection.

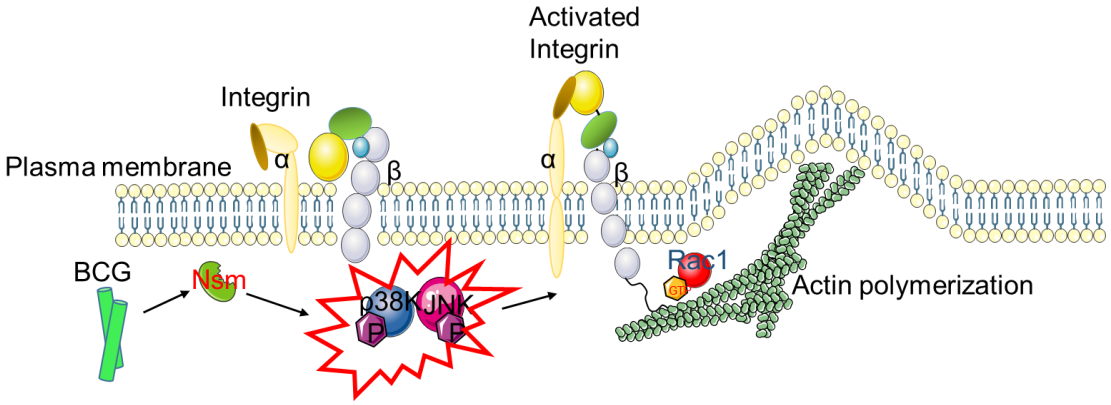

Figure 20. The scenario of β1-integrin regulated cytoskeleton redistribution and granuloma formation upon BCG infection.
BCG infection activates Nsm in macrophages which results in p38K/JNK activation followed by stimulation of surface β1-integrin, Rac1 activation, and actin reorganization.

The rearrangement of actin leads to migration of macrophages and the formation of multiple granulomas *in vivo*.

Nsm and β1-integrin

Integrins are widespread adhesion receptors and migration mediators, as well as mechanosensors transmitting biochemical signals and mechanical forces across cell membranes (Calderwood et al., 2000; Weber et al., 2011). Among these, β1-integrin is one of the most common integrins associated with bacterial adhesion and actin cytoskeleton rearrangements (Calderwood et al., 2000). Also, β1-integrin leads to the invasion of mycobacteria into macrophages, their persistence in these cells, and their spread into other macrophages (Bermudez et al., 1997). It has been documented that the fusion of macrophages and the generation of *in vitro* granulomas are in part dependent on β1-integrin (McNally and Anderson, 2002; Puissegur et al., 2007).

Despite the characterization of β1-integrin in mycobacterial infection, the mechanism behind it remained largely unknown. Notable and recently described functions of active β1-integrin include the regulation of pulmonary metastasis of melanoma cells in mice and of the susceptibility of mice and humans with cystic fibrosis to *P. aeruginosa* infections via Asm/ceramide system (Carpinteiro et al., 2015; Grassme et al., 2017). The present work, for the first time, indicates that active β1-integrin is directly responsible for cell cytoskeleton rearrangement and the formation of granulomas upon mycobacterial infection.

It is known that β1-integrin can exist in three states: an inactive bent state, a primed extended closed state, and an active extended open state (Luo et al., 2007; Su et al., 2016). In the present study, 9EG7 antibodies are used to neutralize active β1-integrin on the cellular surface. The 9EG7 antibody recognizes the activated extended closed or open state form of β1-integrin, which binds to the integrin-epidermal growth factor domain 2 (I-EGF2) within the β1-integrin molecule (Su et al., 2016). Treatment with 9EG7 antibodies recognized β1-integrin and stabilized its activation state, after that it can be endocytosed, thus neutralizing its function.

Therefore, the results of immunoprecipitation with 9EG7 antibodies indicate that BCG infection induces a conformational change of β1-integrin from the inactivated to the activated form and that this conformational change is strictly dependent on Nsm activation. The BCG-induced activation of β1-integrin is insufficient to induce β1-

integrin trafficking and internalization. Neutralization of active β1-integrin with 9EG7 dramatically blocked granuloma formation by approximately 40% and reduced bacterial burden after BCG infection. This effect was dependent on Nsm both *in vitro* and *in vivo*. The results in this study showed marked Nsm- and β1-integrin-dependent phosphorylation of p38K and JNK upon BCG infection. Pretreatment of infection with pharmacological inhibitors of p38K and JNK, SB239063 and SP600125, blocked β1-integrin activation, granuloma formation, and bacterial burden upon infection. These findings are consistent with a previous report, indicating that hypoxia activates β1-integrin via p38K in human vascular smooth muscle cells (Blaschke et al., 2002). Besides, the Karakashian group has reported that the stimulation of JNK phosphorylation is dependent on the Nsm/ceramide-activated protein phosphatase in primary hepatocytes (Karakashian et al., 2004).

Nsm and cytoskeleton

Rac1 has been described to precede foreign body giant cell formation (Jay et al., 2007). This formation seems to be dependent on interleukin-4, which induces multinucleation of murine BMDMs, accompanied by elongation and lamellipodia formation before fusion. Inhibition of Rac1 limited lamellipodia formation in a dose-dependent manner, thus reducing the fusion of macrophages (Jay et al., 2007). The data presented here demonstrate that the activation of β1-integrin induces the stimulation of Rac1 and the generation of F-actin-composed lamellipodia upon BCG infection. Genetic heterozygosity for Nsm or functional blockade of active β1-integrin with 9EG7 in Wt mice leads to apical F-actin depolymerization and Rac1 deactivation. A similar downregulation of granuloma formation was observed after pretreatment with the Rac1 inhibitor NSC23766. Thus, this study demonstrates that Nsm dependent activation of β1-integrin induces cytoskeleton rearrangement, which in turn drives macrophage migration into granuloma formation upon BCG infection.

Nsm and mycobacterial granuloma

The role of granulomas in balancing the host defense and bacterial survival remains controversial because various mechanisms control initiation and maintenance of granuloma formation. Real-time visualization of *Mycobacterium marinum*, a zebrafish model of TB, showed that bacteria-containing macrophages led to the initiation of

granuloma formation (Davis et al., 2002). Studies using zebrafish suggest that, although participating macrophages may partially restrict the growth of mycobacteria, the newly recruited cells transform the granuloma from a protective environment into a hostile surroundings to the host (Clay et al., 2008; Davis and Ramakrishnan, 2009; Pagan and Ramakrishnan, 2014; Pagan et al., 2015). The results of the experiments reported here indicate that BCG uses granulomas for persistence: a reduction in granuloma formation in $Nsm^{+/-}$ mice or in mice treated with anti-β1-integrin antibodies is consistent with a lower bacterial burden. In contrast, Wt mice or mice treated with isotype control antibodies contain more granulomas and higher bacterial burden. Thus, it is suspected that bacteria use active β1-integrin as a driver for the recruitment of newly uninfected cells, which promotes granuloma formation.

Two observations support the possibility that the formation of granulomas in mycobacterial infections affects disease transmission. First, macrophages use classical epithelial pathways to generate mycobacterial granulomas. Because granuloma formation also creates a barrier against immune cell access and thus increases the bacterial load, it also damages the host (Cronan et al., 2016). Second, foamy macrophages, which could be described as lipid synthesis-dysregulated cells, within granulomas support the persistence of bacteria by providing a nutrient-rich reservoir. This changes the tissue pathology, thus resulting in cell destruction and the release of infectious bacteria (Peyron et al., 2008; Russell et al., 2009). The presented *in vivo* studies did not show classical TB granuloma since *in vivo* studies showed neither a tightly organized layer of cells surrounding the center of granuloma nor a necrotic center. This observation is not only due to the fact, that BCG are attenuated mycobacteria, but also because structures of granulomas seem to differ between mice and humans with a lack of necrotic centers even in TB-induced granulomas in mice (Guirado and Schlesinger, 2013; Rhoades et al., 1997). However, lipid droplet accumulations were found in Wt granuloma, which was almost absent in $Nsm^{+/-}$ mice or in Wt mice after treatment with anti-β1-integrin antibodies. It is assumed, that lipid droplets in mycobacterial induced granulomas serve as the sole carbon sources for the bacteria. Therefore, they are essential for mycobacterial survival and growth within granuloma (Peyron et al., 2008; Russell et al., 2009). The observed lipid droplets seem to be quite similar to those found in nascent granulomas detectable in the lungs of humans with TB (Kim et al., 2010).

Previous studies have found that BCG infection in macrophages increases the formation of lipid droplets (D'Avila et al., 2006). Also, ceramide levels are reported to be raised in mycobacteria-induced necrotic lung granulomas (Kim et al., 2010). More recently, Senkal et al. identified a pathway whereby ceramide is converted to acylceramides for storage in lipid droplets (Senkal et al., 2017; Shamseddine et al., 2015). The current study reports that Nsm is rapidly activated after BCG infection in Wt BMDMs and that this activation results in the generation of ceramide at the inner leaflet of the plasma membrane via hydrolysis of sphingomyelin. This finding raises the possibility that ceramide may be a source of lipid droplets in BCG infection and that these droplets could be further translocated and metabolized by bacteria (Airola et al., 2017).

Nsm, sphingosine, and ROS

Previous studies have shown that *M. tuberculosis* can inhibit SphK and block the Ca^{2+} flux to arrest phagosome maturation and to induce a pro-inflammatory response (Malik et al., 2003; Yadav et al., 2006). Also, it has been reported that S1P induces antimicrobial activity in human macrophages (Garg et al., 2004). Together, these findings suggest that the sphingosine metabolism is involved in and mediates mycobacterial infections. Most recently, it has been shown that the accumulation of luminal β1-integrin results in sphingosine depletion and thereby enhances the susceptibility of CF mice towards pulmonary *P. aeruginosa* infection (Grassme et al., 2017). It would be exciting to study the role of sphingosine metabolism in BCG-induced β1-integrin-mediated granuloma formation because it could lead to extended knowledge about mycobacterial infections in the future.

Previous studies have shown that BCG-induced rapid activation of Nsm results in an over-release of superoxide (reactive oxygen species, ROS). Thereby autophagy is suppressed, and bacterial killing is decreased both *in vitro* and *in vivo* (Li et al., 2016). The findings in the present studies show another consequence of Nsm activation during BCG infection, namely, the generation of granulomas via active β1-integrin. It would be intriguing to study whether these two mechanisms are co-orchestrated during mycobacterial infection. Especially since the antimicrobial effect of ROS is also reported to be a necessary condition for necrosis of granulomas (Roca and Ramakrishnan, 2013). The results in this work show that active β1-integrin induces the

activation of Rac1, which may well serve as a contributor to ROS generation via NADPH oxidase (Hordijk, 2006; Li et al., 2017).

Overall, this study suggests that Nsm dependent active β1-integrin plays a central role in macrophage migration and granuloma formation. The study also clearly indicates that an organized granuloma can be a protective niche for *Mycobacteria* (Cronan et al., 2016; Dorhoi and Kaufmann, 2014; Philips and Ernst, 2012; Ramakrishnan, 2012; Volkman et al., 2004). The interruption of granuloma formation by heterozygosity of the Nsm or anti-β1-integrin treatment results in protection against systemic BCG infection. This suggests that existing therapies may be enhanced by modulating the generation of granulomas.

5.2 The role of Asm in mycobacterial infection

The mycobacterial infections have been reported to be mediated by Asm (Roca and Ramakrishnan, 2013; Utermohlen et al., 2008; Vazquez et al., 2016), but the role of Asm in regulating the infection is controversial, and several fundamental questions remain to be answered. It has been shown that Asm regulates cell fusion by changing the lipid composition on the cellular membrane. Thereby, it contributes to the spreading of mycobacterial infection, while the inhibition of Asm prevents uncontrolled mycobacterial infection (Utermohlen et al., 2008). Another study showed that mycobacterial infection leads to activation of the Asm, thereby increasing ceramide, which in turn resulted in necrosis of infected cells (Roca and Ramakrishnan, 2013). Vazquez et al. showed that Asm is forwarded to phagosomes by Sortlin1, thus mediating phagosome-lysosome fusion, and controlling bacterial infection (Vazquez et al., 2016). These findings not only emphasize the importance of Asm in mycobacterial infections but also raise some key questions: how does Asm promote elimination or persistence of mycobacteria and what are the factors involved in this process? Elucidation of the mechanism of Asm mediated mycobacterial infections may explain the discrepancies between the mentioned studies and provide novel therapeutic targets for controlling tuberculosis, one of the most important diseases caused by mycobacteria.

The present data provide a novel mechanistic link between mycobacterial infections and Asm functions. An attenuated mycobacterial strain, BCG, causes a disease in mice, which is similar to tuberculosis in humans. In this study, BCG was used to infect mice to reflect the *in vivo* situation or infect BMDMs isolated from these mice to study the molecular mechanisms of the infection *in vitro*. The findings in this thesis suggest that Asm is essential for controlling BCG infection and limiting BCG survival both *in vivo* (especially in the liver) and *in vitro*. By using BMDMs isolated from Wt and $Asm^{-/-}$ mice, the study elucidates that Asm mediates expression of cathepsin D and degradation of BCG by cathepsin D, thus providing crucial evidence for the involvement of Asm in the fight against mycobacterial infections. The results in the thesis lead to the following scenario (Figure 21): Internalization of BCG induces activation of Asm and Ac, enhances SphK activity and thereby increases the S1P levels. The elevated S1P increases Nox2 subunit $p47^{phox}$ and triggers production of ROS, which in turn activates cathepsin D. Subsequently, BCG are exposed to

cathepsin D, thus triggering bacterial killing. All of these events were abolished in Asm$^{-/-}$ mice, leading to their high susceptibility to BCG infection. The importance of these findings was confirmed in an *in vivo* BMDMs-transplantation model: Asm$^{-/-}$ mice received BMDMs either from Wt mice or Asm deficient mice and were then infected with BCG. This model showed that reduced bacterial burden of Asm$^{-/-}$ mice occurred when Wt BMDMs were transplanted, while transplantation of Asm$^{-/-}$ BMDMs does not affect BCG load in Asm$^{-/-}$ mice. These results suggest that Asm is essential in enhancing anti-mycobacterial immunity in mice and that macrophages are crucially involved in this defense.

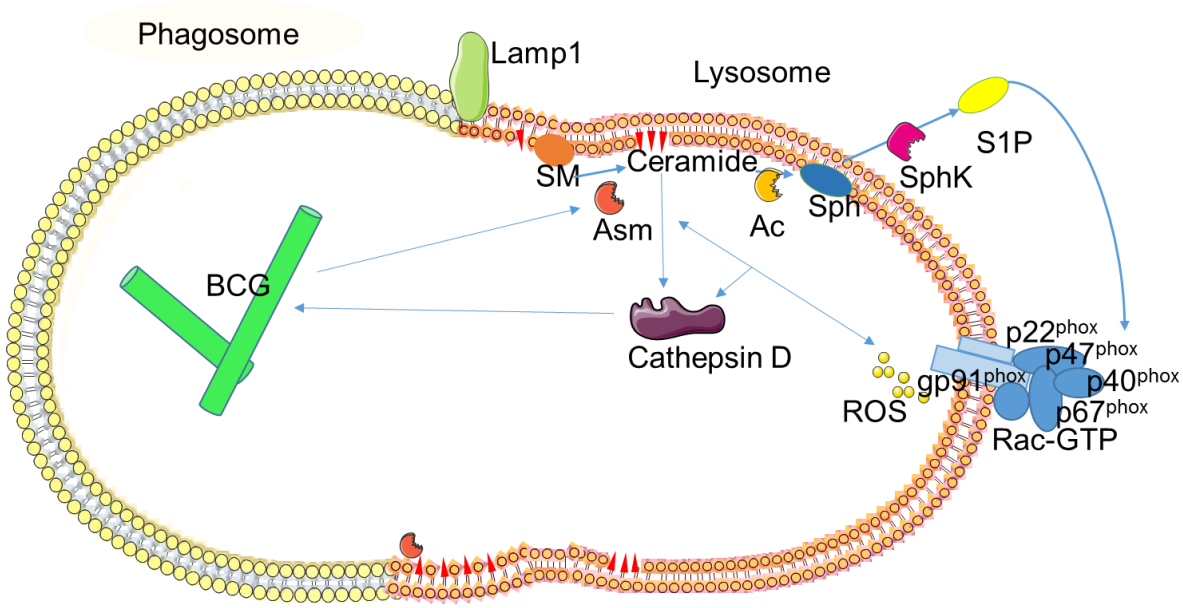

Figure 21. The scenario of Asm regulated BCG infection in macrophages.
BCG infection stimulates Asm and Ac in macrophages which increases S1P by activating SphK and triggers ROS production via Nox2 subunit p47^{phox}. Subsequently, ROS-activated cathepsin D is co-localized with BCG and mediates bacterial killing. Abbreviations: Lamp1, lysosomal-associated membrane protein 1; BCG, Bacillus Calmette-Guérin; SM, sphingomyelin; Asm, acid sphingomyelinase; Ac, acid ceramidase; Sph, sphingosine; SphK, sphingosine kinase; S1P, sphingosine-1-phosphate.

Asm and mycobacterial phagocytosis

The present data show that deficiency of Asm leads to a high sensitivity of BCG infection both *in vitro* and *in vivo*. Furthermore, transplantation of Wt BMDMs to Asm$^{-/-}$ mice partially reverses the susceptibility of Asm$^{-/-}$ mice to BCG infection. These data suggest that macrophages, as professional phagocytes, play an essential role in ingesting mycobacteria. Previous work has linked Asm with bacterial phagocytosis,

reporting either increased bacterial internalization or phagosome-lysosome maturation (Li et al., 2017; Schramm et al., 2008). Recognition of microbial pathogens by phagocyte surface receptors and their phagocytic uptake are the first step of immune defense against bacterial infections. This study here shows that both the binding and internalization of BCG into macrophages are independent of Asm. These results imply that other Asm-independent pathways are relevant in mycobacterial adherence and internalization. Some studies already provide evidence that mycobacteria can be taken up by Asm/ceramide-independent pathways. One potential candidate is complement receptor 3 (CR3) (Velasco-Velazquez et al., 2003). Previous studies showed that CR3 mediates the binding of *M. tuberculosis* to macrophages (Velasco-Velazquez et al., 2003). Alexander Gluschko et al. showed that CR3 is upstream of Asm activation in *L. monocytogenes* infection of macrophages (Gluschko et al., 2018). A Canadian group has demonstrated that CD14, another mycobacteria receptor (Peterson et al., 1995), upregulates CR3 activity during BCG infection and promotes bacterial phagocytosis in THP-1 cells (Sendide et al., 2005). Therefore, CD14 may also be one of the potential Asm independent receptors for mycobacterial binding and internalization. Interestingly, CD14 has been shown to activate Asm, thereby generating ceramide-enriched lipid rafts which cluster the TLR4 receptor upon LPS stimulation (Cuschieri et al., 2007). Thus, TLR4, which acts as a mycobacterial receptor (Sanchez et al., 2010), may not play a significant role in the present study. However, further investigations must be conducted to confirm these hypotheses.

Asm and cathepsins

Mature phagolysosomes contain high levels of cathepsins, the expression of cathepsins in phagolysosomes is critical for killing intracellular bacteria. Previous studies have shown that *M. tuberculosis* infection induces a general down-regulation of cathepsin expression within macrophages (Pires et al., 2016). This was associated with a decrease in cathepsin protein levels and enzymatic activity, favoring an increased intracellular survival of the pathogen. The enzymes significantly downregulated by *M. tuberculosis* in macrophages are cathepsin B, D, and S (Pires et al., 2016). Cathepsin D is a well-known enzyme which is activated by Asm-generated ceramide (Heinrich et al., 1999). An early study has shown that cathepsin D is involved in mycobacterial uptake by phagosomes and phagosomal maturation (Ullrich et al., 1999).

The current study shows that Asm mediates the activation of cathepsin D upon BCG infection, as well as the co-localization of BCG and cathepsin D, which is important for BCG degradation in BMDMs. In contrast, cathepsin D levels progressively decrease upon infection of $Asm^{-/-}$ BMDMs. Similar to the present work, cathepsin D has been shown to facilitate the elimination of *L. monocytogenes* in both macrophages and fibroblasts by degrading its main virulence factor, Listeriolysin O (del Cerro-Vadillo et al., 2006; Prada-Delgado et al., 2001). Another study showed that the infection of macrophages with *Streptococcus pneumonia* activates cathepsin D, thereby inducing apoptosis and facilitating bacterial clearance (Bewley et al., 2011). These findings are consistent with the observation presented in this thesis: The expression and activation of cathepsin D in Wt BMDMs lead to a high bactericidal environment in phagosome and promote degradation of BCG. This mechanism, however, is impaired in $Asm^{-/-}$ BMDMs.

Apart from its role in the bacterial killing, cathepsin D has also been reported to mediate antigen presentation during mycobacterial infection (Singh et al., 2006). A study conducted by Singh et al. (Singh et al., 2006) showed that cathepsin D is required for the generation of the Ag85B (a mycobacterial antigen) epitope by macrophages. Additionally, the silencing of cathepsin D reduced macrophage-induced IL-2 from T cells. Interestingly, they also demonstrated that phagosomes with the virulent mycobacterial strains, BCG and *M. tuberculosis* H37Rv, contained a 46-kDa form of cathepsin D, whereas phagosomes with the avirulent mycobacterial strain, H37Ra, possessed a 30-kDa form of cathepsin D, both being active forms of cathepsin D (Ullrich et al., 1999). Immunobiological studies of macrophages revealed that cathepsin D is involved in antigen processing (Singh et al., 2006). This might explain the high BCG burden in $Asm^{-/-}$ mice livers after 1week and 3 weeks of infection in the current work. Due to a partial inability in antigen processing or a delayed antigen presentation in $Asm^{-/-}$ macrophages (probably Kupffer cells in the liver), the adaptive immune response *in vivo* could be diminished.

An earlier study reported that cathepsin D mediates apoptosis in fibroblasts by cleaving proapoptotic Bcl-2 protein family member, Bid, in Rab5-positive vesicles (Heinrich et al., 2004). A later work demonstrated that some Rab GTPases control the recruitment of cathepsin D to phagosomes during *M. tuberculosis* infection. LysoTracker staining and immunofluorescence microscopy revealed that Rab7, Rab20, Rab22b, Rab32,

Rab34, Rab38 and Rab43 control the recruitment of cathepsin D to the phagosome (Seto et al., 2011). Although the results here suggest that Rab7 trafficking was not altered by Asm deficiency, it might be of interest to investigate whether other Rab family proteins are involved in mediating cathepsin D recruitment.

The current study focused only on the cathepsin D investigation upon BCG infection, while other cathepsins have also been described as being important for infectious diseases. Cathepsins B, G, and S have been shown to directly or indirectly interact with *Cryptococcus neoformans* and mycobacteria, thereby contributing to the elimination of these microorganisms (Hole et al., 2012; Rivera-Marrero et al., 2004; Soualhine et al., 2007; Steinwede et al., 2012). *Cryptococcus neoformans* was taken up by DCs and killed by DC lysosomal enzymes. Their growth was specifically inhibited by cathepsin B (Hole et al., 2012). It has been shown that the infection *M. tuberculosis* of THP-1 monocytes down-regulates cathepsin G and thereby facilitates bacterial viability (Rivera-Marrero et al., 2004). Cathepsin G deficient mice showed significantly impaired BCG killing and pronounced pulmonary granuloma formation upon BCG infection (Steinwede et al., 2012). Intracellular cathepsin S has been demonstrated to improve antigen presentation by MHC class II in BCG-infected macrophages and stimulate CD4(+) T cells (Soualhine et al., 2007). Cathepsins S, F, L, and V have been described to play multiple roles in antigen presentation during infection, to be critical for the balance of proteolytic activity and to have various activity kinetics in different cell types (Beers et al., 2005; Hsing and Rudensky, 2005; Shi et al., 2000; Tang et al., 2006; Villadangos and Ploegh, 2000). On the one hand, the increased activities of the enzymes can kill the bacteria. On the other hand, their reduced activities preserve the epitopes for provoking efficient lymphocyte priming (Pierre and Mellman, 1998; Russell et al., 2009; Savina and Amigorena, 2007; Savina et al., 2006; Yates et al., 2007). Therefore, the investigation of extended profiles of other cathepsins, besides cathepsin D, during BCG infection may help to elucidate the mechanism of Asm-regulated phagosome maturation and BCG killing.

Asm and ROS

The results in this study reveal a new pathway in mycobacterial infection, which suggests that Asm-induced ROS contribute to altering cathepsin D activation and

target BCG to cathepsin D. The rapid ROS accumulation after BCG infection is abolished in Asm$^{-/-}$ BMDMs. Pharmacological inhibition of ROS in BMDMs by using apocynin reduced cathepsin D activation and its co-localization with BCG.

ROS play controversial roles during mycobacterial infections. ROS have been reported as being both, susceptibility and resistance factors, in mycobacterial infections. They initially increase the microbicidal activity of macrophages, but can also rapidly induce programmed necrosis, thereby leading to the release of mycobacteria into the growth-permissive extracellular milieu (Roca and Ramakrishnan, 2013). The activity of NADPH oxidase affects not only the grade of phagosomal proteolysis but also the pattern of proteolytic digestion (Allan et al., 2014). Recently, it has been reported that Nsm-induced ROS inhibit autophagy and thereby negatively control BCG infection (Li et al., 2016). These findings imply a critical role of ROS in directly and indirectly affecting mycobacterial infection.

It has been previously demonstrated that Asm deficiency abolishes ROS release in *P. aeruginosa* and *S. aureus* infections (Li et al., 2017; Peng et al., 2015; Zhang et al., 2008). Asm-generated ceramide-enriched platforms are required for the activation of NADPH oxidase and the subsequent generation of ROS. Two subunits of NADPH oxidase p47^{phox} and gp91^{phox} have been shown to be critically involved in Asm/ceramide-regulated signaling (El-Benna et al., 2009; Reinehr et al., 2006; Zhang et al., 2008). This is consistent with the results reported here that Asm induces ROS release by regulating the Nox2 subunit p47^{phox}.

Other studies show that Asm can be directly activated by oxidation (Zhang and Li, 2010) and that Asm-induced ROS may be part of a positive feedback loop to boost Asm activation during *P. aeruginosa* infection (Zhang et al., 2008). These findings are consistent with the observations here that Asm and ROS have similar kinetics. An increase in Asm activity could be initially observed after 5mpi and peaked at 30 mpi, corresponding to the ROS production kinetics which was also initiated at 5 mpi and reached its peak at 30 mpi. The present study indicates that the positive feedback loop between Asm activity and ROS production is the underlying mechanism of ROS-controlled activation of cathepsin D. Upon BCG infection, the Asm is activated and triggers ROS production via activation of NADPH oxidase. ROS in turn increase Asm activity. The ROS-mediated increase in Asm activity leads to ceramide production. Ceramide is well known to directly interact with cathepsin D

(Heinrich et al., 1999) resulting in activation of the enzyme, which consistent with the results shown in this thesis.

Podinovskaia et al. reported recently that superoxide bursts are enhanced in both *M. tuberculosis*-infected human and murine macrophages (Podinovskaia et al., 2013). They found decreased phagosome acidification is due to enhanced NADPH oxidase activity in human but not in murine macrophages. This is accompanied by a reduction of phagosomal lipolysis and consequently increased retention of lipids. These lipids are known to serve as a nutrition source that might be accessed by bacteria in infected human macrophages (Peyron et al., 2008; Russell et al., 2009).

Interestingly, several studies discovered that Nox2 negatively regulates the levels of cysteine cathepsins within the maturing phagosome of macrophages and dendritic cells (Balce et al., 2011; Mantegazza et al., 2008; Rybicka et al., 2012; Rybicka et al., 2010; Savina et al., 2006). Later on, it was reported that the redox environment within phagolysosomes influences local proteases, including cathepsins S and L. These results indicate altered antigen processing in a cell-specific and antigen-specific manner (Allan et al., 2014). Further studies regarding the crosstalk between ROS and cathepsins in BCG infection would be appropriate.

Asm and SphK/S1P

Previous work suggested that Asm-derived ceramide triggers ROS production (Zhang et al., 2008). The study herein provides an additional mechanical link between Asm and ROS during BCG infection: The Asm-induced ROS production was achieved via the activation of the SphK/S1P system. Anes and coworkers first showed that a large range of sphingolipids is involved in mycobacterial infection to varying degrees. Sphingomyelin, ceramide, sphingosine, and S1P significantly increase the actin polymerization in phagosomes of mycobacteria-infected macrophages, activate phagosome-lysosome fusion, lower phagosomal pH and increase pathogen killing (Anes et al., 2003). These studies are consistent with the presented finding that $Asm^{-/-}$ BMDMs have a significantly lower level of microbicidal lipids, such as sphingomyelin, ceramide, sphingosine, and S1P in comparison to Wt macrophages and are impaired in phagosome and lysosome fusion and bacterial killing.

Other studies provide insights into mechanisms of sphingolipid-controlled mycobacterial infections. Most of these studies showed that SphK and S1P play a prominent role in mycobacterial infections as microbicidal factors. In 2003, Zulfiqar et al. first published a mechanism of *M. tuberculosis*-induced inhibition of phagosome-lysosome fusion and acidification via inhibition of SphK. The inhibition of SphK leads to the failure of Ca^{2+}-dependent phagosome maturation (Malik et al., 2003). Another group revealed that SphK is acting together with phosphoinositide-specific phospholipase C (PI-PLC), and a conventional protein kinase C (cPKC). They are required for ERK1/2 and PI3K activation and secretion of TNF-α, IL-6, RANTES and G-CSF (Yadav et al., 2006). Later on, Prakash et al. showed that the selective inhibition of SphK-1 increases the sensitivity of RAW macrophages to *M. smegmatis* infection. The sensitivity of RAW macrophages to *M.smegmatis* infection is due to the reduction in the generation of NO and secretion of TNF-α via downregulation of p38K (Prakash et al., 2010).

Garg et al. were the first to report a function of S1P in the induction of antimicrobial activity in mycobacterial infection (Garg et al., 2004). *In vitro*, they used human macrophages while *in vivo* mice were either infected with nonpathogenic *M. smegmatis* or pathogenic *M. tuberculosis* H37Rv. They showed that S1P induces host phospholipase D (PLD), which favors the acidification of mycobacteria-containing phagosomes. Mycobacteria-infected mice treated with S1P showed a significant reduction of bacterial load both in the lung and in the spleen, as well as less pulmonary tissue damage (granuloma) (Garg et al., 2004). Another work dealing with *M. tuberculosis*-infected monocytes shows that S1P plays a role in enhancing antigen presentation. Treatment with S1P increases antigen processing and presentation, enhances the frequency of *M. tuberculosis*-specific CD4+ T cells, and regulates IFN-γ production by antigen-specific CD4+ T cells (Santucci et al., 2007).

These studies demonstrate that SphK and S1P influence the bacterial elimination by promoting phagosome-lysosome fusion and play a role in the enhanced antigen presentation and adaptive immune response. However, they did not imply a potential regulator of SphK and S1P during mycobacterial infection. The results in this thesis suggest that Asm regulates SphK and S1P: In Wt BMDMs there was a significant increase of S1P upon BCG infection, whereas the S1P levels in Asm deficient

macrophages were not affected by infection, indicating that Asm is the mediator of SphK and S1P signaling during BCG infection.

The presented study shows that BCG infection induces not only an increased activity of Asm but also of Ac in Wt BMDMs. Mass spectrometry data, analyzing the sphingolipid metabolism, demonstrate a significant increase of S1P but no change in the level of sphingosine upon BCG infection of Wt macrophages. Since Ac hydrolyzes ceramide into sphingosine which can be phosphorylated by SphK into S1P, it is possible that ceramide and sphingosine are consumed and rapidly converted to S1P. Taken together, these results suggest that Asm controls SphK and S1P during BCG infection.

The data in this work suggest that SphK and S1P may also regulate ROS production upon mycobacterial infection. $Asm^{-/-}$ macrophages, which contain low levels of sphingosine and S1P, significantly reduce Nox2 subunit $p47^{phox}$ and ROS production upon BCG infection. Consistent with this, inhibition of SphK by SKI-I in Wt BMDMs also reduces the expression level of $p47^{phox}$ as well as ROS. These findings are consistent with some previous studies. S1P has been reported to increase NADPH oxidase activation in fibroblasts via phosphoinositide-3-kinase (PI3K) and protein kinase C (PKC). Also, the S1P-induced H_2O_2 production is necessary to maximize c-Src kinase activation (Catarzi et al., 2007). Another study reported that S1P transporter spinster homolog 2 (SPN2), S1P receptor 1 (S1PR1) and S1P receptor 2 (S1PR2) play a role in hypoxia-mediated ROS generation (Harijith et al., 2016). Also, $p47^{phox}$ activation and ROS generation were reduced by inhibition of SphK-1 in human lung microvascular endothelial cells (Harijith et al., 2016). However, there are also contrary studies. One study showed that SphK 1 suppresses lipopolysaccharide (LPS)-induced neutrophil oxidant production (Di et al., 2010) and S1PR2 knock out mice were shown to accumulate ROS (Herr et al., 2016). Previous work showed that S1P-mediated amelioration of lung pathology and disease severity in TB patients is mediated by the selective activation or rearrangement of various S1P receptors (S1PRs) particularly S1PR2. Furthermore, S1PR2 is effective in controlling respiratory fungal pathogens (McQuiston et al., 2011). The current data show that in Wt macrophages, intracellular S1P is highly elevated until 30 min of infection and then reduced again. The S1P might be secreted via S1P transporters after infection and interact with other cells via S1P receptors. To elucidate the mechanism of the SphK/S1P regulation of $p47^{phox}$ and

ROS, further studies addressing the role of S1P transporters and receptors may be very promising.

Asm and macrophages

The study presented here indicates that the deficiency of Asm results in high susceptibility of mice to BCG infection. Compared to Wt mice, an increased bacterial burden is observed in the livers of $Asm^{-/-}$ mice throughout the whole observation period (3 weeks). However, in the spleen, a higher burden in $Asm^{-/-}$ mice is only present at the beginning of the infection (1 day). After only 3 days of infection, the number of splenic bacteria in $Asm^{-/-}$ mice was similar to the level of Wt mice.

Similarly, after transplantation of Wt BMDMs into $Asm^{-/-}$ mice, hepatic bacterial load in $Asm^{-/-}$ mice is significantly reduced throughout the whole observation period (3 days) compared to non-transplanted, or $Asm^{-/-}$ BMDM transplanted $Asm^{-/-}$ mice. Instead, spleens of such transplanted $Asm^{-/-}$ mice even show a higher bacterial load than those of non-transplanted mice. The reversed susceptibility to BCG by transplantation of Wt macrophages to $Asm^{-/-}$ mice is observed only in the liver, but not spleen.

The discrepancy in hepatic and splenic bacterial load may be due to different immune responses of resident macrophages and other lymphocytes in those tissues.

One study compared different resident macrophages, murine Kupffer cells, splenic macrophages and peritoneal macrophages phenotypically and functionally (Movita et al., 2012). Under steady-state conditions, liver macrophages exert potent endocytic activities and display relatively high basal levels of ROS compared to splenic and peritoneal macrophages. Additionally, ligation of TLR4, TLR7/8, and TLR9 on Kupffer cells resulted in lower or undetectable levels of IL-12p40 and TNFα, as well as higher CD40 on the surface compared to other macrophages (Movita et al., 2012). These findings suggest that Kupffer cells are specialized phagocytes, which only play a limited immune-regulatory role (Movita et al., 2012). BMDMs have been reported to have similar properties as Kupffer cells (Beattie et al., 2016). Compared to splenic macrophages, BMDMs show a stronger capacity for proliferation and phagocytosis (Wang et al., 2013). However, BMDMs produce high levels of suppressive cytokines (IL-10 and TGFβ), while splenic macrophages maintained high levels of pro-inflammatory cytokines (IL-6, IL-12, and TNFα) (Wang et al., 2013).

Another common notion is that hepatic dendritic cells (DCs) are generally weak activators of immunity, although they are capable of producing inflammatory cytokines, and certain subtypes potently activate T cells. A recent study showed that hepatic DCs are less mature, capture fewer antigens, and induce less T cell stimulation than splenic DCs because of differences in their subtype composition (Pillarisetty et al., 2004). A study based on investigations of the *in situ* expression of MHC class II on hepatic DCs found that these cells do not display measurable levels of the T cell-costimulatory molecules CD40, CD80 and CD86. This implies a low immune-stimulatory capacity of hepatic DCs (Inaba et al., 1994). Furthermore, Kupffer cells have been shown to play a critical role in mycobacterial infections. A recent study investigated *M. tuberculosis* growth in murine Kupffer cells and found that significant increases in autophagy and cytoskeletal molecules contribute to the improved restriction of *M. tuberculosis* growth (Thandi et al., 2018).

These findings may explain differences between liver and spleen in $Asm^{-/-}$ mice upon BCG infection. On the one hand, the different phenotypes of BMDMs and splenic macrophages indicate different mechanisms for regulating the immune response. This suggests that BMDMs in the spleen are dysfunctional despite the success of the transplantation. On the other hand, in the context of mycobacterial infections, tissue-resident macrophages in the liver and spleen may be of varying importance. Other tissue lymphocytes, such as DCs or T lymphocytes, could play a leading role in the spleen. In order to better understand BCG clearance in tissues, further studies on the role of Asm in other cell types are essential.

In summary, these studies point out some potential and new mechanisms for Asm-dependent regulation of mycobacterial infections. The BCG infection activates the Asm/ceramide system, increases S1P and triggers the release of ROS thus activating cathepsin D. Cathepsin D colocalizes with BCG and functions as degrading bacteria.

To better understand the complex molecular mechanisms of the effect of Asm in mycobacterial infections and to develop antibacterial therapies, especially for tuberculosis, further studies are needed.

6 Summary

The presented thesis studied the role of sphingomyelinases in mycobacterial infection, focusing on Nsm and Asm. The work employed *M. bovis* BCG as a model for mycobacterial infection since BCG causes a disease in mice which is similar to tuberculosis in humans caused by *M. tuberculosis*.

The results concerning the role of Nsm in mycobacterial infection suggested a novel mechanism responsible for mycobacteria-induced granuloma. The major findings are:

- BCG infection rapidly induces activation of Nsm in BMDMs.
- The activation of Nsm leads to phosphorylation of p38K/JNK.
- Phosphorylated p38K/JNK activate β1-integrin.
- Activated β1-integrin results in the reorganization of the cytoskeleton.
- Cytoskeleton redistribution leads to the migration of macrophages and the formation of granulomas.
- Neutralization of active β1-integrin reduces granuloma numbers and bacterial burden *in vivo*.

The present data regarding the role of Asm in mycobacterial infection provide a novel mechanistic link between mycobacterial infections and Asm function. The main findings include the following:

- Asm deficiency leads to increased susceptibility of mice to BCG infection in comparison to Wt mice.
- BCG infection rapidly induces the activation of Asm and Ac in BMDMs.
- Asm and Ac activation trigger elevated levels of SphK and S1P.
- SphK/S1P increase $p47^{phox}$ and ROS generation.
- ROS promotes the expression and activity of the lysosomal enzyme, cathepsin D.
- Cathepsin D is important for BCG degradation within BMDMs.
- Transplantation of Wt BMDMs into $Asm^{-/-}$ mice reduces hepatic bacterial burden.

The studies presented in this thesis elucidate the role of sphingomyelinases in mycobacterial infection with regard to two important aspects related to mycobacterial infection, i.e., granuloma formation, and bacterial degradation. A combined study involving both neutral and acid sphingomyelinases may provide a novel therapeutic strategy against mycobacterial infection.

7 References

Abais, J.M., Xia, M., Li, G., Gehr, T.W., Boini, K.M., and Li, P.L. (2014). Contribution of endogenously produced reactive oxygen species to the activation of podocyte NLRP3 inflammasomes in hyperhomocysteinemia. Free radical biology & medicine *67*, 211-220.

Abdel Shakor, A.B., Kwiatkowska, K., and Sobota, A. (2004). Cell surface ceramide generation precedes and controls FcgammaRII clustering and phosphorylation in rafts. The Journal of biological chemistry *279*, 36778-36787.

Adams, D.O. (1976). The granulomatous inflammatory response. A review. The American journal of pathology *84*, 164-192.

Airola, M.V., Shanbhogue, P., Shamseddine, A.A., Guja, K.E., Senkal, C.E., Maini, R., Bartke, N., Wu, B.X., Obeid, L.M., Garcia-Diaz, M.*, et al.* (2017). Structure of human nSMase2 reveals an interdomain allosteric activation mechanism for ceramide generation. Proceedings of the National Academy of Sciences of the United States of America *114*, E5549-E5558.

Allan, E.R., Tailor, P., Balce, D.R., Pirzadeh, P., McKenna, N.T., Renaux, B., Warren, A.L., Jirik, F.R., and Yates, R.M. (2014). NADPH oxidase modifies patterns of MHC class II-restricted epitopic repertoires through redox control of antigen processing. Journal of immunology *192*, 4989-5001.

Anes, E., Kuhnel, M.P., Bos, E., Moniz-Pereira, J., Habermann, A., and Griffiths, G. (2003). Selected lipids activate phagosome actin assembly and maturation resulting in killing of pathogenic mycobacteria. Nature cell biology *5*, 793-802.

Avota, E., Gulbins, E., and Schneider-Schaulies, S. (2011). DC-SIGN mediated sphingomyelinase-activation and ceramide generation is essential for enhancement of viral uptake in dendritic cells. PLoS pathogens *7*, e1001290.

Babior, B.M., Lambeth, J.D., and Nauseef, W. (2002). The neutrophil NADPH oxidase. Arch Biochem Biophys *397*, 342-344.

Bailly, M., and Condeelis, J. (2002). Cell motility: insights from the backstage. Nature cell biology *4*, E292-294.

Balce, D.R., Li, B., Allan, E.R., Rybicka, J.M., Krohn, R.M., and Yates, R.M. (2011). Alternative activation of macrophages by IL-4 enhances the proteolytic capacity of their phagosomes through synergistic mechanisms. Blood *118*, 4199-4208.

Bandhuvula, P., and Saba, J.D. (2007). Sphingosine-1-phosphate lyase in immunity and cancer: silencing the siren. Trends in molecular medicine *13*, 210-217.

Beattie, L., Sawtell, A., Mann, J., Frame, T.C.M., Teal, B., de Labastida Rivera, F., Brown, N., Walwyn-Brown, K., Moore, J.W.J., MacDonald, S.*, et al.* (2016). Bone marrow-derived and resident liver macrophages display unique transcriptomic signatures but similar biological functions. Journal of hepatology *65*, 758-768.

Becker, K.A., Henry, B., Ziobro, R., Tummler, B., Gulbins, E., and Grassme, H. (2012). Role of CD95 in pulmonary inflammation and infection in cystic fibrosis. Journal of molecular medicine *90*, 1011-1023.

Bedard, K., and Krause, K.H. (2007). The NOX family of ROS-generating NADPH oxidases: physiology and pathophysiology. Physiological reviews *87*, 245-313.

Beers, C., Burich, A., Kleijmeer, M.J., Griffith, J.M., Wong, P., and Rudensky, A.Y. (2005). Cathepsin S controls MHC class II-mediated antigen presentation by epithelial cells in vivo. Journal of immunology *174*, 1205-1212.

Bermudez, L.E., Parker, A., and Goodman, J.R. (1997). Growth within macrophages increases the efficiency of Mycobacterium avium in invading other macrophages by a complement receptor-independent pathway. Infection and immunity *65*, 1916-1925.
Bewley, M.A., Marriott, H.M., Tulone, C., Francis, S.E., Mitchell, T.J., Read, R.C., Chain, B., Kroemer, G., Whyte, M.K., and Dockrell, D.H. (2011). A cardinal role for cathepsin d in co-ordinating the host-mediated apoptosis of macrophages and killing of pneumococci. PLoS pathogens *7*, e1001262.
Bezombes, C., Grazide, S., Garret, C., Fabre, C., Quillet-Mary, A., Muller, S., Jaffrezou, J.P., and Laurent, G. (2004). Rituximab antiproliferative effect in B-lymphoma cells is associated with acid-sphingomyelinase activation in raft microdomains. Blood *104*, 1166-1173.
Blaschke, F., Stawowy, P., Goetze, S., Hintz, O., Grafe, M., Kintscher, U., Fleck, E., and Graf, K. (2002). Hypoxia activates beta(1)-integrin via ERK 1/2 and p38 MAP kinase in human vascular smooth muscle cells. Biochemical and biophysical research communications *296*, 890-896.
Bonay, M., Roux, A.L., Floquet, J., Retory, Y., Herrmann, J.L., Lofaso, F., and Deramaudt, T.B. (2015). Caspase-independent apoptosis in infected macrophages triggered by sulforaphane via Nrf2/p38 signaling pathways. Cell death discovery *1*, 15022.
Boucher, L.M., Wiegmann, K., Futterer, A., Pfeffer, K., Machleidt, T., Schutze, S., Mak, T.W., and Kronke, M. (1995). CD28 signals through acidic sphingomyelinase. The Journal of experimental medicine *181*, 2059-2068.
Bright, N.A., Gratian, M.J., and Luzio, J.P. (2005). Endocytic delivery to lysosomes mediated by concurrent fusion and kissing events in living cells. Current biology : CB *15*, 360-365.
Briken, V., Porcelli, S.A., Besra, G.S., and Kremer, L. (2004). Mycobacterial lipoarabinomannan and related lipoglycans: from biogenesis to modulation of the immune response. Molecular microbiology *53*, 391-403.
Calderwood, D.A., Shattil, S.J., and Ginsberg, M.H. (2000). Integrins and actin filaments: reciprocal regulation of cell adhesion and signaling. The Journal of biological chemistry *275*, 22607-22610.
Canton, J. (2014). Phagosome maturation in polarized macrophages. Journal of leukocyte biology *96*, 729-738.
Carpinteiro, A., Becker, K.A., Japtok, L., Hessler, G., Keitsch, S., Pozgajova, M., Schmid, K.W., Adams, C., Muller, S., Kleuser, B.*, et al.* (2015). Regulation of hematogenous tumor metastasis by acid sphingomyelinase. EMBO Mol Med *7*, 714-734.
Catarzi, S., Giannoni, E., Favilli, F., Meacci, E., Iantomasi, T., and Vincenzini, M.T. (2007). Sphingosine 1-phosphate stimulation of NADPH oxidase activity: relationship with platelet-derived growth factor receptor and c-Src kinase. Biochimica et biophysica acta *1770*, 872-883.
Causeret, C., Geeraert, L., Van der Hoeven, G., Mannaerts, G.P., and Van Veldhoven, P.P. (2000). Further characterization of rat dihydroceramide desaturase: tissue distribution, subcellular localization, and substrate specificity. Lipids *35*, 1117-1125.
Christoforidis, S., McBride, H.M., Burgoyne, R.D., and Zerial, M. (1999). The Rab5 effector EEA1 is a core component of endosome docking. Nature *397*, 621-625.
Clarke, C.J., Truong, T.G., and Hannun, Y.A. (2007). Role for neutral sphingomyelinase-2 in tumor necrosis factor alpha-stimulated expression of vascular cell adhesion molecule-1 (VCAM) and intercellular adhesion molecule-1 (ICAM) in lung epithelial cells: p38 MAPK is an upstream regulator of nSMase2. The Journal of biological chemistry *282*, 1384-1396.

Clay, H., Volkman, H.E., and Ramakrishnan, L. (2008). Tumor necrosis factor signaling mediates resistance to mycobacteria by inhibiting bacterial growth and macrophage death. Immunity *29*, 283-294.
Cockburn, T.A. (1964). The Evolution and Eradication of Infectious Diseases. Perspectives in biology and medicine *7*, 498-499.
Cremesti, A.E., Goni, F.M., and Kolesnick, R. (2002). Role of sphingomyelinase and ceramide in modulating rafts: do biophysical properties determine biologic outcome? FEBS letters *531*, 47-53.
Cronan, M.R., Beerman, R.W., Rosenberg, A.F., Saelens, J.W., Johnson, M.G., Oehlers, S.H., Sisk, D.M., Jurcic Smith, K.L., Medvitz, N.A., Miller, S.E.*, et al.* (2016). Macrophage Epithelial Reprogramming Underlies Mycobacterial Granuloma Formation and Promotes Infection. Immunity *45*, 861-876.
Cuschieri, J., Bulger, E., Billgrin, J., Garcia, I., and Maier, R.V. (2007). Acid sphingomyelinase is required for lipid Raft TLR4 complex formation. Surgical infections *8*, 91-106.
D'Avila, H., Melo, R.C., Parreira, G.G., Werneck-Barroso, E., Castro-Faria-Neto, H.C., and Bozza, P.T. (2006). Mycobacterium bovis bacillus Calmette-Guerin induces TLR2-mediated formation of lipid bodies: intracellular domains for eicosanoid synthesis in vivo. Journal of immunology *176*, 3087-3097.
da Veiga Pereira, L., Desnick, R.J., Adler, D.A., Disteche, C.M., and Schuchman, E.H. (1991). Regional assignment of the human acid sphingomyelinase gene (SMPD1) by PCR analysis of somatic cell hybrids and in situ hybridization to 11p15.1----p15.4. Genomics *9*, 229-234.
Daffe, M. (2015). The cell envelope of tubercle bacilli. Tuberculosis *95 Suppl 1*, S155-158.
Davis, J.M., Clay, H., Lewis, J.L., Ghori, N., Herbomel, P., and Ramakrishnan, L. (2002). Real-time visualization of mycobacterium-macrophage interactions leading to initiation of granuloma formation in zebrafish embryos. Immunity *17*, 693-702.
Davis, J.M., and Ramakrishnan, L. (2009). The role of the granuloma in expansion and dissemination of early tuberculous infection. Cell *136*, 37-49.
del Cerro-Vadillo, E., Madrazo-Toca, F., Carrasco-Marin, E., Fernandez-Prieto, L., Beck, C., Leyva-Cobian, F., Saftig, P., and Alvarez-Dominguez, C. (2006). Cutting edge: a novel nonoxidative phagosomal mechanism exerted by cathepsin-D controls Listeria monocytogenes intracellular growth. Journal of immunology *176*, 1321-1325.
Deretic, V., Via, L.E., Fratti, R.A., and Deretic, D. (1997). Mycobacterial phagosome maturation, rab proteins, and intracellular trafficking. Electrophoresis *18*, 2542-2547.
Dheda, K., Schwander, S.K., Zhu, B., van Zyl-Smit, R.N., and Zhang, Y. (2010). The immunology of tuberculosis: from bench to bedside. Respirology *15*, 433-450.
Di, A., Kawamura, T., Gao, X.P., Tang, H., Berdyshev, E., Vogel, S.M., Zhao, Y.Y., Sharma, T., Bachmaier, K., Xu, J.*, et al.* (2010). A novel function of sphingosine kinase 1 suppression of JNK activity in preventing inflammation and injury. The Journal of biological chemistry *285*, 15848-15857.
Dorhoi, A., and Kaufmann, S.H. (2014). Perspectives on host adaptation in response to Mycobacterium tuberculosis: modulation of inflammation. Seminars in immunology *26*, 533-542.
Dreschers, S., Franz, P., Dumitru, C., Wilker, B., Jahnke, K., and Gulbins, E. (2007). Infections with human rhinovirus induce the formation of distinct functional membrane domains. Cellular physiology and biochemistry : international journal of experimental cellular physiology, biochemistry, and pharmacology *20*, 241-254.
Dumitru, C.A., Carpinteiro, A., Trarbach, T., Hengge, U.R., and Gulbins, E. (2007). Doxorubicin enhances TRAIL-induced cell death via ceramide-enriched membrane

platforms. Apoptosis : an international journal on programmed cell death *12*, 1533-1541.
Egen, J.G., Rothfuchs, A.G., Feng, C.G., Winter, N., Sher, A., and Germain, R.N. (2008). Macrophage and T cell dynamics during the development and disintegration of mycobacterial granulomas. Immunity *28*, 271-284.
El-Benna, J., Dang, P.M., Gougerot-Pocidalo, M.A., Marie, J.C., and Braut-Boucher, F. (2009). p47phox, the phagocyte NADPH oxidase/NOX2 organizer: structure, phosphorylation and implication in diseases. Experimental & molecular medicine *41*, 217-225.
Esen, M., Schreiner, B., Jendrossek, V., Lang, F., Fassbender, K., Grassme, H., and Gulbins, E. (2001). Mechanisms of Staphylococcus aureus induced apoptosis of human endothelial cells. Apoptosis : an international journal on programmed cell death *6*, 431-439.
Esmail, H., Barry, C.E., 3rd, Young, D.B., and Wilkinson, R.J. (2014). The ongoing challenge of latent tuberculosis. Philosophical transactions of the Royal Society of London Series B, Biological sciences *369*, 20130437.
Etoc, F., Lisse, D., Bellaiche, Y., Piehler, J., Coppey, M., and Dahan, M. (2013). Subcellular control of Rac-GTPase signalling by magnetogenetic manipulation inside living cells. Nature nanotechnology *8*, 193-198.
Fairn, G.D., and Grinstein, S. (2012). How nascent phagosomes mature to become phagolysosomes. Trends in immunology *33*, 397-405.
Falcone, S., Perrotta, C., De Palma, C., Pisconti, A., Sciorati, C., Capobianco, A., Rovere-Querini, P., Manfredi, A.A., and Clementi, E. (2004). Activation of acid sphingomyelinase and its inhibition by the nitric oxide/cyclic guanosine 3',5'-monophosphate pathway: key events in Escherichia coli-elicited apoptosis of dendritic cells. Journal of immunology *173*, 4452-4463.
Fang, F.C. (2011). Antimicrobial actions of reactive oxygen species. MBio *2*.
Faulstich, M., Hagen, F., Avota, E., Kozjak-Pavlovic, V., Winkler, A.C., Xian, Y., Schneider-Schaulies, S., and Rudel, T. (2015). Neutral sphingomyelinase 2 is a key factor for PorB-dependent invasion of Neisseria gonorrhoeae. Cellular microbiology *17*, 241-253.
Filosto, S., Ashfaq, M., Chung, S., Fry, W., and Goldkorn, T. (2012). Neutral sphingomyelinase 2 activity and protein stability are modulated by phosphorylation of five conserved serines. The Journal of biological chemistry *287*, 514-522.
Flannagan, R.S., Cosio, G., and Grinstein, S. (2009). Antimicrobial mechanisms of phagocytes and bacterial evasion strategies. Nature reviews Microbiology *7*, 355-366.
Flannagan, R.S., Jaumouille, V., and Grinstein, S. (2012). The cell biology of phagocytosis. Annual review of pathology *7*, 61-98.
Galadari, S., Wu, B.X., Mao, C., Roddy, P., El Bawab, S., and Hannun, Y.A. (2006). Identification of a novel amidase motif in neutral ceramidase. The Biochemical journal *393*, 687-695.
Garcia-Ruiz, C., Colell, A., Mari, M., Morales, A., Calvo, M., Enrich, C., and Fernandez-Checa, J.C. (2003). Defective TNF-alpha-mediated hepatocellular apoptosis and liver damage in acidic sphingomyelinase knockout mice. The Journal of clinical investigation *111*, 197-208.
Garg, S.K., Volpe, E., Palmieri, G., Mattei, M., Galati, D., Martino, A., Piccioni, M.S., Valente, E., Bonanno, E., De Vito, P.*, et al.* (2004). Sphingosine 1-phosphate induces antimicrobial activity both in vitro and in vivo. The Journal of infectious diseases *189*, 2129-2138.
Gassert, E., Avota, E., Harms, H., Krohne, G., Gulbins, E., and Schneider-Schaulies, S. (2009). Induction of membrane ceramides: a novel strategy to interfere with T

lymphocyte cytoskeletal reorganisation in viral immunosuppression. PLoS pathogens *5*, e1000623.
Gluschko, A., Herb, M., Wiegmann, K., Krut, O., Neiss, W.F., Utermohlen, O., Kronke, M., and Schramm, M. (2018). The beta2 Integrin Mac-1 Induces Protective LC3-Associated Phagocytosis of Listeria monocytogenes. Cell host & microbe *23*, 324-337 e325.
Goni, F.M., and Alonso, A. (2002). Sphingomyelinases: enzymology and membrane activity. FEBS letters *531*, 38-46.
Gorelik, A., Illes, K., Heinz, L.X., Superti-Furga, G., and Nagar, B. (2016). Crystal structure of mammalian acid sphingomyelinase. Nature communications *7*, 12196.
Grassme, H., Gulbins, E., Brenner, B., Ferlinz, K., Sandhoff, K., Harzer, K., Lang, F., and Meyer, T.F. (1997). Acidic sphingomyelinase mediates entry of N. gonorrhoeae into nonphagocytic cells. Cell *91*, 605-615.
Grassme, H., Henry, B., Ziobro, R., Becker, K.A., Riethmuller, J., Gardner, A., Seitz, A.P., Steinmann, J., Lang, S., Ward, C.*, et al.* (2017). beta1-Integrin Accumulates in Cystic Fibrosis Luminal Airway Epithelial Membranes and Decreases Sphingosine, Promoting Bacterial Infections. Cell Host Microbe *21*, 707-718 e708.
Grassme, H., Jekle, A., Riehle, A., Schwarz, H., Berger, J., Sandhoff, K., Kolesnick, R., and Gulbins, E. (2001). CD95 signaling via ceramide-rich membrane rafts. The Journal of biological chemistry *276*, 20589-20596.
Grassme, H., Jendrossek, V., Bock, J., Riehle, A., and Gulbins, E. (2002). Ceramide-rich membrane rafts mediate CD40 clustering. Journal of immunology *168*, 298-307.
Grassme, H., Jendrossek, V., Riehle, A., von Kurthy, G., Berger, J., Schwarz, H., Weller, M., Kolesnick, R., and Gulbins, E. (2003). Host defense against Pseudomonas aeruginosa requires ceramide-rich membrane rafts. Nature medicine *9*, 322-330.
Grassme, H., Riehle, A., Wilker, B., and Gulbins, E. (2005). Rhinoviruses infect human epithelial cells via ceramide-enriched membrane platforms. The Journal of biological chemistry *280*, 26256-26262.
Grassme, H., Riethmuller, J., and Gulbins, E. (2007). Biological aspects of ceramide-enriched membrane domains. Progress in lipid research *46*, 161-170.
Griffith, D.E., Aksamit, T., Brown-Elliott, B.A., Catanzaro, A., Daley, C., Gordin, F., Holland, S.M., Horsburgh, R., Huitt, G., Iademarco, M.F.*, et al.* (2007). An official ATS/IDSA statement: diagnosis, treatment, and prevention of nontuberculous mycobacterial diseases. Am J Respir Crit Care Med *175*, 367-416.
Guarner, J., Bartlett, J., Whitney, E.A., Raghunathan, P.L., Stienstra, Y., Asamoa, K., Etuaful, S., Klutse, E., Quarshie, E., van der Werf, T.S.*, et al.* (2003). Histopathologic features of Mycobacterium ulcerans infection. Emerg Infect Dis *9*, 651-656.
Guirado, E., and Schlesinger, L.S. (2013). Modeling the Mycobacterium tuberculosis Granuloma - the Critical Battlefield in Host Immunity and Disease. Frontiers in immunology *4*, 98.
Gulbins, A., Schumacher, F., Becker, K.A., Wilker, B., Soddemann, M., Boldrin, F., Muller, C.P., Edwards, M.J., Goodman, M., Caldwell, C.C.*, et al.* (2018). Antidepressants act by inducing autophagy controlled by sphingomyelin-ceramide. Molecular psychiatry.
Gulbins, E., and Li, P.L. (2006). Physiological and pathophysiological aspects of ceramide. Am J Physiol Regul Integr Comp Physiol *290*, R11-26.
Guo, F., Debidda, M., Yang, L., Williams, D.A., and Zheng, Y. (2006). Genetic deletion of Rac1 GTPase reveals its critical role in actin stress fiber formation and focal adhesion complex assembly. The Journal of biological chemistry *281*, 18652-18659.
Gutierrez, M.G. (2013). Functional role(s) of phagosomal Rab GTPases. Small GTPases *4*, 148-158.

Hait, N.C., Oskeritzian, C.A., Paugh, S.W., Milstien, S., and Spiegel, S. (2006). Sphingosine kinases, sphingosine 1-phosphate, apoptosis and diseases. Biochimica et biophysica acta *1758*, 2016-2026.
Hannun, Y.A., and Obeid, L.M. (2008). Principles of bioactive lipid signalling: lessons from sphingolipids. Nature reviews Molecular cell biology *9*, 139-150.
Hanson, P.I., Roth, R., Lin, Y., and Heuser, J.E. (2008). Plasma membrane deformation by circular arrays of ESCRT-III protein filaments. The Journal of cell biology *180*, 389-402.
Harijith, A., Pendyala, S., Ebenezer, D.L., Ha, A.W., Fu, P., Wang, Y.T., Ma, K., Toth, P.T., Berdyshev, E.V., Kanteti, P.*, et al.* (2016). Hyperoxia-induced p47phox activation and ROS generation is mediated through S1P transporter Spns2, and S1P/S1P1&2 signaling axis in lung endothelium. American journal of physiology Lung cellular and molecular physiology *311*, L337-351.
Hauck, C.R., Grassme, H., Bock, J., Jendrossek, V., Ferlinz, K., Meyer, T.F., and Gulbins, E. (2000). Acid sphingomyelinase is involved in CEACAM receptor-mediated phagocytosis of Neisseria gonorrhoeae. FEBS letters *478*, 260-266.
Hed, J. (1986). Methods for distinguishing ingested from adhering particles. Methods in enzymology *132*, 198-204.
Hedlund, M., Duan, R.D., Nilsson, A., and Svanborg, C. (1998). Sphingomyelin, glycosphingolipids and ceramide signalling in cells exposed to P-fimbriated Escherichia coli. Molecular microbiology *29*, 1297-1306.
Heinrich, M., Neumeyer, J., Jakob, M., Hallas, C., Tchikov, V., Winoto-Morbach, S., Wickel, M., Schneider-Brachert, W., Trauzold, A., Hethke, A.*, et al.* (2004). Cathepsin D links TNF-induced acid sphingomyelinase to Bid-mediated caspase-9 and -3 activation. Cell death and differentiation *11*, 550-563.
Heinrich, M., Wickel, M., Schneider-Brachert, W., Sandberg, C., Gahr, J., Schwandner, R., Weber, T., Saftig, P., Peters, C., Brunner, J.*, et al.* (1999). Cathepsin D targeted by acid sphingomyelinase-derived ceramide. The EMBO journal *18*, 5252-5263.
Herr, D.R., Reolo, M.J., Peh, Y.X., Wang, W., Lee, C.W., Rivera, R., Paterson, I.C., and Chun, J. (2016). Sphingosine 1-phosphate receptor 2 (S1P2) attenuates reactive oxygen species formation and inhibits cell death: implications for otoprotective therapy. Scientific reports *6*, 24541.
Hofmann, K., Tomiuk, S., Wolff, G., and Stoffel, W. (2000). Cloning and characterization of the mammalian brain-specific, Mg2+-dependent neutral sphingomyelinase. Proceedings of the National Academy of Sciences of the United States of America *97*, 5895-5900.
Hole, C.R., Bui, H., Wormley, F.L., Jr., and Wozniak, K.L. (2012). Mechanisms of dendritic cell lysosomal killing of Cryptococcus. Scientific reports *2*, 739.
Hordijk, P.L. (2006). Regulation of NADPH oxidases: the role of Rac proteins. Circulation research *98*, 453-462.
Horinouchi, K., Erlich, S., Perl, D.P., Ferlinz, K., Bisgaier, C.L., Sandhoff, K., Desnick, R.J., Stewart, C.L., and Schuchman, E.H. (1995). Acid sphingomyelinase deficient mice: a model of types A and B Niemann-Pick disease. Nature genetics *10*, 288-293.
Hsing, L.C., and Rudensky, A.Y. (2005). The lysosomal cysteine proteases in MHC class II antigen presentation. Immunological reviews *207*, 229-241.
Humphreys, I.R., Stewart, G.R., Turner, D.J., Patel, J., Karamanou, D., Snelgrove, R.J., and Young, D.B. (2006). A role for dendritic cells in the dissemination of mycobacterial infection. Microbes Infect *8*, 1339-1346.
Hurwitz, R., Ferlinz, K., Vielhaber, G., Moczall, H., and Sandhoff, K. (1994). Processing of human acid sphingomyelinase in normal and I-cell fibroblasts. The Journal of biological chemistry *269*, 5440-5445.

Huynh, K.K., Eskelinen, E.L., Scott, C.C., Malevanets, A., Saftig, P., and Grinstein, S. (2007). LAMP proteins are required for fusion of lysosomes with phagosomes. The EMBO journal *26*, 313-324.
Inaba, K., Witmer-Pack, M., Inaba, M., Hathcock, K.S., Sakuta, H., Azuma, M., Yagita, H., Okumura, K., Linsley, P.S., Ikehara, S.*, et al.* (1994). The tissue distribution of the B7-2 costimulator in mice: abundant expression on dendritic cells in situ and during maturation in vitro. The Journal of experimental medicine *180*, 1849-1860.
Jay, S.M., Skokos, E., Laiwalla, F., Krady, M.M., and Kyriakides, T.R. (2007). Foreign body giant cell formation is preceded by lamellipodia formation and can be attenuated by inhibition of Rac1 activation. The American journal of pathology *171*, 632-640.
Jenkins, R.W., Idkowiak-Baldys, J., Simbari, F., Canals, D., Roddy, P., Riner, C.D., Clarke, C.J., and Hannun, Y.A. (2011). A novel mechanism of lysosomal acid sphingomyelinase maturation: requirement for carboxyl-terminal proteolytic processing. The Journal of biological chemistry *286*, 3777-3788.
Kagina, B.M., Abel, B., Scriba, T.J., Hughes, E.J., Keyser, A., Soares, A., Gamieldien, H., Sidibana, M., Hatherill, M., Gelderbloem, S.*, et al.* (2010). Specific T cell frequency and cytokine expression profile do not correlate with protection against tuberculosis after bacillus Calmette-Guerin vaccination of newborns. Am J Respir Crit Care Med *182*, 1073-1079.
Karakashian, A.A., Giltiay, N.V., Smith, G.M., and Nikolova-Karakashian, M.N. (2004). Expression of neutral sphingomyelinase-2 (NSMase-2) in primary rat hepatocytes modulates IL-beta-induced JNK activation. FASEB journal : official publication of the Federation of American Societies for Experimental Biology *18*, 968-970.
Kim, M.J., Wainwright, H.C., Locketz, M., Bekker, L.G., Walther, G.B., Dittrich, C., Visser, A., Wang, W., Hsu, F.F., Wiehart, U.*, et al.* (2010). Caseation of human tuberculosis granulomas correlates with elevated host lipid metabolism. EMBO Mol Med *2*, 258-274.
Kinchen, J.M., and Ravichandran, K.S. (2008). Phagosome maturation: going through the acid test. Nature reviews Molecular cell biology *9*, 781-795.
Kitano, M., Nakaya, M., Nakamura, T., Nagata, S., and Matsuda, M. (2008). Imaging of Rab5 activity identifies essential regulators for phagosome maturation. Nature *453*, 241-245.
Koch, R. (1882). The etiology of tuberculosis. Berl Klin Wochenschr *15*, 221-230.
Lay, G., Poquet, Y., Salek-Peyron, P., Puissegur, M.P., Botanch, C., Bon, H., Levillain, F., Duteyrat, J.L., Emile, J.F., and Altare, F. (2007). Langhans giant cells from M. tuberculosis-induced human granulomas cannot mediate mycobacterial uptake. The Journal of pathology *211*, 76-85.
Lee, S.H., and Dominguez, R. (2010). Regulation of actin cytoskeleton dynamics in cells. Molecules and cells *29*, 311-325.
Levin, R., Grinstein, S., and Canton, J. (2016). The life cycle of phagosomes: formation, maturation, and resolution. Immunological reviews *273*, 156-179.
Li, C., Peng, H., Japtok, L., Seitz, A., Riehle, A., Wilker, B., Soddemann, M., Kleuser, B., Edwards, M., Lammas, D.*, et al.* (2016). Inhibition of neutral sphingomyelinase protects mice against systemic tuberculosis. Frontiers in bioscience *8*, 311-325.
Li, C., Wu, Y., Riehle, A., Orian-Rousseau, V., Zhang, Y., Gulbins, E., and Grassme, H. (2017). Regulation of Staphylococcus aureus Infection of Macrophages by CD44, Reactive Oxygen Species, and Acid Sphingomyelinase. Antioxidants & redox signaling.
Lim, J.J., Grinstein, S., and Roth, Z. (2017). Diversity and Versatility of Phagocytosis: Roles in Innate Immunity, Tissue Remodeling, and Homeostasis. Frontiers in cellular and infection microbiology *7*, 191.

Lin, P.L., Ford, C.B., Coleman, M.T., Myers, A.J., Gawande, R., Ioerger, T., Sacchettini, J., Fortune, S.M., and Flynn, J.L. (2014). Sterilization of granulomas is common in active and latent tuberculosis despite within-host variability in bacterial killing. Nature medicine *20*, 75-79.
Linn, S.C., Kim, H.S., Keane, E.M., Andras, L.M., Wang, E., and Merrill, A.H., Jr. (2001). Regulation of de novo sphingolipid biosynthesis and the toxic consequences of its disruption. Biochemical Society transactions *29*, 831-835.
Liu, J. (2005). Tuberculosis and the Tubercle Bacillus. Emerging Infectious Diseases *11*, 1331-1331.
Luisoni, S., Suomalainen, M., Boucke, K., Tanner, L.B., Wenk, M.R., Guan, X.L., Grzybek, M., Coskun, U., and Greber, U.F. (2015). Co-option of Membrane Wounding Enables Virus Penetration into Cells. Cell host & microbe *18*, 75-85.
Luo, B.H., Carman, C.V., and Springer, T.A. (2007). Structural basis of integrin regulation and signaling. Annual review of immunology *25*, 619-647.
Ma, J., Gulbins, E., Edwards, M.J., Caldwell, C.C., Fraunholz, M., and Becker, K.A. (2017). Staphylococcus aureus alpha-Toxin Induces Inflammatory Cytokines via Lysosomal Acid Sphingomyelinase and Ceramides. Cellular physiology and biochemistry : international journal of experimental cellular physiology, biochemistry, and pharmacology *43*, 2170-2184.
Maglione, P.J., Xu, J., and Chan, J. (2007). B cells moderate inflammatory progression and enhance bacterial containment upon pulmonary challenge with Mycobacterium tuberculosis. Journal of immunology *178*, 7222-7234.
Malik, Z.A., Thompson, C.R., Hashimi, S., Porter, B., Iyer, S.S., and Kusner, D.J. (2003). Cutting edge: Mycobacterium tuberculosis blocks Ca2+ signaling and phagosome maturation in human macrophages via specific inhibition of sphingosine kinase. Journal of immunology *170*, 2811-2815.
Mantegazza, A.R., Savina, A., Vermeulen, M., Perez, L., Geffner, J., Hermine, O., Rosenzweig, S.D., Faure, F., and Amigorena, S. (2008). NADPH oxidase controls phagosomal pH and antigen cross-presentation in human dendritic cells. Blood *112*, 4712-4722.
Marathe, S., Schissel, S.L., Yellin, M.J., Beatini, N., Mintzer, R., Williams, K.J., and Tabas, I. (1998). Human vascular endothelial cells are a rich and regulatable source of secretory sphingomyelinase. Implications for early atherogenesis and ceramide-mediated cell signaling. The Journal of biological chemistry *273*, 4081-4088.
Marchesini, N., and Hannun, Y.A. (2004). Acid and neutral sphingomyelinases: roles and mechanisms of regulation. Biochemistry and cell biology = Biochimie et biologie cellulaire *82*, 27-44.
Marshansky, V., and Futai, M. (2008). The V-type H+-ATPase in vesicular trafficking: targeting, regulation and function. Current opinion in cell biology *20*, 415-426.
Masson, P.L., Heremans, J.F., and Schonne, E. (1969). Lactoferrin, an iron-binding protein in neutrophilic leukocytes. The Journal of experimental medicine *130*, 643-658.
McCann, S.K., and Roulston, C.L. (2013). NADPH Oxidase as a Therapeutic Target for Neuroprotection against Ischaemic Stroke: Future Perspectives. Brain sciences *3*, 561-598.
McCollister, B.D., Myers, J.T., Jones-Carson, J., Voelker, D.R., and Vazquez-Torres, A. (2007). Constitutive acid sphingomyelinase enhances early and late macrophage killing of Salmonella enterica serovar Typhimurium. Infection and immunity *75*, 5346-5352.
McNally, A.K., and Anderson, J.M. (2002). Beta1 and beta2 integrins mediate adhesion during macrophage fusion and multinucleated foreign body giant cell formation. The American journal of pathology *160*, 621-630.

McQuiston, T., Luberto, C., and Del Poeta, M. (2011). Role of sphingosine-1-phosphate (S1P) and S1P receptor 2 in the phagocytosis of Cryptococcus neoformans by alveolar macrophages. Microbiology *157*, 1416-1427.
Miller, J.L., Velmurugan, K., Cowan, M.J., and Briken, V. (2010). The type I NADH dehydrogenase of Mycobacterium tuberculosis counters phagosomal NOX2 activity to inhibit TNF-alpha-mediated host cell apoptosis. PLoS pathogens *6*, e1000864.
Miller, M.E., Adhikary, S., Kolokoltsov, A.A., and Davey, R.A. (2012). Ebolavirus requires acid sphingomyelinase activity and plasma membrane sphingomyelin for infection. Journal of virology *86*, 7473-7483.
Minakami, R., and Sumimotoa, H. (2006). Phagocytosis-coupled activation of the superoxide-producing phagocyte oxidase, a member of the NADPH oxidase (nox) family. International journal of hematology *84*, 193-198.
Miura, Y., Gotoh, E., Nara, F., Nishijima, M., and Hanada, K. (2004). Hydrolysis of sphingosylphosphocholine by neutral sphingomyelinases. FEBS letters *557*, 288-292.
Movita, D., Kreefft, K., Biesta, P., van Oudenaren, A., Leenen, P.J., Janssen, H.L., and Boonstra, A. (2012). Kupffer cells express a unique combination of phenotypic and functional characteristics compared with splenic and peritoneal macrophages. Journal of leukocyte biology *92*, 723-733.
Nakatsuji, T., Tang, D.C., Zhang, L., Gallo, R.L., and Huang, C.M. (2011). Propionibacterium acnes CAMP factor and host acid sphingomyelinase contribute to bacterial virulence: potential targets for inflammatory acne treatment. PloS one *6*, e14797.
Nessar, R., Cambau, E., Reyrat, J.M., Murray, A., and Gicquel, B. (2012). Mycobacterium abscessus: a new antibiotic nightmare. The Journal of antimicrobial chemotherapy *67*, 810-818.
Nienhuis, W.A., Stienstra, Y., Thompson, W.A., Awuah, P.C., Abass, K.M., Tuah, W., Awua-Boateng, N.Y., Ampadu, E.O., Siegmund, V., Schouten, J.P.*, et al.* (2010). Antimicrobial treatment for early, limited Mycobacterium ulcerans infection: a randomised controlled trial. Lancet *375*, 664-672.
Nunes-Alves, C., Booty, M.G., Carpenter, S.M., Jayaraman, P., Rothchild, A.C., and Behar, S.M. (2014). In search of a new paradigm for protective immunity to TB. Nature reviews Microbiology *12*, 289-299.
Pagan, A.J., and Ramakrishnan, L. (2014). Immunity and Immunopathology in the Tuberculous Granuloma. Cold Spring Harbor perspectives in medicine *5*.
Pagan, A.J., Yang, C.T., Cameron, J., Swaim, L.E., Ellett, F., Lieschke, G.J., and Ramakrishnan, L. (2015). Myeloid Growth Factors Promote Resistance to Mycobacterial Infection by Curtailing Granuloma Necrosis through Macrophage Replenishment. Cell host & microbe *18*, 15-26.
Pai, M., Behr, M.A., Dowdy, D., Dheda, K., Divangahi, M., Boehme, C.C., Ginsberg, A., Swaminathan, S., Spigelman, M., Getahun, H.*, et al.* (2016). Tuberculosis. Nature reviews Disease primers *2*, 16076.
Pandey, A.K., and Sassetti, C.M. (2008). Mycobacterial persistence requires the utilization of host cholesterol. Proceedings of the National Academy of Sciences of the United States of America *105*, 4376-4380.
Parsons, J.T., Horwitz, A.R., and Schwartz, M.A. (2010). Cell adhesion: integrating cytoskeletal dynamics and cellular tension. Nature reviews Molecular cell biology *11*, 633-643.
Pauwels, A.M., Trost, M., Beyaert, R., and Hoffmann, E. (2017). Patterns, Receptors, and Signals: Regulation of Phagosome Maturation. Trends in immunology *38*, 407-422.

Peng, H., Li, C., Kadow, S., Henry, B.D., Steinmann, J., Becker, K.A., Riehle, A., Beckmann, N., Wilker, B., Li, P.L., *et al.* (2015). Acid sphingomyelinase inhibition protects mice from lung edema and lethal Staphylococcus aureus sepsis. Journal of molecular medicine *93*, 675-689.
Peterson, P.K., Gekker, G., Hu, S., Sheng, W.S., Anderson, W.R., Ulevitch, R.J., Tobias, P.S., Gustafson, K.V., Molitor, T.W., and Chao, C.C. (1995). CD14 receptor-mediated uptake of nonopsonized Mycobacterium tuberculosis by human microglia. Infection and immunity *63*, 1598-1602.
Pewzner-Jung, Y., Ben-Dor, S., and Futerman, A.H. (2006). When do Lasses (longevity assurance genes) become CerS (ceramide synthases)?: Insights into the regulation of ceramide synthesis. The Journal of biological chemistry *281*, 25001-25005.
Peyron, P., Vaubourgeix, J., Poquet, Y., Levillain, F., Botanch, C., Bardou, F., Daffe, M., Emile, J.F., Marchou, B., Cardona, P.J., *et al.* (2008). Foamy macrophages from tuberculous patients' granulomas constitute a nutrient-rich reservoir for M. tuberculosis persistence. PLoS pathogens *4*, e1000204.
Philipp, S., Puchert, M., Adam-Klages, S., Tchikov, V., Winoto-Morbach, S., Mathieu, S., Deerberg, A., Kolker, L., Marchesini, N., Kabelitz, D., *et al.* (2010). The Polycomb group protein EED couples TNF receptor 1 to neutral sphingomyelinase. Proceedings of the National Academy of Sciences of the United States of America *107*, 1112-1117.
Philips, J.A. (2008). Mycobacterial manipulation of vacuolar sorting. Cellular microbiology *10*, 2408-2415.
Philips, J.A., and Ernst, J.D. (2012). Tuberculosis pathogenesis and immunity. Annual review of pathology *7*, 353-384.
Pierre, P., and Mellman, I. (1998). Developmental regulation of invariant chain proteolysis controls MHC class II trafficking in mouse dendritic cells. Cell *93*, 1135-1145.
Pillarisetty, V.G., Shah, A.B., Miller, G., Bleier, J.I., and DeMatteo, R.P. (2004). Liver dendritic cells are less immunogenic than spleen dendritic cells because of differences in subtype composition. Journal of immunology *172*, 1009-1017.
Pires, D., Marques, J., Pombo, J.P., Carmo, N., Bettencourt, P., Neyrolles, O., Lugo-Villarino, G., and Anes, E. (2016). Role of Cathepsins in Mycobacterium tuberculosis Survival in Human Macrophages. Scientific reports *6*, 32247.
Podinovskaia, M., Lee, W., Caldwell, S., and Russell, D.G. (2013). Infection of macrophages with Mycobacterium tuberculosis induces global modifications to phagosomal function. Cellular microbiology *15*, 843-859.
Prada-Delgado, A., Carrasco-Marin, E., Bokoch, G.M., and Alvarez-Dominguez, C. (2001). Interferon-gamma listericidal action is mediated by novel Rab5a functions at the phagosomal environment. The Journal of biological chemistry *276*, 19059-19065.
Prakash, H., Luth, A., Grinkina, N., Holzer, D., Wadgaonkar, R., Gonzalez, A.P., Anes, E., and Kleuser, B. (2010). Sphingosine kinase-1 (SphK-1) regulates Mycobacterium smegmatis infection in macrophages. PloS one *5*, e10657.
Pryor, P.R., and Luzio, J.P. (2009). Delivery of endocytosed membrane proteins to the lysosome. Biochimica et biophysica acta *1793*, 615-624.
Puissegur, M.P., Botanch, C., Duteyrat, J.L., Delsol, G., Caratero, C., and Altare, F. (2004). An in vitro dual model of mycobacterial granulomas to investigate the molecular interactions between mycobacteria and human host cells. Cellular microbiology *6*, 423-433.
Puissegur, M.P., Lay, G., Gilleron, M., Botella, L., Nigou, J., Marrakchi, H., Mari, B., Duteyrat, J.L., Guerardel, Y., Kremer, L., *et al.* (2007). Mycobacterial lipomannan

induces granuloma macrophage fusion via a TLR2-dependent, ADAM9- and beta1 integrin-mediated pathway. Journal of immunology *178*, 3161-3169.
Qiu, H., Edmunds, T., Baker-Malcolm, J., Karey, K.P., Estes, S., Schwarz, C., Hughes, H., and Van Patten, S.M. (2003). Activation of human acid sphingomyelinase through modification or deletion of C-terminal cysteine. The Journal of biological chemistry *278*, 32744-32752.
Qrafli, M., Asekkaj, I., Bourkadi, J.E., El Aouad, R., and Sadki, K. (2017). New variant identified in major susceptibility locus to tuberculosis on chromosomal region 8q12-q13 in Moroccan population: a case control study. BMC infectious diseases *17*, 712.
Raas-Rothschild, A., Pankova-Kholmyansky, I., Kacher, Y., and Futerman, A.H. (2004). Glycosphingolipidoses: beyond the enzymatic defect. Glycoconjugate journal *21*, 295-304.
Ramakrishnan, L. (2012). Revisiting the role of the granuloma in tuberculosis. Nature reviews Immunology *12*, 352-366.
Randhawa, P.S. (1990). Lymphocyte subsets in granulomas of human tuberculosis: an in situ immunofluorescence study using monoclonal antibodies. Pathology *22*, 153-155.
Reinehr, R., Becker, S., Braun, J., Eberle, A., Grether-Beck, S., and Haussinger, D. (2006). Endosomal acidification and activation of NADPH oxidase isoforms are upstream events in hyperosmolarity-induced hepatocyte apoptosis. The Journal of biological chemistry *281*, 23150-23166.
Rhoades, E.R., Frank, A.A., and Orme, I.M. (1997). Progression of chronic pulmonary tuberculosis in mice aerogenically infected with virulent Mycobacterium tuberculosis. Tubercle and lung disease : the official journal of the International Union against Tuberculosis and Lung Disease *78*, 57-66.
Rink, J., Ghigo, E., Kalaidzidis, Y., and Zerial, M. (2005). Rab conversion as a mechanism of progression from early to late endosomes. Cell *122*, 735-749.
Rivera-Marrero, C.A., Stewart, J., Shafer, W.M., and Roman, J. (2004). The down-regulation of cathepsin G in THP-1 monocytes after infection with Mycobacterium tuberculosis is associated with increased intracellular survival of bacilli. Infection and immunity *72*, 5712-5721.
Roca, F.J., and Ramakrishnan, L. (2013). TNF dually mediates resistance and susceptibility to mycobacteria via mitochondrial reactive oxygen species. Cell *153*, 521-534.
Rosales, C., and Uribe-Querol, E. (2017). Phagocytosis: A Fundamental Process in Immunity. BioMed research international *2017*, 9042851.
Russell, D.G., Vanderven, B.C., Glennie, S., Mwandumba, H., and Heyderman, R.S. (2009). The macrophage marches on its phagosome: dynamic assays of phagosome function. Nat Rev Immunol *9*, 594-600.
Rybicka, J.M., Balce, D.R., Chaudhuri, S., Allan, E.R., and Yates, R.M. (2012). Phagosomal proteolysis in dendritic cells is modulated by NADPH oxidase in a pH-independent manner. The EMBO journal *31*, 932-944.
Rybicka, J.M., Balce, D.R., Khan, M.F., Krohn, R.M., and Yates, R.M. (2010). NADPH oxidase activity controls phagosomal proteolysis in macrophages through modulation of the lumenal redox environment of phagosomes. Proceedings of the National Academy of Sciences of the United States of America *107*, 10496-10501.
Sanchez, D., Rojas, M., Hernandez, I., Radzioch, D., Garcia, L.F., and Barrera, L.F. (2010). Role of TLR2- and TLR4-mediated signaling in Mycobacterium tuberculosis-induced macrophage death. Cellular immunology *260*, 128-136.
Santucci, M.B., Greco, E., De Spirito, M., Arcovito, G., De Angelis, G., Cauda, R., and Fraziano, M. (2007). Sphingosine 1-phosphate promotes antigen processing and

presentation to CD4+ T cells in Mycobacterium tuberculosis-infected monocytes. Biochemical and biophysical research communications *361*, 687-693.
Savina, A., and Amigorena, S. (2007). Phagocytosis and antigen presentation in dendritic cells. Immunological reviews *219*, 143-156.
Savina, A., Jancic, C., Hugues, S., Guermonprez, P., Vargas, P., Moura, I.C., Lennon-Dumenil, A.M., Seabra, M.C., Raposo, G., and Amigorena, S. (2006). NOX2 controls phagosomal pH to regulate antigen processing during crosspresentation by dendritic cells. Cell *126*, 205-218.
Schissel, S.L., Keesler, G.A., Schuchman, E.H., Williams, K.J., and Tabas, I. (1998). The cellular trafficking and zinc dependence of secretory and lysosomal sphingomyelinase, two products of the acid sphingomyelinase gene. The Journal of biological chemistry *273*, 18250-18259.
Schneider, P.B., and Kennedy, E.P. (1967). Sphingomyelinase in normal human spleens and in spleens from subjects with Niemann-Pick disease. J Lipid Res *8*, 202-209.
Schorey, J.S., and Cooper, A.M. (2003). Macrophage signalling upon mycobacterial infection: the MAP kinases lead the way. Cellular microbiology *5*, 133-142.
Schramm, M., Herz, J., Haas, A., Kronke, M., and Utermohlen, O. (2008). Acid sphingomyelinase is required for efficient phago-lysosomal fusion. Cellular microbiology *10*, 1839-1853.
Schuchman, E.H., Levran, O., Pereira, L.V., and Desnick, R.J. (1992). Structural organization and complete nucleotide sequence of the gene encoding human acid sphingomyelinase (SMPD1). Genomics *12*, 197-205.
Schutze, S., Potthoff, K., Machleidt, T., Berkovic, D., Wiegmann, K., and Kronke, M. (1992). TNF activates NF-kappa B by phosphatidylcholine-specific phospholipase C-induced "acidic" sphingomyelin breakdown. Cell *71*, 765-776.
Schwandner, R., Wiegmann, K., Bernardo, K., Kreder, D., and Kronke, M. (1998). TNF receptor death domain-associated proteins TRADD and FADD signal activation of acid sphingomyelinase. The Journal of biological chemistry *273*, 5916-5922.
Segui, B., Cuvillier, O., Adam-Klages, S., Garcia, V., Malagarie-Cazenave, S., Leveque, S., Caspar-Bauguil, S., Coudert, J., Salvayre, R., Kronke, M.*, et al.* (2001). Involvement of FAN in TNF-induced apoptosis. The Journal of clinical investigation *108*, 143-151.
Sendide, K., Reiner, N.E., Lee, J.S., Bourgoin, S., Talal, A., and Hmama, Z. (2005). Cross-talk between CD14 and complement receptor 3 promotes phagocytosis of mycobacteria: regulation by phosphatidylinositol 3-kinase and cytohesin-1. Journal of immunology *174*, 4210-4219.
Senkal, C.E., Salama, M.F., Snider, A.J., Allopenna, J.J., Rana, N.A., Koller, A., Hannun, Y.A., and Obeid, L.M. (2017). Ceramide Is Metabolized to Acylceramide and Stored in Lipid Droplets. Cell metabolism *25*, 686-697.
Seto, S., Tsujimura, K., and Koide, Y. (2011). Rab GTPases regulating phagosome maturation are differentially recruited to mycobacterial phagosomes. Traffic *12*, 407-420.
Shamseddine, A.A., Airola, M.V., and Hannun, Y.A. (2015). Roles and regulation of neutral sphingomyelinase-2 in cellular and pathological processes. Advances in biological regulation *57*, 24-41.
Shi, G.P., Bryant, R.A., Riese, R., Verhelst, S., Driessen, C., Li, Z., Bromme, D., Ploegh, H.L., and Chapman, H.A. (2000). Role for cathepsin F in invariant chain processing and major histocompatibility complex class II peptide loading by macrophages. The Journal of experimental medicine *191*, 1177-1186.

Shin, D.M., Jeon, B.Y., Lee, H.M., Jin, H.S., Yuk, J.M., Song, C.H., Lee, S.H., Lee, Z.W., Cho, S.N., Kim, J.M., *et al.* (2010). Mycobacterium tuberculosis eis regulates autophagy, inflammation, and cell death through redox-dependent signaling. PLoS pathogens *6*, e1001230.
Simonis, A., Hebling, S., Gulbins, E., Schneider-Schaulies, S., and Schubert-Unkmeir, A. (2014). Differential activation of acid sphingomyelinase and ceramide release determines invasiveness of Neisseria meningitidis into brain endothelial cells. PLoS pathogens *10*, e1004160.
Singh, A., Guidry, L., Narasimhulu, K.V., Mai, D., Trombley, J., Redding, K.E., Giles, G.I., Lancaster, J.R., Jr., and Steyn, A.J. (2007). Mycobacterium tuberculosis WhiB3 responds to O2 and nitric oxide via its [4Fe-4S] cluster and is essential for nutrient starvation survival. Proceedings of the National Academy of Sciences of the United States of America *104*, 11562-11567.
Singh, C.R., Moulton, R.A., Armitige, L.Y., Bidani, A., Snuggs, M., Dhandayuthapani, S., Hunter, R.L., and Jagannath, C. (2006). Processing and presentation of a mycobacterial antigen 85B epitope by murine macrophages is dependent on the phagosomal acquisition of vacuolar proton ATPase and in situ activation of cathepsin D. Journal of immunology *177*, 3250-3259.
Singh, V., Jamwal, S., Jain, R., Verma, P., Gokhale, R., and Rao, K.V. (2012). Mycobacterium tuberculosis-driven targeted recalibration of macrophage lipid homeostasis promotes the foamy phenotype. Cell host & microbe *12*, 669-681.
Slauch, J.M. (2011). How does the oxidative burst of macrophages kill bacteria? Still an open question. Molecular microbiology *80*, 580-583.
Soualhine, H., Deghmane, A.E., Sun, J., Mak, K., Talal, A., Av-Gay, Y., and Hmama, Z. (2007). Mycobacterium bovis bacillus Calmette-Guerin secreting active cathepsin S stimulates expression of mature MHC class II molecules and antigen presentation in human macrophages. Journal of immunology *179*, 5137-5145.
Steinwede, K., Maus, R., Bohling, J., Voedisch, S., Braun, A., Ochs, M., Schmiedl, A., Langer, F., Gauthier, F., Roes, J., *et al.* (2012). Cathepsin G and neutrophil elastase contribute to lung-protective immunity against mycobacterial infections in mice. Journal of immunology *188*, 4476-4487.
Su, Y., Xia, W., Li, J., Walz, T., Humphries, M.J., Vestweber, D., Cabanas, C., Lu, C., and Springer, T.A. (2016). Relating conformation to function in integrin alpha5beta1. Proceedings of the National Academy of Sciences of the United States of America *113*, E3872-3881.
Szollosi, J., Tron, L., Damjanovich, S., Helliwell, S.H., Arndt-Jovin, D., and Jovin, T.M. (1984). Fluorescence energy transfer measurements on cell surfaces: a critical comparison of steady-state fluorimetric and flow cytometric methods. Cytometry *5*, 210-216.
Tafesse, F.G., Ternes, P., and Holthuis, J.C. (2006). The multigenic sphingomyelin synthase family. The Journal of biological chemistry *281*, 29421-29425.
Tailleux, L., Schwartz, O., Herrmann, J.L., Pivert, E., Jackson, M., Amara, A., Legres, L., Dreher, D., Nicod, L.P., Gluckman, J.C., *et al.* (2003). DC-SIGN is the major Mycobacterium tuberculosis receptor on human dendritic cells. The Journal of experimental medicine *197*, 121-127.
Takahashi, T., Suchi, M., Desnick, R.J., Takada, G., and Schuchman, E.H. (1992). Identification and expression of five mutations in the human acid sphingomyelinase gene causing types A and B Niemann-Pick disease. Molecular evidence for genetic heterogeneity in the neuronopathic and non-neuronopathic forms. The Journal of biological chemistry *267*, 12552-12558.

Tang, C.H., Lee, J.W., Galvez, M.G., Robillard, L., Mole, S.E., and Chapman, H.A. (2006). Murine cathepsin F deficiency causes neuronal lipofuscinosis and late-onset neurological disease. Molecular and cellular biology *26*, 2309-2316.
Tani, M., and Hannun, Y.A. (2007). Neutral sphingomyelinase 2 is palmitoylated on multiple cysteine residues. Role of palmitoylation in subcellular localization. The Journal of biological chemistry *282*, 10047-10056.
Tavakoli, S., and Asmis, R. (2012). Reactive oxygen species and thiol redox signaling in the macrophage biology of atherosclerosis. Antioxid Redox Signal *17*, 1785-1795.
Teichgraber, V., Ulrich, M., Endlich, N., Riethmuller, J., Wilker, B., De Oliveira-Munding, C.C., van Heeckeren, A.M., Barr, M.L., von Kurthy, G., Schmid, K.W.*, et al.* (2008). Ceramide accumulation mediates inflammation, cell death and infection susceptibility in cystic fibrosis. Nature medicine *14*, 382-391.
Thandi, R.S., Tripathi, D., Radhakrishnan, R.K., Paidipally, P., and Vankayalapati, R. (2018). Kupffer cells restricts Mycobacterium tuberculosis growth better than alveolar macrophages. The Journal of Immunology *200*, 173.120-173.120.
Thorne, K.J., Oliver, R.C., and Barrett, A.J. (1976). Lysis and killing of bacteria by lysosomal proteinases. Infection and immunity *14*, 555-563.
Tonnetti, L., Veri, M.C., Bonvini, E., and D'Adamio, L. (1999). A role for neutral sphingomyelinase-mediated ceramide production in T cell receptor-induced apoptosis and mitogen-activated protein kinase-mediated signal transduction. The Journal of experimental medicine *189*, 1581-1589.
Tsai, M.C., Chakravarty, S., Zhu, G., Xu, J., Tanaka, K., Koch, C., Tufariello, J., Flynn, J., and Chan, J. (2006). Characterization of the tuberculous granuloma in murine and human lungs: cellular composition and relative tissue oxygen tension. Cellular microbiology *8*, 218-232.
Tschop, J., Nogueiras, R., Haas-Lockie, S., Kasten, K.R., Castaneda, T.R., Huber, N., Guanciale, K., Perez-Tilve, D., Habegger, K., Ottaway, N.*, et al.* (2010). CNS leptin action modulates immune response and survival in sepsis. The Journal of neuroscience : the official journal of the Society for Neuroscience *30*, 6036-6047.
Ullrich, H.J., Beatty, W.L., and Russell, D.G. (1999). Direct delivery of procathepsin D to phagosomes: implications for phagosome biogenesis and parasitism by Mycobacterium. European journal of cell biology *78*, 739-748.
Uribe-Querol, E., and Rosales, C. (2017). Control of Phagocytosis by Microbial Pathogens. Frontiers in immunology *8*, 1368.
Utermohlen, O., Herz, J., Schramm, M., and Kronke, M. (2008). Fusogenicity of membranes: the impact of acid sphingomyelinase on innate immune responses. Immunobiology *213*, 307-314.
Utermohlen, O., Karow, U., Lohler, J., and Kronke, M. (2003). Severe impairment in early host defense against Listeria monocytogenes in mice deficient in acid sphingomyelinase. Journal of immunology *170*, 2621-2628.
van Ingen, J. (2017). Infectious Disease Vol 2, 4 edn (Elsevier).
Vazquez, C.L., Rodgers, A., Herbst, S., Coade, S., Gronow, A., Guzman, C.A., Wilson, M.S., Kanzaki, M., Nykjaer, A., and Gutierrez, M.G. (2016). The proneurotrophin receptor sortilin is required for Mycobacterium tuberculosis control by macrophages. Scientific reports *6*, 29332.
Velasco-Velazquez, M.A., Barrera, D., Gonzalez-Arenas, A., Rosales, C., and Agramonte-Hevia, J. (2003). Macrophage--Mycobacterium tuberculosis interactions: role of complement receptor 3. Microbial pathogenesis *35*, 125-131.
Venable, M.E., Lee, J.Y., Smyth, M.J., Bielawska, A., and Obeid, L.M. (1995). Role of ceramide in cellular senescence. The Journal of biological chemistry *270*, 30701-30708.

Vergne, I., Chua, J., Lee, H.H., Lucas, M., Belisle, J., and Deretic, V. (2005). Mechanism of phagolysosome biogenesis block by viable Mycobacterium tuberculosis. Proceedings of the National Academy of Sciences of the United States of America *102*, 4033-4038.
Vieira, O.V., Botelho, R.J., Rameh, L., Brachmann, S.M., Matsuo, T., Davidson, H.W., Schreiber, A., Backer, J.M., Cantley, L.C., and Grinstein, S. (2001). Distinct roles of class I and class III phosphatidylinositol 3-kinases in phagosome formation and maturation. The Journal of cell biology *155*, 19-25.
Vieira, O.V., Bucci, C., Harrison, R.E., Trimble, W.S., Lanzetti, L., Gruenberg, J., Schreiber, A.D., Stahl, P.D., and Grinstein, S. (2003). Modulation of Rab5 and Rab7 recruitment to phagosomes by phosphatidylinositol 3-kinase. Molecular and cellular biology *23*, 2501-2514.
Villadangos, J.A., and Ploegh, H.L. (2000). Proteolysis in MHC class II antigen presentation: who's in charge? Immunity *12*, 233-239.
Volkman, H.E., Clay, H., Beery, D., Chang, J.C., Sherman, D.R., and Ramakrishnan, L. (2004). Tuberculous granuloma formation is enhanced by a mycobacterium virulence determinant. PLoS biology *2*, e367.
Wang, C., Yu, X., Cao, Q., Wang, Y., Zheng, G., Tan, T.K., Zhao, H., Zhao, Y., Wang, Y., and Harris, D. (2013). Characterization of murine macrophages from bone marrow, spleen and peritoneum. BMC immunology *14*, 6.
Wayne, L.G. (1982). Microbiology of tubercle bacilli. The American review of respiratory disease *125*, 31-41.
Weber, G.F., Bjerke, M.A., and DeSimone, D.W. (2011). Integrins and cadherins join forces to form adhesive networks. J Cell Sci *124*, 1183-1193.
Weiss, G., and Schaible, U.E. (2015). Macrophage defense mechanisms against intracellular bacteria. Immunological reviews *264*, 182-203.
WHO (2018a). Leprosy. http://wwwwhoint/en/news-room/fact-sheets/detail/leprosy.
WHO (2018b). Tuberculosis. http://wwwwhoint/en/news-room/fact-sheets/detail/tuberculosis.
Wijesinghe, D.S., Massiello, A., Subramanian, P., Szulc, Z., Bielawska, A., and Chalfant, C.E. (2005). Substrate specificity of human ceramide kinase. J Lipid Res *46*, 2706-2716.
Wolf, A.J., Desvignes, L., Linas, B., Banaiee, N., Tamura, T., Takatsu, K., and Ernst, J.D. (2008). Initiation of the adaptive immune response to Mycobacterium tuberculosis depends on antigen production in the local lymph node, not the lungs. The Journal of experimental medicine *205*, 105-115.
Wu, Y., Gulbins, E., and Grassme, H. (2017). Crosstalk Between Sphingomyelinases and Reactive Oxygen Species in Mycobacterial Infection. Antioxid Redox Signal.
Wu, Y., Gulbins, E., and Grassme, H. (2018). The function of sphingomyelinases in mycobacterial infections. Biological chemistry.
Xu, M., Li, X.X., Ritter, J.K., Abais, J.M., Zhang, Y., and Li, P.L. (2013). Contribution of NADPH oxidase to membrane CD38 internalization and activation in coronary arterial myocytes. PloS one *8*, e71212.
Xu, R., Jin, J., Hu, W., Sun, W., Bielawski, J., Szulc, Z., Taha, T., Obeid, L.M., and Mao, C. (2006). Golgi alkaline ceramidase regulates cell proliferation and survival by controlling levels of sphingosine and S1P. FASEB journal : official publication of the Federation of American Societies for Experimental Biology *20*, 1813-1825.
Yadav, M., Clark, L., and Schorey, J.S. (2006). Macrophage's proinflammatory response to a mycobacterial infection is dependent on sphingosine kinase-mediated activation of phosphatidylinositol phospholipase C, protein kinase C, ERK1/2, and phosphatidylinositol 3-kinase. Journal of immunology *176*, 5494-5503.

Yang, C.S., Shin, D.M., Kim, K.H., Lee, Z.W., Lee, C.H., Park, S.G., Bae, Y.S., and Jo, E.K. (2009). NADPH oxidase 2 interaction with TLR2 is required for efficient innate immune responses to mycobacteria via cathelicidin expression. Journal of immunology *182*, 3696-3705.

Yates, R.M., Hermetter, A., Taylor, G.A., and Russell, D.G. (2007). Macrophage activation downregulates the degradative capacity of the phagosome. Traffic *8*, 241-250.

Yu, H., Zeidan, Y.H., Wu, B.X., Jenkins, R.W., Flotte, T.R., Hannun, Y.A., and Virella-Lowell, I. (2009). Defective acid sphingomyelinase pathway with Pseudomonas aeruginosa infection in cystic fibrosis. American journal of respiratory cell and molecular biology *41*, 367-375.

Zhang, C., and Li, P.L. (2010). Membrane raft redox signalosomes in endothelial cells. Free radical research *44*, 831-842.

Zhang, Y., Li, X., Becker, K.A., and Gulbins, E. (2009). Ceramide-enriched membrane domains--structure and function. Biochimica et biophysica acta *1788*, 178-183.

Zhang, Y., Li, X., Carpinteiro, A., and Gulbins, E. (2008). Acid sphingomyelinase amplifies redox signaling in Pseudomonas aeruginosa-induced macrophage apoptosis. Journal of immunology *181*, 4247-4254.

Zhang, Y., Li, X., Grassme, H., Doring, G., and Gulbins, E. (2010). Alterations in ceramide concentration and pH determine the release of reactive oxygen species by Cftr-deficient macrophages on infection. Journal of immunology *184*, 5104-5111.

Zink, A.R., Sola, C., Reischl, U., Grabner, W., Rastogi, N., Wolf, H., and Nerlich, A.G. (2003). Characterization of Mycobacterium tuberculosis complex DNAs from Egyptian mummies by spoligotyping. Journal of clinical microbiology *41*, 359-367.

Appendix

Publications

Wu, Y., Li C., Riehle, A., Pollmeier, B., Gulbins, E., and Grassme, H. (2018b) Mycobacterial infection is promoted by neutral sphingomyelinase 2 regulating a signaling cascade leading to activation of β1-integrin. Cellular physiology and biochemistry *51*, 1815-1829.

Wu.Y., Riehle, A., Pollmeier, B., Gulbins, E., and Grassme, H. Acid sphingomyelinase is essential for mycobacteria degradation in macrophages. *In preparation*.

Cao Li, Anni Wang, **Yuqing Wu**, Erich Gulbins, Heike Grassmé, Zhigang Zhao. Acid sphingomyelinase-ceramide system in bacterial infections. *Accepted*.

Wu, Y., Gulbins, E., and Grassme, H. (2018). The function of sphingomyelinases in mycobacterial infections. Biological chemistry.

Wu, Y., Gulbins, E., and Grassme, H. (2017). Crosstalk Between Sphingomyelinases and Reactive Oxygen Species in Mycobacterial infection. Antioxid Redox Signal.

Li, C., **Wu, Y**., Riehle, A., Ma, J., Kamler, M., Gulbins, E., and Grassme, H. (2017a). *Staphylococcus aureus* Survives in Cystic Fibrosis Macrophages, Forming a Reservoir for Chronic Pneumonia. Infection and immunity.

Li, C., **Wu, Y**., Riehle, A., Orian-Rousseau, V., Zhang, Y., Gulbins, E., and Grassme, H. (2017b). Regulation of *Staphylococcus aureus* Infection of Macrophages by CD44, Reactive Oxygen Species, and Acid Sphingomyelinase. Antioxid Redox Signal.s in Mycobacterial Infection. Antioxid Redox Signal.

Posters and Presentations

Science Slam – Research Day, University of Duisburg-Essen, December 7th, 2018, Essen, Germany: **Presentation** – Game of immune system.

International Workshop- “Sphingolipids - from basic science to novel therapeutic concepts” June 28th-30th, 2018, Würzburg, Germany: **Presentation** - The role of acid sphingomyelinase in mycobacterial infection.

Meeting of SFB 1039 and GRK 2098, June 26th-27th, 2018, Frankfurt, Germany: **Presentation** - The role of acid sphingomyelinase in mycobacterial infection.

Gordon Research Conference- glycolipid and sphingolipid biology, February 11th-16th, 2018, Galveston, Texas, United States: **Poster prize winner** - Inhibition of neutral sphingomyelinase dependent granuloma formation via β1-integrin protects mice against systemic tuberculosis.

Research day, University of Duisburg-Essen, November 17th, 2017, Essen, Germany: **Poster** - Inhibition of neutral sphingomyelinase dependent granuloma formation via β1-integrin protects mice against systemic tuberculosis.

Symposium des GRK 2098 und der DFG-Forschergruppe 2123, June 21st-22nd, 2017, Würzburg, Germany: **Presentation** - Role of neutral sphingomyelinase in mycobacterial infection.

Forschergruppen Meeting (FOR2123), October 7th, 2016, Würzburg, Germany: **Poster** - Role of neutral sphingomyelinase in mycobacterial infection.

Acknowledgments

First, I would like to thank Prof. Dr. Erich Gulbins and Dr. Heike Grassmé for giving me the opportunity to work on the lab, studying the projects and most importantly, supporting me with their excellent scientific guidance.

I am very grateful for the academic support from Dr. Heike Grassmé and for her patience and encouragement throughout my Ph.D. time.

I would like to thank the graduate schools- FOR 2123 and GRK 2098 for the arrangement of the Ph.D. program and meeting so many experienced scientists to enthusiast my study.

I would also like to thank the members of the thesis committee for taking the time to evaluate my Ph.D. thesis.

I would like to thank my collaboration partner, Dr. Fabian Schumacher at the Department of Toxicology/Institute of Nutritional Science in Potsdam.

A huge thank you is to my past and present colleagues at the Department of Molecular Biology, for helping me and creating a kind work environment: Dr. Katrin Becker-Flegler, Dr. Nadine Beckmann, Salina Begum, Dr. Alexander Carpinterio, Hannelore Disselhoff, Gabriele Hessler, Karen Hung, Dr. Stephanie Kadow, Simone Keitsch, Anne Koch, Melanie Kramer, Claudine Kühn, Dr. Cao Li, Jie Ma, Siegfried Moyrer, Eyad Naser, Helga Pätsch, Bettina Peter, Carolin Sehl, Matthias Soddeman, and Barbara Wilker.

In particular, I would also like to thank Andrea Riehle and Bärbel Pollmeier, who always offered a helping hand in time and provided excellent technical support. Bettina Peter, Helga Pätsch, and Siegfried Moyrer, thank you very much for the great support in pharmacy orderings, invoice reimbursements, Visa applications and software's installments and instructions. Matthias Soddeman, thank you very much for teaching me to use the Cryotome and helping me to cut tissues.

I also want to thank my friends I have met here, Anne Koch, Salina Begum and Karen Hung. We spent so much time together and shared our studies and lives. Simone

Keitsch, thank you for supporting me in the lab for the mice. Also, we had so many fun going out together.

Finally, I would like to thank my family, particularly my parents, my parents in law, my daughter, and my husband. My parents, thank you for your unconditional love and belief in me. My parents in law, especially my mom in law, thank you for visiting and helping us. My daughter and my husband, thank you for your companying and supporting all the time.

Curriculum Vitae

"The biography is not included in the online version for reasons of data protection".

Declarations

Erklärung:

Hiermit erkläre ich, gem. § 7 Abs. (2) d) + f) der Promotionsordnung der Fakultät für Biologie zur Erlangung des Dr. rer. nat., dass ich die vorliegende Dissertation selbständig verfasst und mich keiner anderen als der angegebenen Hilfsmittel bedient, bei der Abfassung der Dissertation nur die angegeben Hilfsmittel benutzt und alle wörtlich oder inhaltlich übernommenen Stellen als solche gekennzeichnet habe.

Essen, den _____ _____
Unterschrift des Doktoranden

Erklärung:

Hiermit erkläre ich, gem. § 7 Abs. (2) e) + g) der Promotionsordnung der Fakultät für Biologie zur Erlangung des Dr. rer. nat., dass ich keine anderen Promotionen bzw. Promotionsversuche in der Vergangenheit durchgeführt habe und dass diese Arbeit von keiner anderen Fakultät/Fachbereich abgelehnt worden ist.

Essen, den _____ _____
Unterschrift des Doktoranden

Erklärung:

Hiermit erkläre ich, gem. § 6 Abs. (2) g) der Promotionsordnung der Fakultät für Biologie zur Erlangung der Dr. rer. nat., dass ich das Arbeitsgebiet, dem das Thema „**Role of sphingomyelinases in mycobacterial infection**“ zuzuordnen ist, in Forschung und Lehre vertrete und den Antrag von **Yuqing Wu** befürworte und die Betreuung auch im Falle eines Weggangs, wenn nicht wichtige Gründe dem entgegenstehen, weiterführen werde.

_____
Name des Mitglieds der Universität Duisburg-Essen in Druckbuchstaben

Essen, den _____ _____
Unterschrift eines Mitglieds der Universität Duisburg-Essen